MODELING AND POWER MANAGEMENT OF A HYBRID WIND-MICROTURBINE POWER GENERATION SYSTEM

by

Sreedhar Reddy Guda

A thesis submitted in partial fulfillment
of the requirements for the degree

of

Master of Science

in

Electrical Engineering

MONTANA STATE UNIVERSITY
Bozeman, Montana

July 2005

APPROVAL

of a thesis submitted by

Sreedhar Reddy Guda

This thesis has been read by each member of the thesis committee and has been found to be satisfactory regarding content, English usage, format, citations, bibliographic style, and consistency, and is ready for submission to the College of Graduate Studies.

Dr. Hashem Nehrir

Approved for the Department of Electrical and Computer Engineering

Dr. James Peterson

Approved for the College of Graduate Studies

Dr. Joseph Fedock

STATEMENT OF PERMISSION TO USE

In presenting this thesis in partial fulfillment of the requirements for a master's degree at Montana State University, I agree that the Library shall make it available to borrowers under rules of the Library.

If I have indicated my intention to copyright this thesis by including a copyright notice page, copying is allowable only for scholarly purposes, consistent with "fair use" as prescribed in the U.S. Copyright Law. Requests for permission for extended quotation from or reproduction of this thesis in whole or in parts may be granted only by the copyright holder.

Sreedhar Reddy Guda

July 2005

ACKNOWLEDGEMENTS

I am grateful to acknowledge and thank all of those who assisted me in my graduate program at Montana State University. First, I would like to thank Dr. M. H. Nehrir, my academic advisor here at MSU. The guidance, support, patience and personal time he invested throughout my years as a graduate student have been truly appreciated. Special thanks are extended to my other graduate committee members, Dr. H. Gao and Dr. R. Gunderson. Mr. C. Wang, my fellow student and colleague, deserves deepest thanks for his time and the clarifying conversations that were so useful to my understanding of this thesis and other matters. Most importantly, I would like to thank my family and friends for their support throughout all the years.

TABLE OF CONTENTS

TABLE OF CONTENTS - CONTINUED

TABLE OF CONTENTS - CONTINUED

LIST OF TABLES

LIST OF FIGURES

LIST OF FIGURES - CONTINUED

LIST OF FIGURES - CONTINUED

LIST OF FIGURES - CONTINUED

LIST OF FIGURES - CONTINUED

ABSTRACT

The goal of this thesis is to evaluate the performance of a hybrid wind-microturbine energy system through computer simulation studies. The primary focus of this study is the development of dynamic models for a standalone wind energy conversion system and a microturbine generation system. The system model developed is suitable for power management in distributed generation studies.

The developed model of the wind energy conversion system consists of dynamic models for a wind turbine as well as an electric generator. A detailed model of the wind turbine based on a set of nonlinear curves is presented. The electric generator, driven by the wind turbine, is a self-excited asynchronous (induction) generator suitable for isolated and grid-connected operations. Modeling of the electric generator, complete with saturation characteristic, is done using *dq*-axis theory. Also, the importance of excitation-capacitors during isolated mode of operation is explained.

A dynamic model for the microturbine generation system is achieved by integrating models of a microturbine and an electric generator driven by it. The model illustrates the dynamics of the microturbine and its control systems. A set of mathematical equations are used to model a permanent magnet synchronous machine acting as the electric generator of the microturbine generation system. The developed system is capable of simulating the dynamics of the microturbine generation system, demonstrating its ability to meet load power requirements.

The dynamic models of the wind energy conversion system and the microturbine generation system are integrated using power electronics interfacing and simulated in MATLAB/Simulink. Simulation results indicate the suitability of the developed model to study the dynamic behavior of the hybrid generation system under different load conditions.

CHAPTER 1

INTRODUCTION

Background

This thesis is concerned with the development of a computer simulation model to evaluate the performance of a stand-alone hybrid generation system comprising of a wind energy conversion system and a microturbine generation system. Models representing each system components are developed, integrated and used to observe the overall system behavior.

The ever increasing energy demands, dwindling sources of fossil fuels and concern about pollution levels in the environment has been the driving force behind electricity generation using renewable energy sources. Tapping the energy available from the renewable resources allows the attainment of notable reductions in the pollution levels and worrying climate changes. On the other hand, the availability of energy from renewable sources like wind energy, solar energy, etc. is unpredictable and is affected by factors beyond human control. Therefore, such renewable energy systems should be backed up by conventional sources of energy or energy storage devices in order to ensure continuity of the energy supply. This leads us to the topic of hybrid generation units comprising conventional or unconventional sources of energy or both, where two or more individual generation systems operate in parallel supplementing each other. A typical

hybrid generation system relies on power electronic interfacing for functioning and interfacing between different generating units and with the distribution network (in grid-connected operation).

In remote and isolated areas far from the grid, it may not be an economically viable option to supply electric power from the grid. This is due to the high cost of transmission lines and higher transmission losses that accompany distribution of centrally generated power to remote areas. The deregulation of electricity market has made it possible for the hybrid systems to be installed as isolated units or grid-connected units (not discussed in this thesis) acting as distributed generations (DG) sources. It is well documented in the literature that DGs could have positive impacts on the operation of power systems to which they are connected. DGs come in different forms such as on-site gas or diesel fired turbines, reciprocating engines, microturbines, small hydro induction generators, wind turbines and fuel cells. DG technology promises to be an efficient, environmentally friendly and reliable power source. Proper modeling of these DGs, which constitute hybrid generation systems, is needed in order to study their operation and impact on power systems.

Hybrid Generation System

Hybrid generation systems usually combine renewable sources like wind power with conventional sources of energy like gas turbines (or microturbines) to from an equivalent of a miniature (or virtual) grid. Such a configuration addresses two important issues

namely, higher emissions because of conventional generation techniques and high cost of energy capture from renewable sources. For wind energy systems, the renewable source of energy considered in this thesis, the emissions are nil but it has relatively high capital costs. With modern microturbine systems, the other generating system in the hybrid generation system, the energy costs are relatively lower and the emissions of undesired gases is also low. In this thesis, these two systems models are integrated to form a model of the hybrid generation system as explained in the following paragraphs.

A hybrid system could be designed to operate either in isolated mode or in grid-connected mode, through power electronic interface. The power electronic interface should have the ability to maintain the hybrid generation system parameters like voltage, frequency etc., at prescribed (acceptable) levels. It is essential to have a good control of the power angle and the voltage level by means of an inverter which is the main block of the power electronic interface. Control of the inverter's output voltage and the power angle controls the flow of real power and reactive power. A typical wind-microturbine hybrid generation system, along with its power electronics interface, is shown in Figure 1.1.

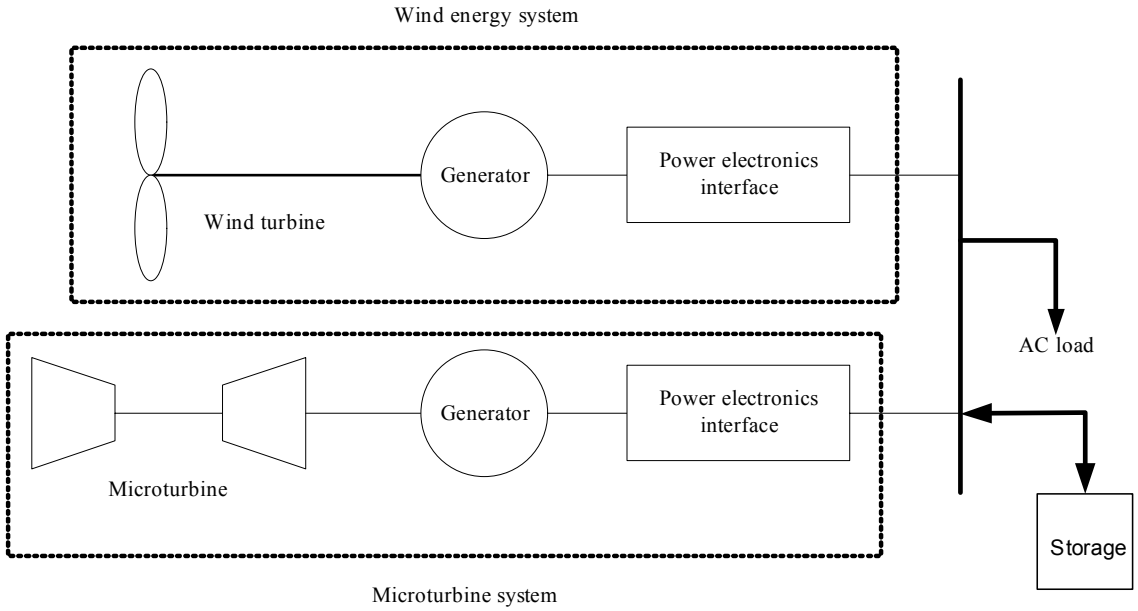

Figure 1.1 A typical wind-microturbine hybrid generation system.

The hybrid system presented in this thesis comprises of a wind energy conversion system (WECS) acting as the renewable source of energy and a microturbine generation (MTG) system serving as the conventional source of energy. In general, it also includes a storage unit which helps to increase the overall system efficiency (Figure 1.1). However, as the emphasis is on MTG and WECS systems, the hybrid system considered in this thesis doesn't have a storage device.

Electricity generation by wind promises to be the best source of renewable energy, as rapid advances in wind turbine technology have made utilization of wind energy for electricity generation possible. Moreover, the economic aspects of these technologies are now sufficiently promising to justify their use.

The other component of the proposed hybrid generation system (Figure 1.1), which tries to offset the high installation costs involved with the wind energy system, is the microturbine system. With the combination of high reliability and low installation costs microturbines are seen as one of the key components in the distributed generation. The emission levels of microturbines are low and they are capable of working on a variety of fuels like natural gas, sour gas, propane etc.

Literature Review

This section offers a brief review of some of the published work on the hybrid generating systems. The work referred in the following sections is focused mostly on the modeling of individual components of the hybrid system. However, this section doesn't offer any review on the modeling of power electronics interface, as it is beyond the scope of this thesis.

Reference [1.1] presents a hybrid configuration comprising of a wind–diesel system originally developed by the Hydro-Quebec, aimed at reducing the cost of electricity supply in remote areas. The two main blocks of the system presented are, diesel- driven synchronous generator and the wind turbine driven by the asynchronous (induction) generator. The wind turbine block uses a 2-dimensional lookup table to compute the turbine torque output as a function of wind speed and turbine speed. At low wind speeds both the induction generator and the diesel-driven synchronous generator are required to feed the load. When the wind power exceeds the load demand, it is possible to shut down

the diesel-generator. In this all-wind mode, the synchronous machine is used as a synchronous condenser and its excitation system controls the grid voltage at its nominal value. A secondary load bank is used to regulate the system frequency by absorbing the wind power exceeding consumer demand.

Reference [1.2] presents a hybrid generation system referred as a virtual power plant. The system consists of a wind farm and a gas turbine driven synchronous generator whose outputs are combined before connecting to the grid. In this paper, the authors developed dynamic models for the synchronous generator and induction generator and, the dynamic model of a wind turbine is scaled appropriately to represent the output of a wind farm. The voltage and the output power are controlled via the gas turbine and the synchronous generator model with the help of an automatic voltage regulator (AVR) and a power system stabilizer (PSS) attached to the synchronous generator.

Literature Review on Wind Energy Conversion System

Wind energy conversion systems (WECS) are the devices which are used to convert the wind energy to electrical energy. There exists a large collection of literature on the modeling of wind energy conversion systems more specifically on the modeling of individual system components of a wind energy conversion system. A wind energy conversion system is mainly comprised of two subsystems, namely a wind turbine part and an electric generator part. Detailed descriptions of these concepts can be found in text

books on wind energy [1.3]-[1.5]. A summary of the typical wind turbine models and their control strategies is presented in [1.4].

Literature Review on Wind Turbines. In the literature, most of the models used to represent a wind turbine are based on a non linear relationship between rotor power coefficient and linear tip speed of the rotor blade [1.3]-[1.9].

Muljadi and Butterfield [1.6] mention the advantages of employing a variable speed wind turbine and present a model of it with pitch control. In this model, during low to medium wind speeds, the generator and the power converter control the wind turbine to maximize the energy capture by maintaining the rotor speed at a predetermined optimum value. For high wind speeds the wind turbine is controlled to maintain the aerodynamic power produced by the wind turbine either by pitch control or by generator load control. However, generator load control in the high wind regions, in some cases suffers from the disadvantage of exceeding the rated current values of the stator windings of the generator. Care should be taken not to exceed the rated values of the current.

References [1.7] and [1.8] propose a detailed model of the variable speed pitch controlled wind turbine suitable for studying the transient stability of multi- megawatt sized wind turbines. The simulated model is based on a set of non linear curves depicting the relation between the blade tip speed, rotor power coefficient and pitch angle of the wind turbine. The references also consider a detailed model for the wind input which includes the effects of gust, noise added to the base value of wind input. Reference [1.7]

uses transfer-functions to represent the dynamics of the electrical generator driven by the wind turbine, while [1.8] uses *dq-axis* representation for the synchronous machine acting as an electrical generator. A proportional integral (PI) controller is used to implement the pitch angle controller to limit the wind turbine output in the high wind speed regimes. Simulation results obtained for these models indicate a good approximation of the dynamic performance of a large wind turbine generator subjected to turbulent wind conditions.

As an extension to this work done in [1.7] and [1.8], Slootweg *et al* [1.9] presented a general model that can be used to represent all types of variable speed wind turbines in power system dynamic simulations. The modeling of the wind turbine given by the authors retains the pitch angle controller, which reduces wind turbine rotor efficiency at high wind speeds, as given in [1.7] and [1.8]. The wind turbine dynamics are approximated using nonlinear curves, which are numerical approximations, to estimate the value of wind turbine rotor efficiency for given values of rotor tip speed and pitch angle of the blade. The authors offer a comparison between the per-unit power curves of two commercial wind turbines and the one obtained theoretically by using the numerical approximation. The results indicate that a general numerical approximation can be used to simulate different types of wind turbines.

Literature Review on Self-excited Induction Generator. The conversion of mechanical power of the wind turbine into the electrical power can be accomplished by an electrical generator which can be a DC machine, a synchronous machine, or an Induction machine.

DC machine was used widely until 1980s, in smaller power installations below 100 kW, because of its extremely easy speed control [1.3]. The presence of commutators in DC machines has low reliability and high maintenance costs. The second kind of electric generators are synchronous generators, suitable for constant speed systems. Requirement of DC field current and reduced wind energy capture of constant speed systems, compared to variable speed systems, are discouraging factors in their use in wind systems [1.3]. Another choice for the electric generator in a WECS is a permanent magnet synchronous generator. Reference [1.10] presents a model of the variable speed wind turbine connected to a permanent magnet synchronous generator (PMSG). But PMSGs suffer from uncontrollable magnetic field decaying over a period of time, their generated voltage tends to fall steeply with load and is not ideal for isolated operation [1.11]. Induction generators, on the other hand, have many advantages over conventional synchronous generators due to their ruggedness, no need for DC filed current, low maintenance requirements and low cost [1.3].

References [1.12] and [1.13] give a model of the WECS using doubly fed induction generator (DFIG). DFIGs allow one to produce power both from the stator and the rotor of a (wound rotor) induction generator. However increase in the power output comes with increased cost of power electronics, and their control, for the rotor circuit. One advantage of this configuration is its suitability for grid-connected operations where reactive power is supplied by the grid.

One of the early works done on the process of self-excitation in induction machines was by Basset and Potter [1.14]. In this paper the author shows that the induction machine, driven by a prime mover, can be self-excited using a bank of capacitors connected across its stator terminals. This facilitates the operation of induction machine as an isolated generator by using excitation capacitors to address the reactive power needs of the machine, while still enjoying the basic advantages of using induction machines for electricity generation. Additional benefits include a self-protection mechanism against short circuits. The authors also discuss the importance of the saturation curve and the excitation capacitance reactance. The author draws conclusion that induction generator can be made to handle any type of load, provided that the loads are compensated to present unity power factor characteristics to the generator.

As a continuation to this work Wagner [1.15] proposed a method to predetermine the induction machine characteristics when operating as self-excited induction generator (SEIG). His analysis is based on equating the reactive power of the whole induction generator system to zero. He points out that the value to which the terminal voltage of the SEIG will rise due to self-excitation is dependent upon the speed of the rotor, value of the capacitor, and the load. In a capacitor-excited generator used as an isolated power source, both the terminal voltage and the frequency are unknown and have to be computed for a given speed, capacitance and load. The analysis is complicated owing to the magnetic saturation in the machine. Murthy *et al* [1.16] proposed an analytical technique using the 'Newton-Raphson' method to identify the saturated parameters, and the generated

frequency for given operating conditions (speed, load and capacitance value). This method uses a steady-state equivalent circuit to estimate the (steady-state) parameters using the values obtained from the analytical analysis. Although, the method is suitable for computer simulations, it is efficient for steady-state analysis only.

In [1.17], Elder *et al* examine the phenomenon of self-excitation in induction machines by offering a physical interpretation of the process. The authors compare the initiation of the machine excitation with the response of a resonant circuit (induction machine with capacitors), caused by the action of remnant magnetism present in the rotor circuit of the machine. They rightly acknowledge the importance of residual magnetism for self-excitation to occur, in addition to the parameters identified in the earlier works. As a continuation of this work, the authors [1.18] examine the use of a self-excited induction machine as low-cost stand-alone generator, using *dq*-axis representation, addressing the problem of guaranteed excitation in the case of loss of residual magnetism. In this paper the authors also examine the behavior of the generator under balanced and unbalanced conditions. The results obtained are used to evaluate the static VAR sources available to control the machine excitation. The authors conclude that the excitation problem is minimal if added capacitance or increased machine speed are allowed.

Grantham *et al* [1.19] have proposed a method for predicting the minimum and maximum values of capacitance necessary to initiate self-excitation in a stand-alone induction generator. The maximum capacitance is usually so large to have any practical significance. Subsequently, their method has been extended to predict the transient

voltage build-up initial stages of self-excitation. Also, steady-state voltage and frequency are obtained theoretically as well as by practical means, taking into account the rotor parameter variations with frequency. The analysis was done using *dq* axis theory. In [1.20] the authors continued their work by simulating a wind energy conversion system (WECS) obtained by integrating the *dq*-axis SEIG model with a wind turbine model. The wind turbine model is modeled using the torque-speed characteristic of a wind turbine. The effects of magnetizing inductance on self-excitation and the loading analysis of induction generator are studied theoretically as well as in a laboratory set up.

In a work related to estimate the minimum value of excitation capacitance for self-excitation to occur, Al-Jabri and Alolah [1.21] presented a method to estimate the value of capacitance when inductive load is connected. This was done by solving two nonlinear equations which are obtained by applying loop-impedance method on the steady-state per phase equivalent circuit of the induction generator. Also, using this method it is possible to predict the (rotor) speed threshold below which self-excitation fails to occur.

In a similar work Malik and Al-Baharani [1.22] have examined the effect of the exciting capacitors on the steady-state performance of an isolated SEIG with a balanced three-phase load. They conclude that the terminal voltage is independent of the load power factor and depends only on the magnitude of the load impedance.

Li wang and Jian-Yi Su [1.23], in their paper showed and compared the dynamic performance of an isolated SEIG under different power factor loading conditions, using

both simulations and laboratory experiments. Similar to [1.19], they employed *dq*-axis theory for the analysis and simulated the saturation characteristic of the SEIG as a function of magnetizing reactance and magnetizing component of the current.

From the above mentioned references, it is clear that the analysis using the steady-state per-phase equivalent circuit of the induction machine is mostly used to predict the steady-state operating parameters of the machine, and the excitation capacitance needed for initiation of the self-excitation. The other method used [1.18], [1.19], [1.23] is, the *dq*-axis model based on the machine theory, to study the transient as well as the steady-state response of the induction machine.

Literature Review on Microturbine Generation System

A microturbine generation (MTG) system comprises of a microturbine driving an electrical generator. The following paragraphs give a brief summary on the earlier work done on the microturbine part of the MTG system as well as a brief review of its electrical generator part.

Microturbines are small high-speed versions of conventional heavy-duty gas turbines. Hence the dynamic model of a conventional gas turbine, with relatively small thermodynamic constants, can be adopted to study the impacts of a microturbine on the overall system. Rowen [1.24] was among the first ones who presented a model of a heavy-duty gas turbine suitable for use in dynamic power studies and in analyses of connected equipment. The author gave a mathematical model of a single-shaft gas turbine

in terms of p.u. values. The control systems of the given model include speed control, acceleration control, and fuel system. Also, the developed model is suitable for both isolated and parallel operation.

Hannett and Afzal Khan [1.25], in continuation to Rowen's work, validated the gas turbine model by comparing its dynamic performance with that of an operating gas turbine generation system. The authors conclude that the model proposed by Rowen is adequate for the representation of a gas turbine.

In [1.26], the authors used the validated model of the gas turbine [1.25] to simulate the response of a combined cycle plant. Their system comprises of a gas turbine model and a steam turbine model which uses the waste heat from the gas turbine through a heat recovery system. This simulated (combined cycle) model can be used for system dynamic performance studies.

In an extension to this work, Jurado *et al* [1.27] studied the influence of microturbines on distribution networks stability. They also examined the transient and voltage stability of the system. The authors conclude that the microturbines, acting as distributed resources, are capable of providing effective load following service in a distribution system. In [1.28] the authors utilize the proposed model of the microturbine to develop a control system with an adaptive controller for a fuel cell-microturbine hybrid power plant. The developed adaptive controller has the ability to stabilize the system for different disturbances affecting the plant like load power variation or a change in the

plant model parameters such as gas composition. Continuing their work in [1.29], the authors used autoregression with exogenous signal (ARX) identification algorithm to arrive at the transfer-function of a microturbine model. These transfer-functions have the same dynamic response as the original dynamic model of the microturbine, with the added advantage of significant reduction in the model order.

Amer Al-Hinai and Ali Feliachi [1.30] presented a complete model of the MTG system, used as a distributed generator, by making use of the microturbine model discussed in the earlier paragraphs. It includes the power electronic interfacing and is suitable for transient analysis as well as simulation of unbalanced three-phase power system. This paper also presents the simulation results obtained in MATLAB/Simulink.

The electric generator used in a modern MTG system is usually a permanent magnet synchronous generator (PMSG). The equations to model a PMSG are can be found in any standard textbook on electric machines e.g. [1.11].

Objective of this Thesis and Organization of Remaining Chapters

The objective of this thesis is to develop and integrate simulation model of various components of a hybrid generation system. Achieving this objective, involves performance evaluation of all the system components (MTG and WECS) and demonstrating its power management ability with the help of simulation results. The simulation model is suitable to study the impacts of DGs on the power systems besides

being able to simulate the behavior of the overall hybrid system under different operating conditions.

The remaining part of this thesis is organized in to four chapters. Chapter 2 introduces a variable speed WECS and gives detailed modeling of the wind turbine part of it. Dynamic modeling of the electric generator part is explained in chapter 3. Chapter 4 presents modeling of the MTG system followed by the overall hybrid generation system complete with power electronics interfacing given, in chapter 5. Chapter 6 gives the conclusion of this thesis and aspects worthy of future work. Simulation results obtained in MATLAB/Simulink are given at the end of each chapter and simulation models are given in the appendix at the end of this thesis.

REFERENCES

1.1 MATLAB/Simulink SimPowerSystems Documentation. Available: http://www.mathworks.com

1.2 M.F.Gillie and W.E.Leithead "Operation and regulation of a wind and gas virtual power plant," in *17th intl. conf. Electricity Dist*., Barcelona, May 20003.

1.3 Mukund. R. Patel, *Wind Power Systems*, CRC Press, 1999, ch. 4-6.

1.4 J.F. Manwell, J.G. McGowan and A.L. Rogers, *Wind energy Explained – Theory, Design and application*, John Wiley& Sons, 2002, ch. 7.

1.5 Tony Burton, David sharpe, Nick Jenkins and Ervin Bossanyi, *Wind Energy handbook*, John Wiley& Sons, 2001, ch. 4.

1.6 Eduard Muljadi and C. P. Butterfield, "Pitch-controlled variable-speed wind turbine generation," *IEEE Transactions on Industry Applications* , vol. 37, no. 1, pp. 240-246, Jan/Feb 2001.

1.7 P.M.Anderson and Anjan Bose, "Stability simulation of wind turbine systems," *IEEE Trans. on Power and Apparatus and Systems*, vol. PAS-102, no. 12, pp. 3791-3795, Dec. 1983.

1.8 O. Wasynczuk, D.T. Man and J. P. Sullivan, "Dynamic behavior of a class of wind turbine generators during random wind fluctuations," *IEEE Transactions on Power and Apparatus and Systems*, vol. PAS-100, no. 6, pp. 2837-2845, June 1981.

1.9 J. G. Slootweg, S.W.H. de Haan, H. Polinder and W.L. Kling, "General model for representing variable speed wind turbines in power system dynamics simulations," *IEEE Transactions on Power Systems*, vol. 18, no. 1, pp. 144-151 , Feb. 2003.

1.10 Antonios E. Haniotis; Konstantinos S. Soutis, Antonios G. Kladas, and John A. Tegopoulos, "Grid connected variable speed wind turbine modeling, dynamic performance and control," in *IEEE PES Power Syst. Conf. Expos*., vol. 2, pp. 759-764, Oct 10-13 2004, New York, NY, United States.

1.11 Bimal K.Bose, *Modern Power Electronics and AC Drives*, Pearson Education, 2003.

1.12 Anca D.Hansen, Florin Iov, Poul Sorensen, and Frede Blaabjerg, "Overall control strategy of variable speed doubly-fed induction generator wind turbine," in *2004 Nordic Wind Power Conference*, Chalmers University of Technology, Sweden.

1.13 Rajib Datta and V. T. Ranganathan, "Variable-speed wind power generation using doubly fed wound rotor induction machine – A comparison with alternative schemes," *IEEE Transactions on Energy Conversion*, vol. 17, no. 3, pp. 414-420, Sept. 2002.

1.14 E. D. Basset and F. M. Potter, "Capacitive excitation of induction generators," *Trans. Amer. Inst. Elect. Eng*, vol. 54, no.5, pp. 540-545, May 1935.

1.15 C. F. Wagner, "Self-excitation of induction motors," *Trans. Amer. Inst. Elect. Eng*, vol. 58, pp. 47-51, Feb. 1939.

1.16 S. S. Murthy, O. P. Malik and A. K. Tandon, "Analysis of self excited induction generators," *Proceedings, IEE*, pt. C, vol. 129, no. 6, pp. 260-265, Nov.1982.

1.17 J. M. Elder, J. T. Boys and J. L. Woodward, "The process of self excitation in induction generators," *Proceedings, IEE*, pt. B, vol. 130, no. 2, pp. 103-108, Mar. 1983.

1.18 J. M. Elder, J. T. Boys and J. L. Woodward, "Self-excited induction machine as a small low-cost generator," *Proceedings IEE*, pt. C, vol. 131, no. 2, pp. 33-41, Mar. 1984.

1.19 C. Grantham, D. Sutanto and B. Mismail, "Steady-state and transient analysis of self-excited induction generators," *Proceedings, IEE*, pt. B, vol. 136, no. 2, pp. 61-68, Mar. 1989.

1.20 Dawit Seyoum, Colin Grantham and M. F. Rahman, "The dynamic characteristics of an isolated self-excited induction generator driven by a wind turbine," *IEEE Trans. Industry Applications*, vol.39, no. 4, pp.936-944, July/August 2003.

1.21 A. K. Al Jabri and A.I. Alolah, "Capacitance requirements for isolated self-excited induction generator," *Proceedings IEE*, pt. B, vol. 137, no. 3, pp. 154-159, May 1990.

1.22 N. H. Malik and A. H. Al-Bahrani, "Influence of the terminal capacitor on the performance characterstics of a self-excited induction generator," *Proceedings IEE*, pt. C, vol. 137, no. 2, pp. 168-173, Mar. 1990.

1.23 Li Wang and Jian-Yi Su, "Dynamic performance of an isolated self-excited induction generator under various loading conditions," *IEEE Transactions on Energy Conversion*, vol. 14, no. 1, pp.93-100, Mar. 1999.

1.24 W. I. Rowen, "Simplified mathematical representations of heavy duty gas turbines," *Journal of Engineering for Power, Transactions ASME*, vol. 105, no. 4, pp. 865-869, Oct, 1983.

1.25 L. N. Hannet and Afzal Khan, "Combustion turbine dynamic model validation from tests," *IEEE Transactions on Power Systems*, vol. 8, no. 1, pp. 152-158, Feb. 1993.

1.26 Working Group on Prime Mover and Energy Supply Models for System Dynamic Performance Studies, "Dynamic models for combined cycle plants in power system studies," *IEEE Transactions on Power Systems*, vol. 9, no. 3, pp. 1698-1708, August 1994.

1.27 A. Cano, F. Jurado and J. Carpio, "Influence of micro-turbines on distribution networks stability," in *Proceedings, IEEE PES General Meeting*, vol. 4, pp. 2153-2158, Jul. 2003, Toronto, Canada.

1.28 F. Jurado and A. Cano, "Use of ARX algorithms for modeling micro-turbines on the distribution feeder," in *Proceedings, IEE: Generation Transmission and Distribution*, vol. 151, no. 2, pp. 232-238, Mar. 2004.

1.29 Francisco Jurado and Jose Ramon Saenz, "Adaptive control of a fuel cell-microturbine hybrid power plant," *IEEE Transactions on Energy Conversion*, vol. 18 no.2, pp. 342-347, June 2003.

1.30 Amer Al-Hinai and Ali Feliachi, "Dynamic model of a microturbine used as a distributed generator," in *Proceedings, 34th Southeastern Symposium on System Theory*, Huntsville, pp.209-213, Alabama, March 2002.

CHAPTER 2

WIND ENERGY CONVERSION SYSTEM – WIND TURBINE MODELING

Introduction

One way of addressing the rising energy demands and growing environmental concerns, is to harness green sources of power. Among these, tapping wind energy with wind turbines appears to be the most promising source of renewable energy. Wind energy conversion systems are used to capture the energy available in the wind to convert into electrical energy.

In this chapter, a functional structure of a wind energy conversion system is introduced, before making a comparison between the two typical wind turbine operating schemes in operation, namely constant-speed wind turbine and variable-speed wind turbine. In addition, the modeling and dynamic behavior of a variable speed wind turbine with pitch control capability is explained in detail.

The average commercial turbine size of the wind installations was 300kW until the mid ninety's [2.1]. Newer machines of larger capacity (up to 5MW) have been developed and are being installed. Wind, when available, is an infinite source of energy. Other environmental impacts of wind power are limited as well.

A schematic diagram of a wind energy conversion system is presented in the next section along with a detailed description of wind turbine and its modeling. The

functionality of other system components is also discussed briefly. In the last section, simulation results, obtained for the variable speed wind turbine, are presented to give a better understanding of the wind turbine dynamics.

Functional Structure of Wind Turbines

The functional structure of a typical wind energy conversion system is as shown in Figure 2.1:

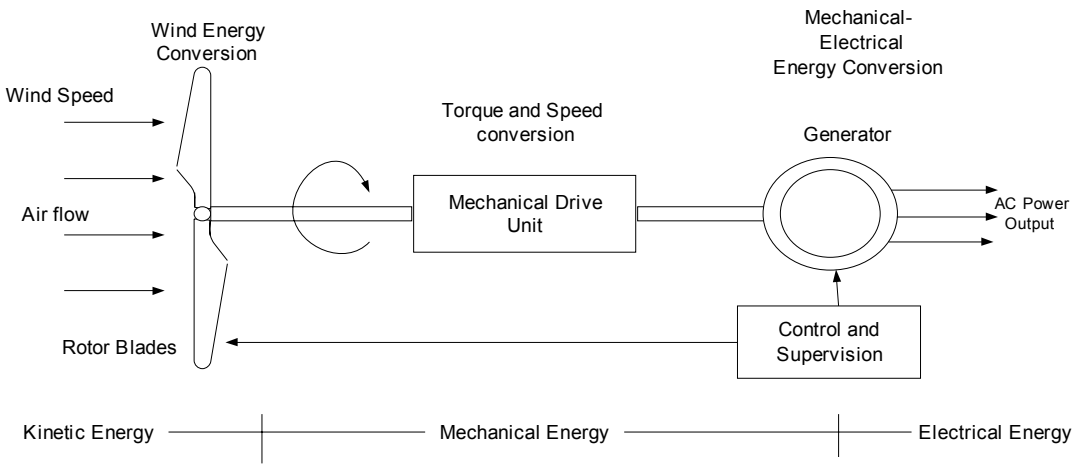

Figure 2.1. Power transfer in a wind energy converter.

A wind energy conversion system is a complex system in which knowledge from a wide array of fields comprising of aerodynamics, mechanical, civil and electrical engineering come together. The principle components of a modern wind turbine are the tower, the rotor and the nacelle, which accommodates the transmission mechanisms and the generator. The wind turbine captures the wind's kinetic energy in the rotor consisting of two or more blades mechanically coupled to an electrical generator. The main

component of the mechanical assembly is the gearbox, which transforms the slower rotational speeds of the wind turbine to higher rotational speeds on the electrical generator side. The rotation of the electrical generator's shaft driven by the wind turbine generates electricity, whose output is maintained as per specifications, by employing suitable control and supervising techniques. Besides monitoring the output, these control systems also include protection systems to protect the overall system.

In this thesis self-excited induction generator (SEIG) is used as the generator for electrical power generation, whose dynamics are simulated in the next chapter. The developed SEIG model is suitable for both steady-state and transient operations. It also includes the effects of saturation of magnetizing inductance, which is very important in the process of self-excitation.

Two distinctly different design configurations are available for a wind turbine, the horizontal axis configuration and the vertical axis configuration. The vertical axis machine has the shape of an egg beater, and is often called the Darrieus rotor after its inventor. However, most modern turbines use horizontal axis design [2.1]. In this chapter the dynamic model of a horizontal axis turbine is developed and simulated in the MATLAB/Simulink, based on the turbine performance curves.

Wind Turbine Modeling

As noted above, a WECS is a complex system converting wind energy to rotational energy and then to electrical energy. The output power or torque of a wind turbine is

determined by several factors like wind velocity, size and shape of the turbine, etc. A dynamic model of the wind turbine, involving these parameters, is needed to understand the behavior of a wind turbine over its region of operation. By studying its modeling, it is possible to control a wind turbine's performance to meet a desired operational characteristic. In the following pages we will look at different performance characteristics and variables that play an important role in wind power generation, by deriving the speed and power relations. The control principles of the wind turbine are also discussed in this section.

Inputs and Outputs of a Wind Turbine

The inputs and output variables of wind turbine can be broken into the following:

1. The independent input quantity *wind speed*, determines the energy input to the wind turbine.

2. Machine-specific input quantities, arising particularly from rotor geometry and arrangement (i.e., different configurations like horizontal axis or vertical axis turbines, area of the blades, etc.).

3. *Turbine speed*, *rotor blade tilt*, and *rotor blade pitch angle*, arising from the transmission system of the wind energy conversion system.

4. Turbine output quantities, namely *Power* or *Drive torque*, which may be controlled by varying the above three input quantities.

Power Extraction from the Air stream

With the identification of the wind turbine's input and output variables, now it is possible to derive an expression relating these two values. The relation between the power and wind speed is derived as follows [2.1]:

The kinetic energy in air of mass m moving with speed V is given by the following:

$$Kinetic\ energy = \frac{1}{2}.m.V^2\ Joules \tag{2.1}$$

The power in moving air flow is the flow rate of kinetic energy per second.

$$Power = \frac{1}{2}.(mass\ flow\ rate\ per\ second).V^2 \tag{2.2}$$

The actual power extracted by the rotor blades is the difference between the upstream and the down stream wind powers. Therefore, equation (2.2) results in

$$P = \frac{1}{2}.(mass\ flow\ rate\ per\ second).\left(V^2 - V_o^2\right) \tag{2.3}$$

Where:

P is the mechanical power extracted by the rotor in watts.

V is the upstream wind velocity at the entrance of the rotor blades in m/s.

V_o is the downstream wind velocity at the exit of the rotor blades in m/s.

Let ρ be the air density in (kg/m^3) and A is the area swept by the rotor blades in (m^2); then, the mass flow rate of air through the rotating blades is given by multiplying the air density with the average velocity.

$$mass\ flow\ rate = \rho . A . \frac{V + V_o}{2} \tag{2.4}$$

From (2.3) and (2.4), the mechanical power extracted by the rotor is given by:

$$P = \frac{1}{2} . \left[\rho . A . \frac{(V + V_o)}{2} \right] . \left(V^2 - V_o^2 \right) \tag{2.5}$$

After algebraic rearrangement of the terms, we have:

$$P = \frac{1}{2} \rho . A . V^3 . C_p \tag{2.6}$$

Where:

$C_p = \dfrac{\left(1 + \dfrac{V_o}{V}\right)\left(1 - \left(\dfrac{V_o}{V}\right)^2\right)}{2}$ is the fraction of the upstream wind power, which is captured by the rotor blades and has a theoretical maximum value of 0.59. It is also referred as the *power coefficient of the rotor* or the *rotor efficiency*. In practical designs, the maximum achievable C_p is between 0.4 and 0.5 for high-speed, two-blade turbines and between 0.2 and 0.4 for slow-speed turbines with more blades [2.1].

From (2.6), we see that the power absorption and operating conditions of a turbine are determined by the effective area of the rotor blades, wind speed, and wind flow conditions at the rotor. Thus, the output power of the turbine can be varied by effective area and by changing the flow conditions at the rotor system, which forms the basis of control of WECS.

Tip Speed Ratio

The tip speed ratio λ, defined as the ratio of the linear speed at the tip of the blade to the free stream wind speed and is given by the following expression [2.1-2.4]:

$$TSR = \lambda = \frac{\omega R}{V} \tag{2.7}$$

Where:

R is the rotor blade radius in meters.

ω is the rotor angular speed in rad/sec.

TSR is related to the wind turbine operating point for extracting maximum power. The maximum rotor efficiency C_p is achieved at a particular *TSR*, which is specific to the aerodynamic design of a given turbine. The rotor must turn at high-speed at high wind, and at low-speed at low wind, to keep *TSR* constant at the optimum level at all times. The larger the *TSR*, the faster is the rotation of the wind turbine rotor at a given wind speed. High (rotational) speed turbines are preferred for efficient electricity generation. From

(2.7), for a particular value of wind speed V, turbines with large blade radius R result in low rotational speed ω, and vice versa. For operation over a wide range of wind speeds, wind turbines with high tip speed ratios are preferred [2.3].

Typical Wind Turbine Operating Systems

There are mainly two kinds of wind energy conversion systems in operation; *fixed-speed* or *constant speed wind turbines* which operate at a nearly constant speed, predetermined by the generator design and gearbox ratio, and *variable speed wind turbines*.

The overall operating strategy determines how the various components are controlled. For example, as part of the overall control strategy, the rotor torque can be controlled to maximize energy capture, or pitch angle control can help control the power output at high wind speeds. *Fixed-speed stall-regulated turbines* have no options for control input. In these turbines the turbine blades are designed with fixed pitch to operate near the optimal *TSR* at a specific wind speed. As wind speed increases, so, too does the angle of attack, and an increasingly large part of the blade, starting at the blade root, enters the stall region resulting in the reduced rotor efficiency and limitation of the power output. A variation of the stall regulated concept involves operating the wind turbine at two distinct, constant operating speeds, by either changing the number of poles of the electrical generator or changing the gear ratio. The principal advantage of stall control is its simplicity, but there are significant disadvantages; for instance, the stall regulated wind

turbine will not be able to capture wind energy in an efficient manner at wind speeds other than that it is designed for.

Fixed-speed pitch-regulated turbines typically use pitch regulation for start-up and, and after start-up only to control the power above the rated wind speed of the turbine. Variable speed wind turbines typically use generator torque control for optimization of power output. They use pitch control to control the output power, only above their rated wind speed. With variable speed, there will be 20-30% increase in the energy capture compared to the fixed-speed operation [2.1-2.5].

Typical curves for a constant speed and variable speed wind turbine are as shown in the Figure 2.2 [2.2].

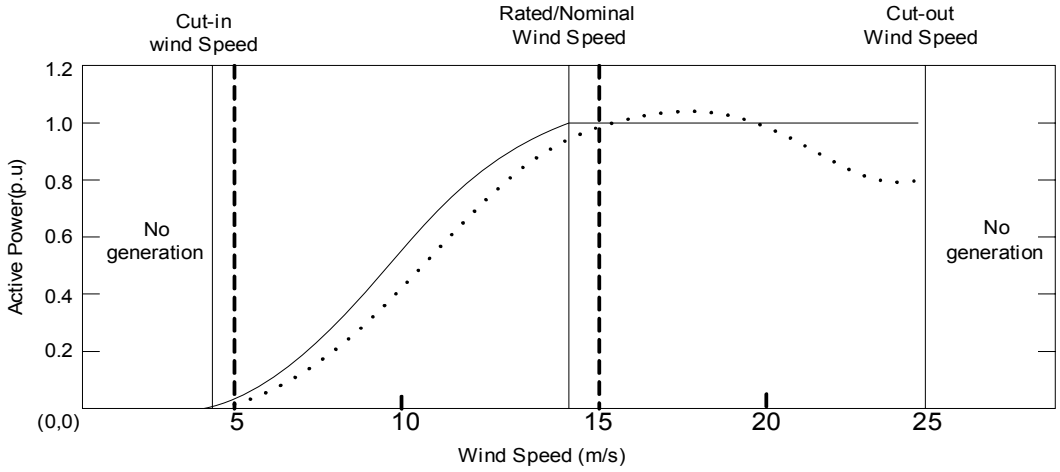

Figure 2.2 Typical curves for a constant speed, stall-controlled (dotted) and variable speed pitch controlled (solid) wind turbine.

In a constant speed, stall-controlled wind turbine the turbine output power peaks somewhat higher than the rated limit, then decreases until the cut-out speed is reached.

This feature provides an element of passive power output regulation, ensuring that the generator is not overloaded as the wind speed reaches above nominal values [2.5]. With variable speed operation although the energy capture is more, the cost of variable speed control is added to the overall system cost. This tradeoff between the energy increase and cost increase has to be optimized in the system design. The advantages and disadvantages of the variable and fixed-speed operations can be summarized in the following table [2.1, 2.2].

Table 2.1 Comparison of Fixed and Variable Speed wind turbine systems.

	Constant Speed	Variable Speed
Advantages	Simple and robust	Less mechanical stress
	Inexpensive electrical system	Higher energy capture
	Electrically efficient	Aerodynamically efficient
	Fewer parts, hence high reliability	Low transient torque
	No frequency conversion, hence, no current harmonics	Mechanical damping system not needed, the electrical system could provide the damping
	Lower capital cost	No synchronization problems. Stiff electrical controls can reduce voltage sags
Disadvantages	Aerodynamically less efficient	Electrically less efficient
	Mechanical stress	Expensive
	Noisy	Sometimes, involves complex control strategies

Variable Speed Wind Turbine System

A typical variable speed pitch-regulated wind turbine is as shown in Figure 2.3. Many parameters that characterize a variable-speed wind turbine are linked [2.6]. For example:

1. The turbine power coefficient curve, the nominal rotor speed, and the rotor diameter determine the nominal wind speed for a wind turbine of a given nominal power

2. The allowable amount of rotor over speeding and the rated power determines the parameters of the pitch controller.

3. The rotor inertia determines the turbine cut-in wind speed.

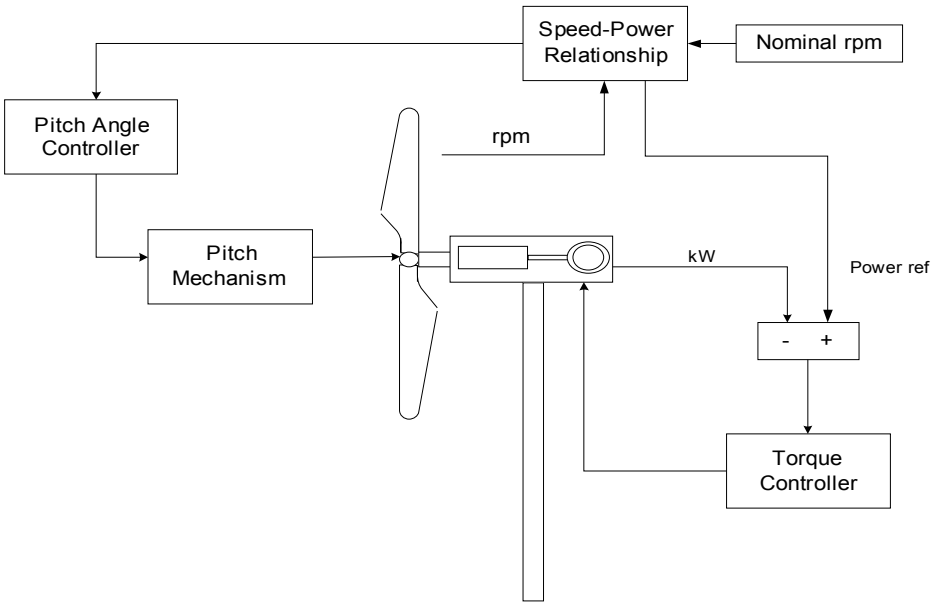

Figure 2.3 Typical pitch-regulated variable-speed wind turbine.

Variable speed pitch-regulated wind turbines have two methods for affecting the turbine operation, namely speed changes and blade pitch changes. In other terms, the control strategies employed in the operation of variable speed wind turbine system are [2.7]:

1. *Power optimization strategy*, employed when the speed is below the rated wind speed, to optimize the energy capture by maintaining the optimum tip speed ratio. This can be achieved by maintaining a constant speed corresponding to the optimum tip speed ratio. If the speed is changed by controlling the electrical load, the generator will be overloaded for wind speeds above nominal value. To avoid such scenario, methods like generator torque control are used to control the speed.

2. *Power limitation strategy,* used above the rated wind speed of the turbine to limit the output power to the rated power by changing the blade pitch to reduce the aerodynamic efficiency, thereby reducing the wind turbine power to acceptable levels.

The regions of the above mentioned control strategies of a variable speed wind turbine system are as shown in the Figure 2.4:

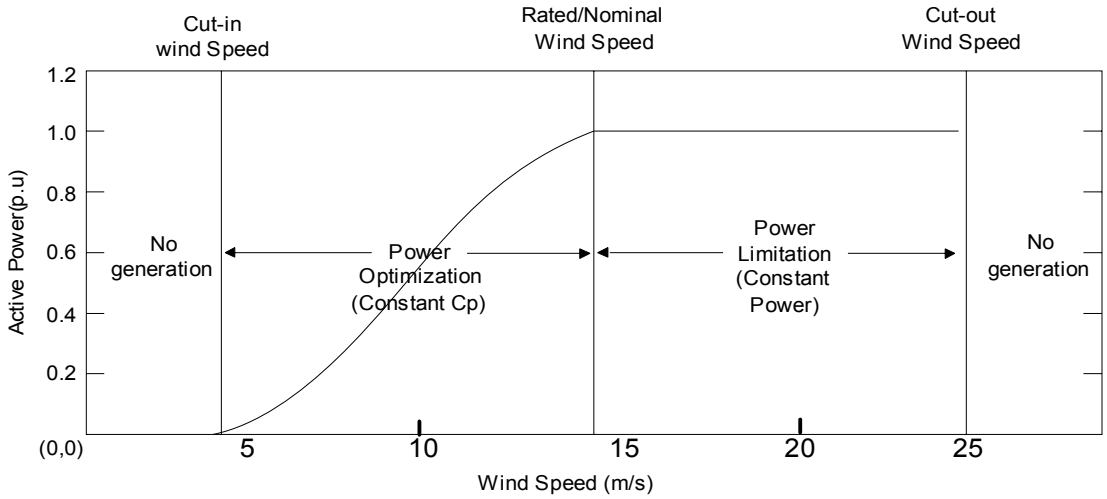

Figure 2.4 Variable Speed pitch controlled wind turbine operation.

Pitch Angle Controller. As mentioned in the previous subsection, pitch controller controls the wind flow around the wind turbine blade, thereby controlling the toque exerted on the turbine shaft. If the wind speed is less than the rated wind speed of the wind turbine, the pitch angle is kept constant at its optimum value. It should be noted that the pitch angle can change at a finite rate, which may be quite low due to the size of the rotor blades. The maximum rate of change of the pitch angle is in the order of 3 to 10 degrees/second. In this controller a slight over-speeding of the rotor above its nominal value can be allowed without causing problems for the wind turbine structure [2.6, 2.8].

The pitch angle controller used in this thesis, employs a PI controller as shown below [2.7, 2.9-2.11]:

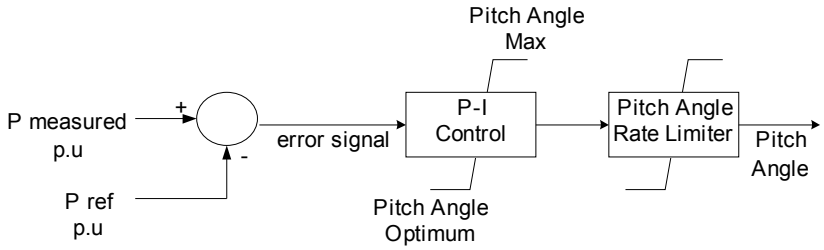

Figure 2.5 Pitch Angle Controller.

As long as the wind turbine output power is lower than the rated power of the wind turbine, the error signal is negative and pitch angle is kept at its optimum value. But once the wind turbine output power exceeds the rated power P_{ref}, the error signal is positive and the pitch angle changes to a new value, at a finite rate, thereby reducing the effective area of the blade resulting in the reduced power output. Inputs to the PI controller are in per-unit and the parameters for the controller are obtained form reference [2.11].

Performance Curves

The performance of variable speed pitch-regulated wind turbines is determined by the characteristic curves relating the power coefficient C_p, tip speed ratio *TSR* and pitch angle θ. Groups of $C_p - \lambda$ curves obtained by measurement or by computation can also be approximated in closed form by non linear functions [2.3], which can be shown as:

$$C_p = C_1(C_2 - C_3\theta - C_4\theta^x - C_5)\, e^{-C_6(\lambda_i)} \tag{2.8}$$

Where:

θ is the pitch angle and λ is the tip speed ratio.

The values chosen for C_1-C_5 and λ_i in this thesis are:

$$\frac{1}{\lambda_i} = \frac{1}{\lambda + 0.08\theta} - \frac{0.035}{\theta^3 + 1}$$

$$C_1 = 0.5 \qquad C_2 = \frac{116}{\lambda_i} \qquad C_3 = 0.4 \qquad C_4 = 0 \qquad C_5 = 5 \qquad C_6 = \frac{21}{\lambda_i}$$

According to the characteristics chosen, the coefficients C_1-C_5 should be modified to obtain a close simulation of the machine in consideration. The differences between the curves of various wind turbines are small and can be neglected in dynamic simulations [2.3]. In [2.6], a comparison was made between the power curves of two commercial wind turbines using the general numerical approximation similar to (2.8).

Simulation Results

In this section, the simulations results of a variable speed pitch controlled wind turbine model are presented. All the simulations were carried out using MATLAB/Simulink. The dynamics of the wind turbine model can be represented with the help of a flow chart, as shown in the Figure 2.6 followed by a brief description of the simulated model.

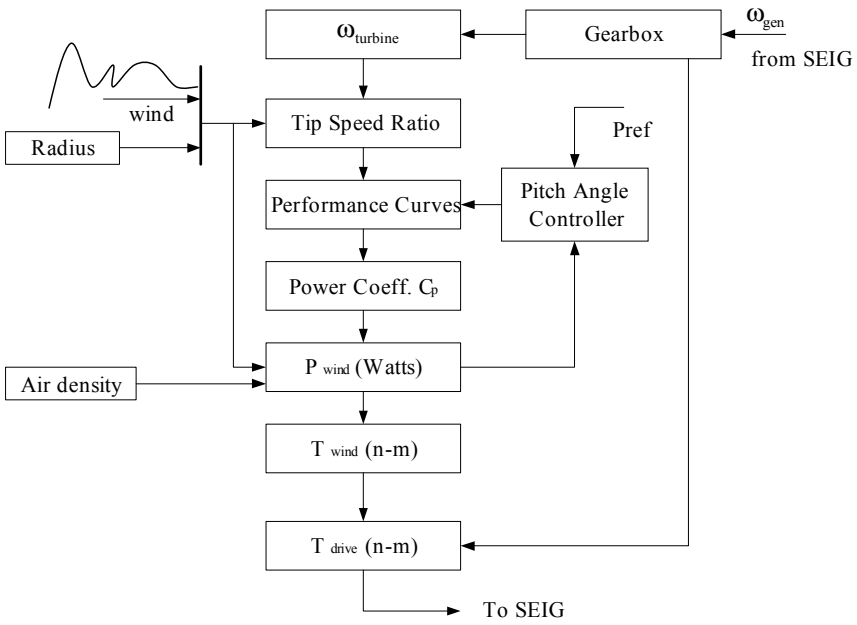

Figure 2.6 Simulation model of the variable speed pitch-regulated wind turbine.

The inputs for the wind turbine model are, wind speed, air density, radius of the wind turbine, mechanical speed of the rotor referred to the wind turbine side and power reference for the pitch angle controller. The output is the drive torque T_{drive} which drives the electrical generator. The wind turbine calculates the tip speed ratio from the input values and estimates the value of power coefficient from the performance curves. The pitch angle controller maintains the value of the blade pitch at optimum value until the power output of the wind turbine exceeds the reference power input.

The performance curves used in this thesis (from (2.8)) are as shown below:

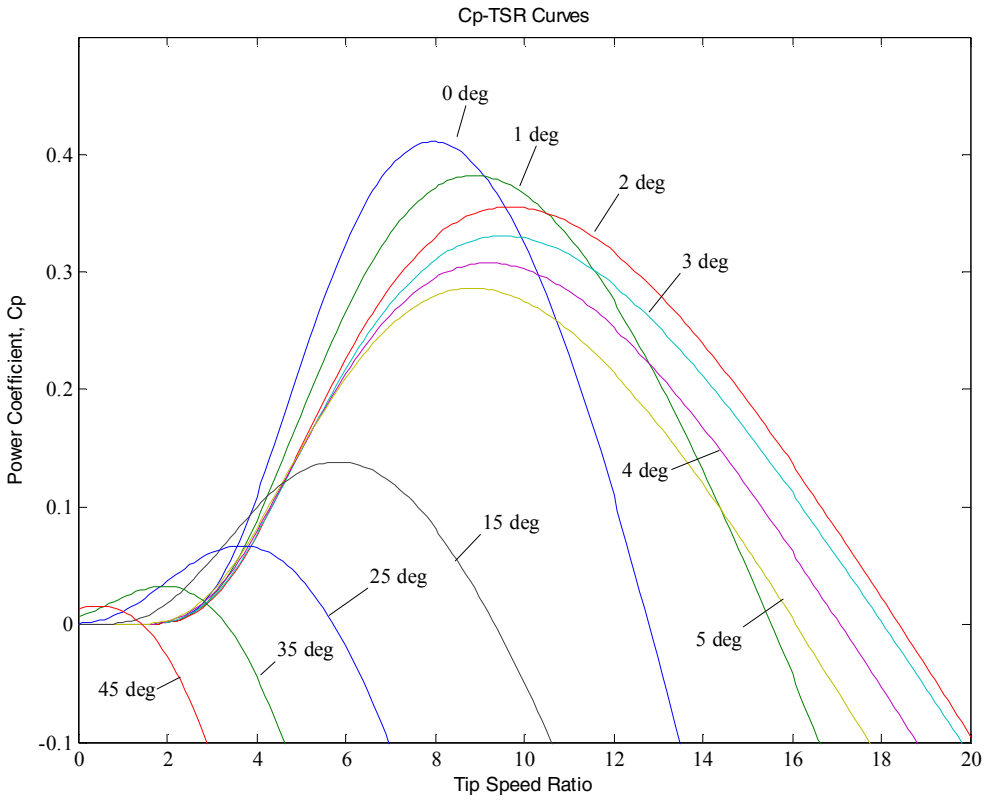

Figure 2.7 $C_p - \lambda$ characteristics (blade pitch angle θ as the parameter).

From the above set of curves (Figure 2.7), we can observe that when pitch angle is equal to 2 degrees, the tip speed ratio has a wide range and a maximum C_p value of 0.35, suitable for wind turbines designed to operate over a wide range of wind speeds. With an increase in the pitch angle, the range of *TSR* and the maximum value of power coefficient decrease considerably.

The parameters used for the simulation are as follows:

Rated power of the wind turbine = 370 kW.

Radius of the wind turbine blade = 20 m.

Gearbox turns ratio = 1:20.

Air density = 1 kg/ m^3.

Figure 2.8 shows the wind turbine output power of the simulated model for different wind velocities. It can be observed that the output power is kept constant at higher wind velocities, even though the wind turbine has the potential to produce more power; this power limit is used and to prevent the over speeding of the rotor and to protect the electrical system.

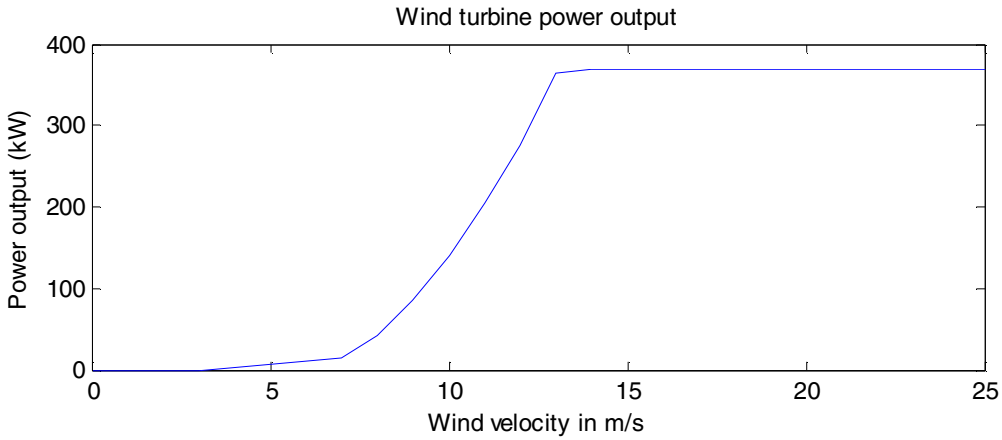

Figure 2.8 Output power of the wind turbine for different wind velocities.

For the following simulation results, the wind turbine starts with an initial wind velocity of 11m/s at no-load, and load was applied on the machine at t=10 seconds. At t=15 seconds there was a step input change in the wind velocity reaching a final value of

14 m/s. In both cases the power reference remained the same (370 kW). The simulation results obtained for the above mentioned conditions are as follows:

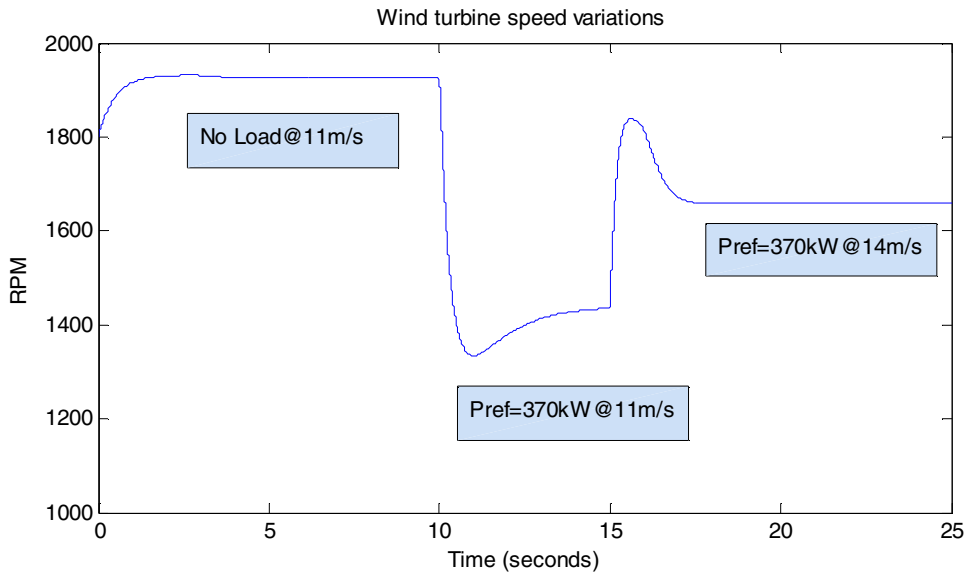

Figure 2.9 Wind turbine rotor speed (referred to generator side) variations with wind.

From Figures 2.9 and 2.10 we can see the changes in the tip speed ratio corresponding to the changes in the rotor speed for different wind and load conditions. During no-load operation, the wind turbine is not connected to the load and therefore rotates freely under the influence of wind attaining high angular velocities. From (2.7), which gives the relation between the tip speed ratio and angular velocity of the wind turbine, it can be concluded that higher angular velocities result in higher tip speed ratios. In this case as *TSR* reaches a value grater than 18, the value of the power coefficient obtained from the set of performance curves is almost zero. As the rotor power coefficient value is zero, the energy captured by the rotor blades is also zero. Therefore, the torque exerted on the generator shaft also equals to zero.

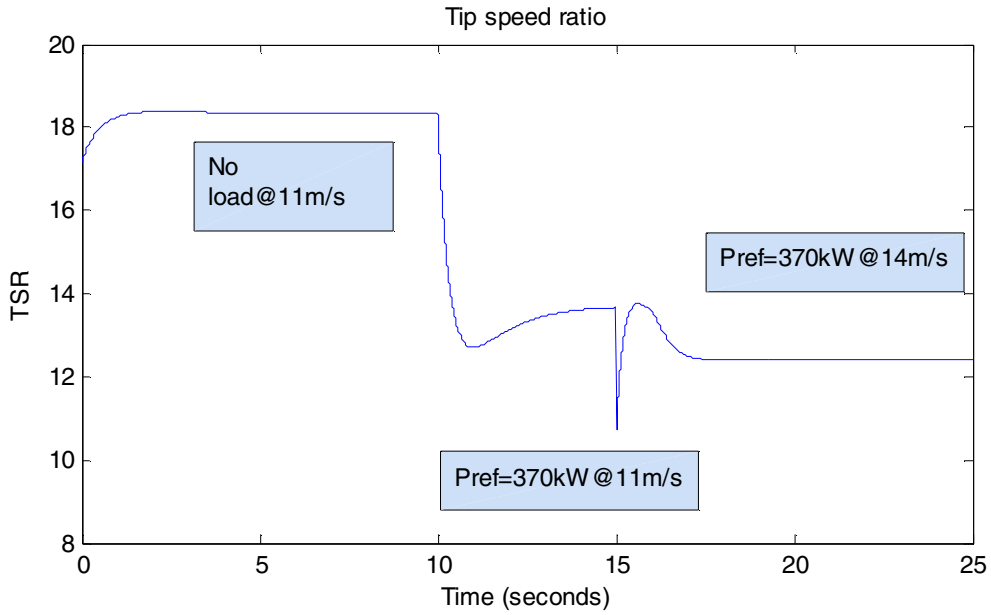

Figure 2.10 Tip speed ratio of the wind turbine.

As load is applied on the wind energy conversion system, the speed of the electrical generator (to be discussed in the next chapter) drops which reduces the speed of the wind turbine (as they are coupled through a gear box, Figure 2.9). This drop in angular speed of the wind turbine reduces the value of *TSR* resulting in a higher value of the power coefficient as can be observed from the power coefficient curves (Figure 2.7). Since rotor power coefficient is now a positive, non-zero, the rotor blades extract energy form the wind resulting in some output power.

Figure 2.11 shows the changes in the power coefficient with changes in the tip speed ratio. From Figure 2.7 it can be seen that, on the right hand side (after reaching the peak value) of the C_p Vs λ curves, with increase in the value of *TSR* the value of C_p decreases. Figure 2.11 shows that lower wind velocities (higher *TSR*, see (2.7)) result in high power

coefficient, and higher wind velocities (lower *TSR*) result in lower power coefficient values, so that the wind turbine output does not exceed its rated power.

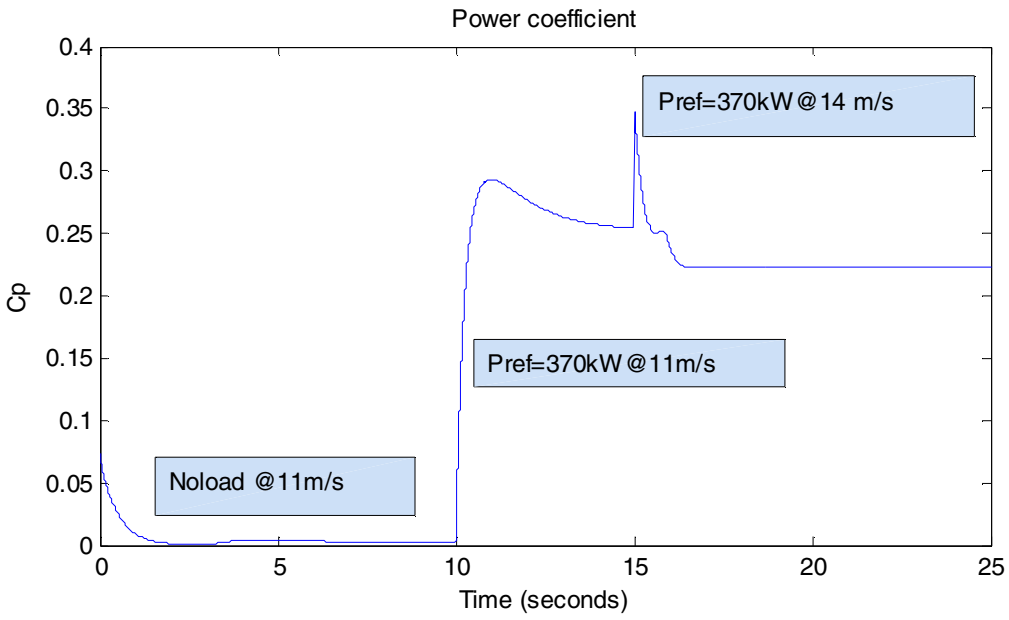

Figure 2.11 Variation of power coefficient with wind.

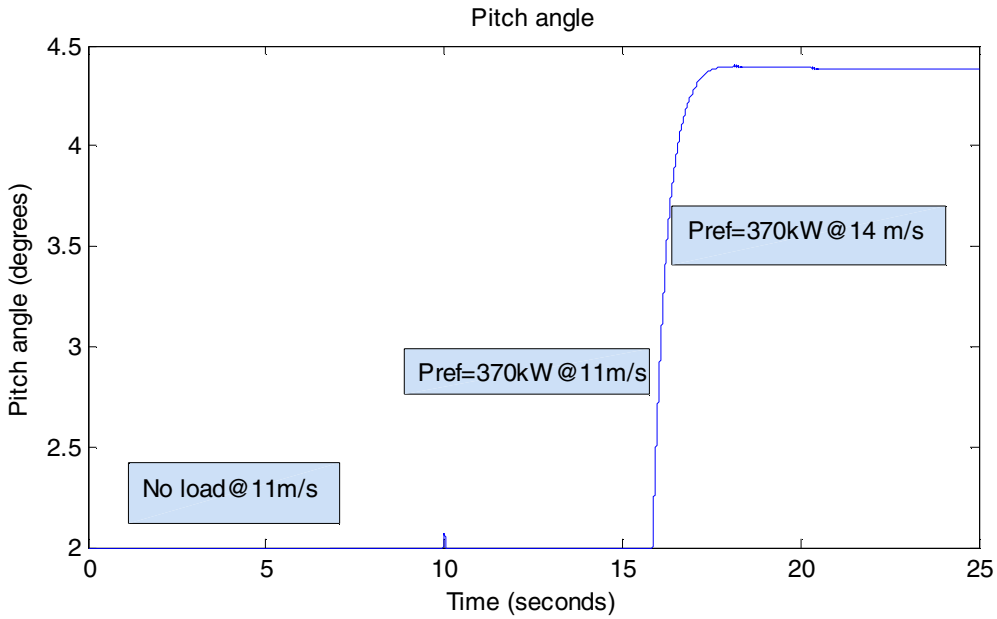

Figure 2.12 Pitch angle controller response to the wind speed change.

Observe that the pitch angle is kept constant by the pitch controller at an optimal value of 2 degrees (Figure 2.12) until the wind turbine reaches above the nominal wind speed (13.5 m/s), where it has the capability to produce more power than the rated power of the system. In this region pitch control alters the pitch of the blade, at a finite rate, thereby changing the airflow around the blades resulting in the reduced efficiency of wind turbine rotor. Also, from Figure 2.7 we see that with increase in the pitch angle the range of *TSR* which produces a positive value for rotor power coefficient reduces sharply.

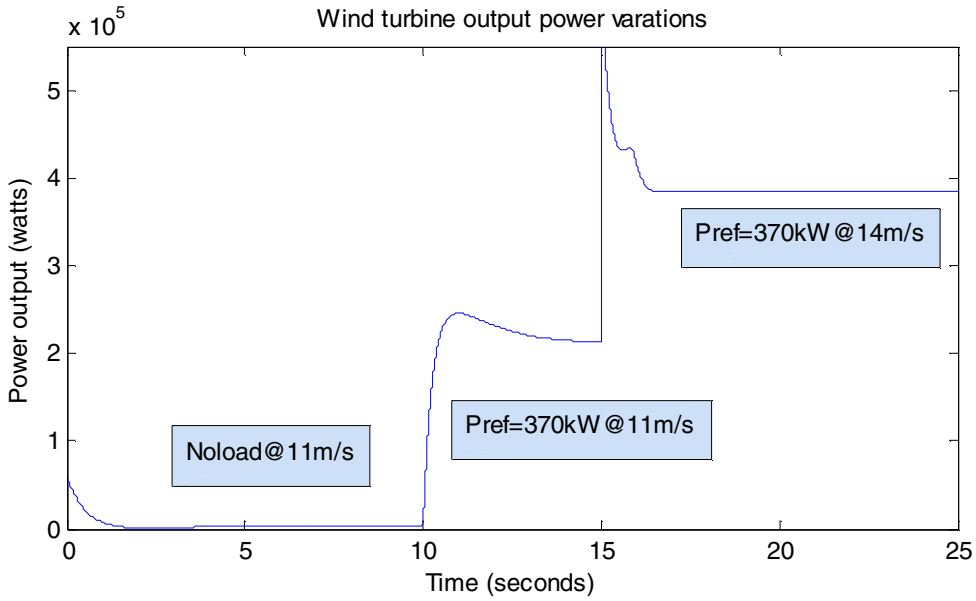

Figure 2.13 Wind turbine output power variation with change in wind speed.

From Figures 2.12 and 2.13 we see that the output of the wind turbine is about 220 kW at 11 m/s and has the ability to supply more than rated power of 370 kW at 14 m/s. As explained above, the wind turbine output power is limited to the rated power by the pitch controller.

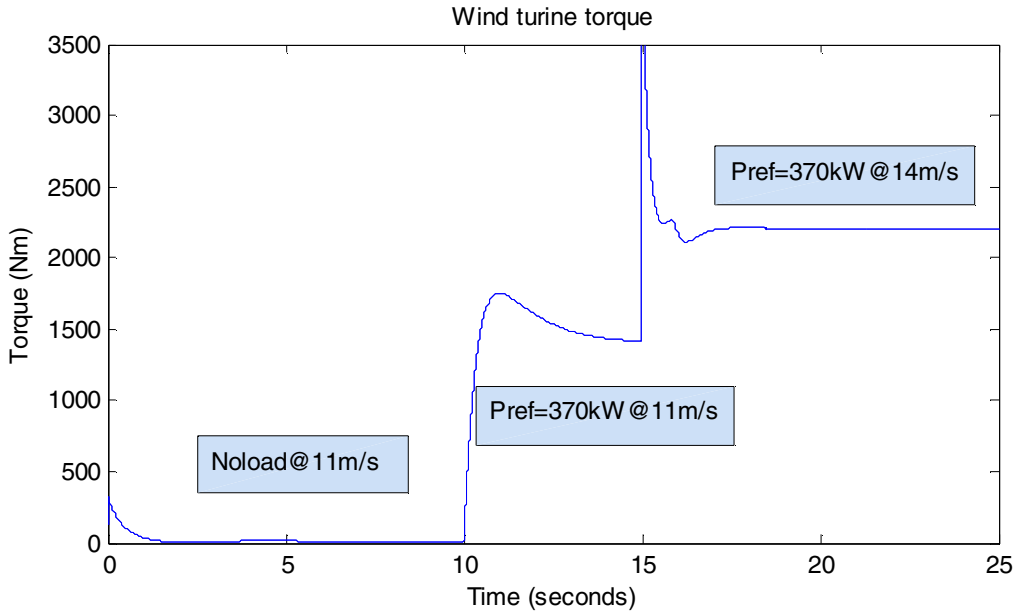

Figure 2.14 Wind turbine torque variation with wind.

The driving torque produced by the wind turbine as observed in Figure 2.14, varies based on the input (wind) and load conditions. When the system is not loaded the driving torque produced the wind turbine is zero, since the energy captured by the rotor is zero. When load is applied at t=10 seconds, we can see a rise in the value of the torque produced by the wind turbine. With a step increase in wind velocity (to 14 m/s), the torque increases from its previous value, and delivers a higher toque to the electrical generator. Torque seen here is obtained by dividing the power extracted from the wind by the angular velocity of the rotor and then referring it on to the generator side.

Conclusion. In this chapter a variable speed wind energy conversion system has been presented. Emphasis has been laid on the wind turbine part of the total system. A comparison was made between the two typical existing wind turbine systems after a brief introduction of each system. A variable speed wind turbine model was simulated based

on the power coefficient curves. The response of the simulated model was observed with dynamic load and changing wind conditions. It was observed with the help of the simulation results, that the power limitation strategy can be successfully enforced by using a pitch controller. This chapter also sets the ground for the next chapter, where a detailed analysis of the electrical generator part of the wind energy conversion system is carried out.

REFERENCES

2.1 Mukund. R. Patel, *Wind Power Systems*, CRC Press, 1999, ch. 4-6.

2.2 J.G. Slootweg, "Wind power: modeling and impact on power system dynamics," PhD dissertation, Dept. Elect. Eng., Delft University of Technology, Delft, Netherlands, 2003.

2.3 Siegfried Heier, *Grid Integration of Wind energy Conversion Systems*, John Wiley& Sons, 1998, ch. 1-2.

2.4 J.F. Manwell, J.G. McGowan and A.L. Rogers, *Wind energy Explained – Theory, Design and Application*, John Wiley& Sons, 2002, ch. 7.

2.5 Tony Burton, David sharpe, Nick Jenkins and Ervin Bossanyi, *Wind Energy Handbook*, John Wiley& Sons, 2001, ch. 4.

2.6 J. G. Slootweg, S.W.H. de Haan, H. Polinder and W.L. Kling, "General model for representing variable speed wind turbines in power system dynamics simulations," *IEEE Transactions on Power Systems*, vol. 18, no. 1, pp. 144-151 , Feb. 2003.

2.7 Anca D.Hansen, Florin Iov, Poul Sorensen, and Frede Blaabjerg, "Overall control strategy of variable speed doubly-fed induction generator wind turbine," in *2004 Nordic Wind Power Conference*, Chalmers University of Technology, Sweden.

2.8 Eduard Muljadi and C. P. Butterfield., "Pitch-controlled variable-speed wind turbine generation," *IEEE Transactions on Industry Applications* , vol. 37, no. 1, pp. 240-246, Jan/Feb 2001

2.9 P.M.Anderson and Anjan Bose., " Stability simulation of wind turbine systems," *IEEE Trans. on Power and Apparatus and Systems*, vol. PAS-102, no. 12, pp. 3791-3795, Dec. 1983.

2.10 O. Wasynczuk, D.T. Man and J. P. Sullivan, "Dynamic Behavior of a class of wind turbine generators during random wind fluctuations," *IEEE Transactions on Power and Apparatus and Systems*, vol. PAS-100, no. 6, pp. 2837-2845, June 1981.

2.11 MATLAB/Simulink Documentation. Available: http://www.mathworks.com

CHAPTER 3

WIND ENERGY CONVERSION SYSTEM - SELF-EXCITED INDUCTION GENERATOR (SEIG) MODELING

Introduction

Induction machine is used in a wide variety of applications as a means of converting electric power to mechanical work. The primary advantage of the induction machine is its rugged brushless construction and no need for separate DC field power. These machines are very economical, reliable, and are available in the ranges of fractional horse power (FHP) to multi –megawatt capacity. Also, unlike synchronous machines, induction machines can be operated at variable speeds. For economy and reliability many wind power systems use induction machines, driven by a wind turbine through a gear box, as an electrical generator. The need for gearbox arises from the fact that lower rotational speeds on the wind turbine side should be converted to high rotor speeds, on the electrical generator side, for electrical energy production.

There are two types of induction machine based on the rotor construction namely, squirrel cage type and wound rotor type. Squirrel cage rotor construction is popular because of its ruggedness, lower cost and simplicity of construction and is widely used in stand-alone wind power generation schemes. Wound rotor machine can produce high starting torque and is the preferred choice in grid-connected wind generation scheme.

Another advantage with wound rotor is its ability to extract rotor power at the added cost of power electronics in the rotor circuit.

This chapter focuses on the electrical generation part of a wind energy conversion system. After a brief introduction of the induction machine, the electrical generator used in this thesis, a detailed analysis of the induction machine operated in stand-alone mode is presented. As a generator, induction machines have the drawback of requiring reactive power for excitation. This necessitates the use of shunt capacitors in the circuit. The effect of magnetization inductance on self-excitation of the induction generator is discussed. Also, this chapter presents the two existing methods to analyze the process of self-excitation in induction machine and the role of excitation-capacitors in its initiation.

Simulation results of the self-excited induction generator driven by the variable speed wind turbine are presented in the last section of this chapter. The process of voltage build up and the effect of saturation characteristics are also explained in the same section.

Induction Machine

In the electromagnetic structure of the Induction machine, the stator is made of numerous coils with three groups (phases), and is supplied with three phase current. The three coils are physically spread around the stator periphery (space-phase), and carry currents which are out of time-phase. This combination produces a rotating magnetic field, which is a key feature of the working of the induction machine. Induction machines are asynchronous speed machines, operating below synchronous speed when motoring

and above synchronous speed when generating. The presence of negative resistance (i.e., when slip is negative), implies that during the generating mode, power flows from the rotor to the stator in the induction machine.

Equivalent Electrical Circuit of Induction Machine

The theory of operation of induction machine is represented by the per phase equivalent circuit shown in Figure. 3.1 [3.1-3.3].

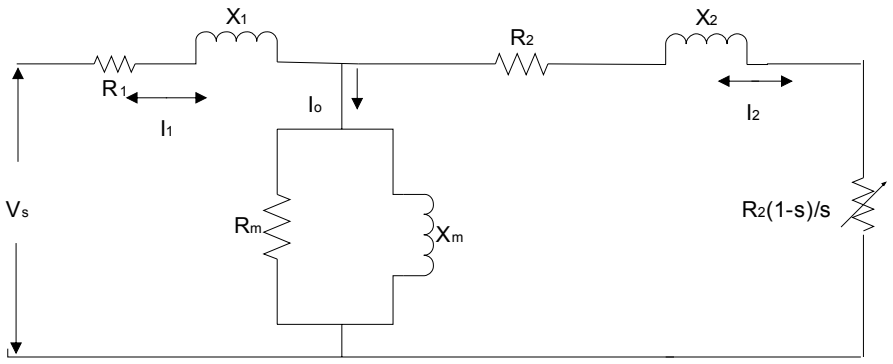

Figure 3.1 Per-phase equivalent circuit of the induction machine referred to the stator.

In the above figure, *R* and *X* refer to the resistance and inductive reactance respectively. Subscripts 1, 2 and *m* represent stator, rotor values referred to the stator side and magnetizing components, respectively.

Induction machine needs AC excitation current for its running. The machine is either self-excited or externally excited. Since the excitation current is mainly reactive, a stand-alone system is self-excited by shunt capacitors. In grid-connected operation, it draws excitation power from the network, and its output frequency and voltage values are

dictated by the grid. Where the grid capacity of supplying the reactive power is limited, local capacitors can be used to partly supply the needed reactive power [3.3].

Self-Excited Induction Generator (SEIG)

Self-excited induction generator (SEIG) works just like an induction machine in the saturation region except the fact that it has excitation capacitors connected across its stator terminals. These machines are ideal choice for electricity generation in stand-alone variable speed wind energy systems, where reactive power from the grid is not available. The induction generator will self-excite, using the external capacitor, only if the rotor has an adequate remnant magnetic field. In the self-excited mode, the generator output frequency and voltage are affected by the speed, the load, and the capacitance value in farads [3.3]. The steady-state per-phase equivalent circuit of a self-excited induction generator is shown in the Figure 3.2.

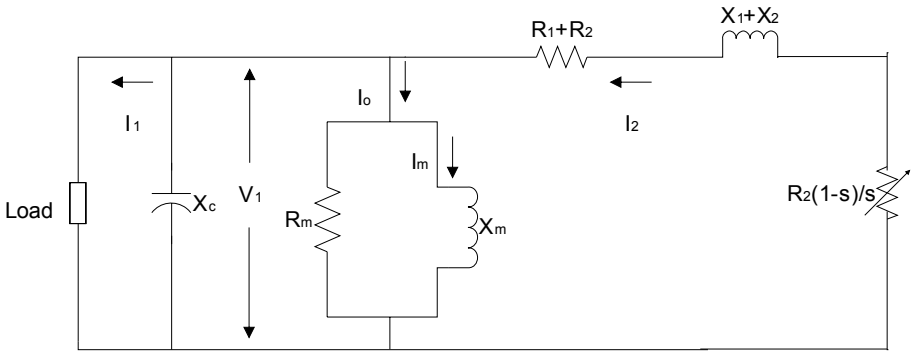

Figure 3.2 Self-excited induction generator with external capacitor.

The process of self-excitation in induction machines has been known for many decades [3.4]. When capacitors are connected across the stator terminals of an induction

machine, driven by an external prime mover, voltage will be induced at its terminals. The induced electromotive force (EMF) and current in the stator windings will continue to rise until the steady-state condition is reached, influenced by the magnetic saturation of the machine. At this operating point the voltage and the current will be stabilized at a given peak value and frequency. In order for the self-excitation to occur, for a particular capacitance value there is a corresponding minimum speed [3.5]-[3.8]. So, in stand-alone mode of operation, it is necessary for the induction generator to be operated in the saturation region. This guarantees one and only one intersection between the magnetization curve and the capacitor reactance line, as well as output voltage stability under load as seen in the Figure 3.3:

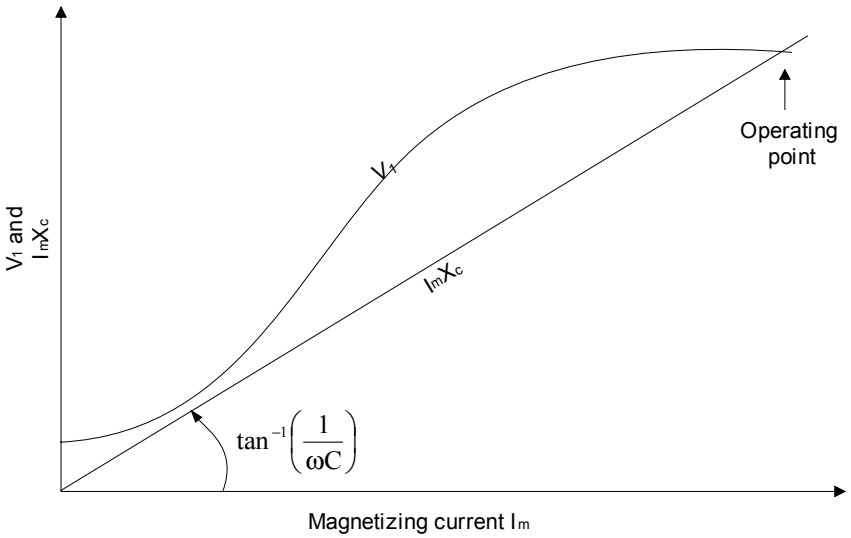

Figure 3.3 Determination of stable operation of self-excited induction generator.

At no-load, the capacitor current $I_c = V_1/X_c$ must be equal to the magnetizing current $I_m = V_1/X_m$. The voltage V_1 is a function of I_m, linearly rising until the saturation

point of the magnetic core is reached. The output frequency of the self-excited generator is, $f = 1/(2\pi CX_m)$ and $\omega = 2\pi f$ where C is self-exciting capacitance.

Methods of Analysis

There are two fundamental circuit models employed for examining the characteristics of a SEIG. One is the per-phase equivalent circuit which includes the loop-impedance method adopted by Murthy *et al* [3.9] and Malik and Al-Bahrani [3.10], and the nodal admittance method proposed by Ouazene and Mcpherson[3.11] and Chan [3.12]. This method is suitable for studying the machine's steady-state characteristics. The other method is the *dq*-axis model based on the generalized machine theory proposed by Elder *et al* [3.6] and Grantham *et al* [3.7], and is employed to analyze the machine's transient state as well as steady-state.

Steady-state Model

Steady-state analysis of induction generators is of interest both from the design and operational points of view. By knowing the parameters of the machine, it is possible to determine the performance of the machine at a given speed, capacitance and load conditions.

Loop impedance and nodal admittance methods used for the analysis of SEIG are both based on per-phase steady-state equivalent circuit of the induction machine (Figure 3.4), modified for the self-excitation case. They make use of the principle of conservation

of active and reactive powers, by writing loop equations [3.9], [3.10], [3.13] or nodal equations [3.11], [3.12], for the equivalent circuit. These methods are very effective in calculating the minimum value of capacitance needed for guaranteeing self-excitation of the induction generator. For stable operation, *excitation capacitance* must be slightly higher than the minimum value. Also there is a speed threshold, below which no excitation is possible, called as the cutoff speed of the machine. In the following paragraph, of loop impedance method is given for better understanding.

The per-unit per-phase steady-state circuit of a self-excited induction generator under RL load is shown in Figure 3.4 [3.9], [3.11].

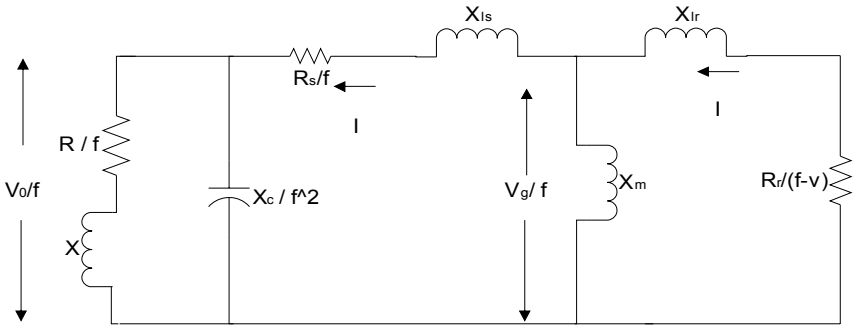

Figure 3.4 Equivalent circuit of self-excited induction generator with R-L Load.

Where:

R_s, R_r, R : p.u. per-phase stator, rotor (referred to stator) and load resistance respectively.

X_{ls}, X_{lr}, X, X_m : p.u. per-phase stator leakage, rotor leakage (referred to stator), load and magnetizing reactances (at base frequency), respectively.

X_{smax} : p.u. maximum saturated magnetizing reactance.

C : per-phase terminal-excitation capacitance.

X_c : p.u. per-phase capacitive reactance (at base frequency) of the terminal excitation capacitor.

f, v : p.u.frequency and speed, respectively.

N : base speed in rev/min

Z_b : per-phase base impedance

f_b : base frequency

V_g, V_0 : per-phase air gap and output voltages, respectively.

In the analysis of SEIG the following assumptions were made [3.9]:

1. Only the magnetizing reactance X_m is assumed to be affected by magnetic saturation, and all other parameters of the equivalent circuit are assumed to be constant. Self-excitation results in the saturation of the main flux and the value of X_m reflect the magnitude of the main flux. Leakage flux passes mainly in the air, and thus these fluxes are not affected to any large extent by the saturation of the main flux.

2. Stator and rotor leakage reactances, in per-unit are taken to be equal. This assumption is normally valid in induction machine analysis.

3. Core loss in the machine is neglected.

For the circuit shown in Figure 3.4, the loop equation for the current can be written as:

$$I\,Z = 0 \tag{3.1}$$

where Z is the net loop impedance given by

$$Z = \left(\left(\frac{R_r}{f - v} \right) + jX_{lr} \,\|\, jX_m \right) + \frac{R_s}{f} + jX_{ls} + \left(\frac{-jX_c}{f^2} \,\Big\|\, \left(\frac{R}{f} + jX \right) \right) \tag{3.2}$$

Since at steady-state excitation $I \neq 0$, it follows from (3.1) that $Z = 0$, which implies that both the real and imaginary parts of Z are zeros. These two equations can be solved simultaneously for any two unknowns (usually voltage and frequency). For successful voltage-buildup, the load-capacitance combination and the rotor speed should result in a value such that X_m=X_{smax}, which yields the minimum value of excitation capacitance below which the SEIG fails to self-excite.

Steady-state and Transient Model (*abc-dq0* transformation)

The process of self-excitation is a transient phenomenon and is better understood if analyzed using a transient model. To arrive at transient model of an induction generator, *abc-dq0* transformation is used.

abc-dq0 Transformation. The *abc-dq0* transformation transfers an *abc* (in any reference frame) system to a rotating *dq0* system. Krause *et al.*[3.1] noted that, all time varying inductances can be eliminated by referring the stator and rotor variables to a frame of reference rotating at any angular velocity or remaining stationary. All transformations are then obtained by assigning the appropriate speed of rotation to this (*arbitrary*) *reference frame*. Also, if the system is balanced the zero component will be equal to zero [3.1].

A change of variables which formulates a transformation of the 3-phase variables of stationary circuit elements to the arbitrary reference frame may be expressed as [3.1]:

$$f_{qdos} = K_s f_{abcs} \tag{3.3}$$

Where:

$$f_{qd0s} = \begin{bmatrix} f_{qs} \\ f_{ds} \\ f_{0s} \end{bmatrix}; f_{abcs} = \begin{bmatrix} f_{as} \\ f_{bs} \\ f_{cs} \end{bmatrix}; K_s = \frac{2}{3} \begin{bmatrix} \cos\theta & \cos\left(\theta - \frac{2\pi}{3}\right) & \cos\left(\theta + \frac{2\pi}{3}\right) \\ \sin\theta & \sin\left(\theta - \frac{2\pi}{3}\right) & \sin\left(\theta + \frac{2\pi}{3}\right) \\ \frac{1}{2} & \frac{1}{2} & \frac{1}{2} \end{bmatrix}; \theta = \int_0^t \omega(\xi) d\xi + \theta(0);$$

ξ is the dummy variable of integration.

For the inverses transformation:

$$(K_s)^{-1} = \begin{bmatrix} \cos\theta & \sin\theta & 1 \\ \cos\left(\theta - \frac{2\pi}{3}\right) & \sin\left(\theta - \frac{2\pi}{3}\right) & 1 \\ \cos\left(\theta + \frac{2\pi}{3}\right) & \sin\left(\theta + \frac{2\pi}{3}\right) & 1 \end{bmatrix}$$

In (3.3), f can represent voltage, current, flux linkage, or electric charge. The subscript s indicates the variables, parameters and transformation associated with stationary circuits. This above transformation could also be used to transform the time-varying rotor windings of the induction machine. It is convenient to visualize the transformation equations as trigonometric relationships between variables as shown in Figure 3.5.

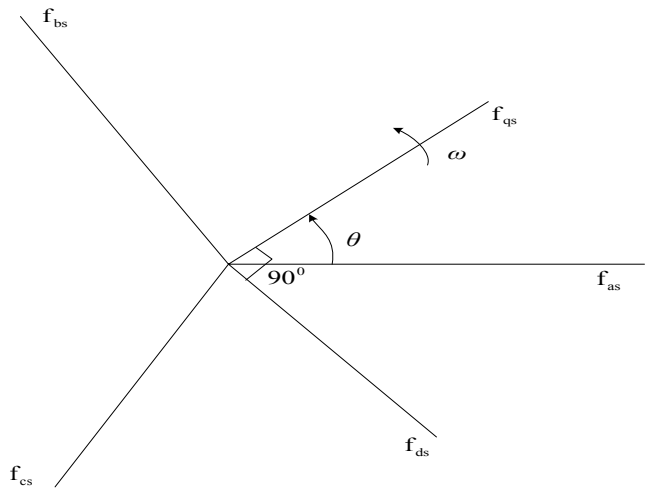

Figure 3.5 Transformation for stationary circuits portrayed by trigonometric relationships.

The equations of transformation may be thought of as if the f_{qs} and f_{ds} variables are directed along axes orthogonal to each other and rotating at an angular velocity of ω, whereupon f_{as}, f_{bs}, and f_{cs} (instantaneous quantities which may be any function of time), considered as variables directed along stationary paths each displaced by 120^0. Although the waveforms of the *qs* and *ds* voltages, currents and flux linkages, and electric charges are dependent upon the angular velocity of the frame of reference, the waveform of the total power is same regardless of the reference frame in which it is evaluated [3.1].

Voltage Equations in Arbitrary Reference-Frame Variables. The winding arrangement for a 2-pole, 3-phase, wye-connected, symmetrical induction machine is shown in Figure 3.6.

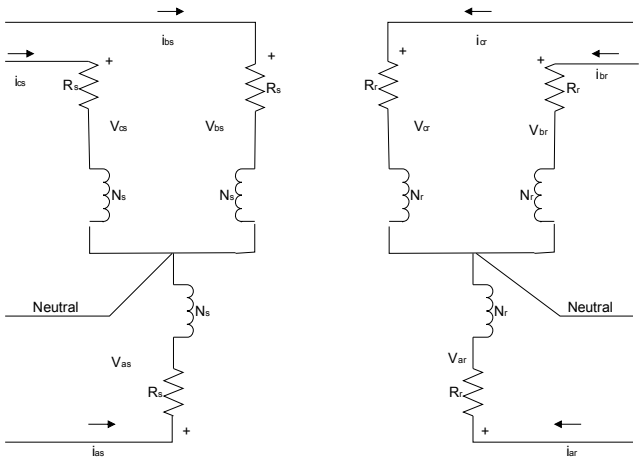

Figure 3. 6 Two-pole, 3-phase, wye connected symmetrical induction machine

The stator windings are identical sinusoidally distributed windings, displaced 120^0, with N_s equivalent turns and resistance r_s. The rotor is consists of three identical

sinusoidally distributed windings, with N_r equivalent turns and resistance r_r. Note that positive *a*, *b*, *c* sequence is used in both in Figures 3.5 and 3.6.

The voltage equations in machine variables can be expressed as [3.1]:

$$V_{abcs} = r_s i_{abcs} + p\lambda_{abcs} \tag{3.4}$$

$$V_{abcr} = r_r i_{abcr} + p\lambda_{abcr} \tag{3.5}$$

Where:

Subscript *s* denotes parameters and variables associated with the stator.

Subscript *r* denotes parameters and variables associated with the rotor.

V_{abcs}, V_{abcr} are phase voltages.

I_{abcs}, I_{abcr} are phase currents.

λ_{abcs}, λ_{abcr} are the flux linkages and $p = d/dt$.

By using the *abc-dq0* transformation and expressing flux linkages as product of currents and winding inductances, we obtain the following expressions for voltage in arbitrary reference frame [3.1]:

$$V_{qdos} = r_s i_{qdos} + \omega\lambda_{dqs} + p\lambda_{qdos} \tag{3.6}$$

$$V'_{qdor} = r'_r i'_{qdor} + (\omega - \omega_r)\lambda'_{dqr} + p\lambda'_{qdor} \tag{3.7}$$

Where:

ω is the electrical angular velocity of the arbitrary reference frame.

ω_r is the electrical angular velocity of the rotor.

$(\lambda_{dqs})^T = [\lambda_{ds} \quad -\lambda_{qs} \quad 0]$; $(\lambda'_{dqr})^T = [\lambda'_{dr} \quad -\lambda'_{qr} \quad 0]$.

"′" denotes rotor values referred to the stator side.

Using the relations between the flux linkages and currents in the arbitrary reference frame and substituting them in (3.6) & (3.7), the voltage and flux equations are expressed as follows:

$$V_{qs} = r_s i_{qs} + \omega\lambda_{ds} + p\lambda_{qs} \tag{3.8}$$

$$V_{ds} = r_s i_{ds} - \omega\lambda_{qs} + p\lambda_{ds} \tag{3.9}$$

$$V'_{qr} = r'_r i'_{qr} + (\omega - \omega_r)\lambda'_{dr} + p\lambda'_{qr} \tag{3.10}$$

$$V'_{dr} = r'_r i'_{dr} - (\omega - \omega_r)\lambda'_{qr} + p\lambda'_{dr} \tag{3.11}$$

$$\lambda_{qs} = L_{ls} i_{qs} + L_m (i_{qs} + i'_{qr}) \tag{3.12}$$

$$\lambda_{ds} = L_{ls} i_{ds} + L_m (i_{ds} + i'_{dr}) \tag{3.13}$$

$$\lambda'_{qr} = L'_{lr} i'_{qr} + L_m (i_{qs} + i'_{qr}) \tag{3.14}$$

$$\lambda'_{dr} = L'_{lr} i'_{dr} + L_m (i_{ds} + i'_{dr}) \tag{3.15}$$

Where:

L_{ls} and L_{ms} are leakage and magnetizing inductances of the stator respectively.

L_{lr} and L_{mr} are leakage and magnetizing inductances of the rotor respectively.

Magnetizing inductance, $L_m = \frac{3}{2} L_{ms}$

The voltage and flux linkage equations suggest the following equivalent circuits for the induction machine:

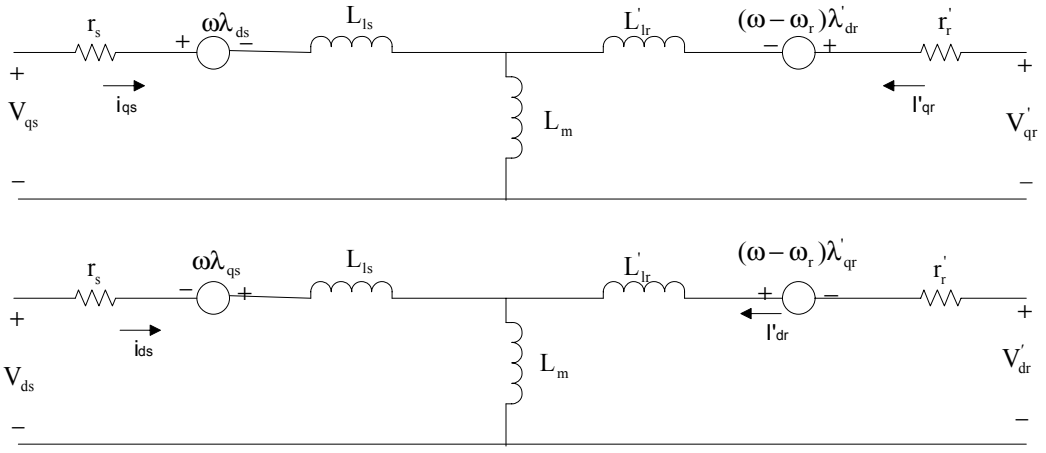

Figure 3.7 Arbitrary reference-frame equivalent circuits for a 3-phase, symmetrical induction machine.

Torque Equations. The expression for electromagnetic torque, positive for motor operation and negative for generator operation, in terms of the arbitrary reference variables can be expressed as [3.1]:

For motor action, $T_e = \left(\frac{3}{2}\right)\left(\frac{P}{2}\right) L_m (i_{qs} i'_{dr} - i_{ds} i'_{qr})$ (3.16)

For generator action, $T_e = \left(\frac{3}{2}\right)\left(\frac{P}{2}\right) L_m (i_{ds} i'_{qr} - i_{qs} i'_{dr})$ (3.17)

The torque and speed are related by the following expressions:

For the motor operation, $T_{e-motor} = J\left(\frac{2}{P}\right) p\omega_r + T_D$ (3.18)

For the generator operation, $T_D = J\left(\frac{2}{P}\right) p\omega_r + T_{e-gen}$ (3.19)

Where:

P: Number of poles.

J: Inertia of the rotor in (Kg m^2).

T_D : Drive torque in (Nm).

Stationary Reference Frame. Although the behavior of the induction machine may be described by any frame of reference, there are three which are commonly used [3.1]. The voltage equations for each of these reference frames can be obtained from the voltage equations in the arbitrary reference frame by assigning the appropriate speed to ω. That

is, for the stationary reference frame, $\omega = 0$, for the rotor reference frame, $\omega = \omega_r$ and for the synchronous reference frame, $\omega = \omega_e$.

Generally, the conditions of operation will determine the most convenient reference frame for analysis and/or simulation purposes. The stator reference frame is used when the stator voltages are unbalanced or discontinuous and the rotor applied voltages are balanced or zero. The rotor reference frame is used when the rotor voltages are unbalanced or discontinuous and the stator applied voltages are balanced. The stationary frame is used when all (stator and rotor) voltages are balanced and continuous. In this thesis, the *stationary reference frame* $(\omega = 0)$ is used for simulating the model of the self-excited induction generator (SEIG).

In all asynchronously rotating reference frames $(\omega \neq \omega_e)$ with $\theta(0) = 0$ (see (3.3)), the phasor representing phase *a* variables (with subscript *as*) is equal to phasor representing *qs* variables. In other terms, for the rotor reference frame and the stationary reference frame, $f_{as} = f_{qs}$, $f_{bs} = f_{as} \angle 120^0$ and $f_{cs} = f_{as} \angle 240^0$ [3.1].

SEIG Model. As discussed above, the *dq* model of the SEIG in the stationary reference frame is obtained by substituting $\omega = 0$ in the arbitrary reference frame equivalent of the induction machine shown in Figure 3.7. Figure 3.8 shows a complete *dq*-axis model, of the SEIG with load, in the stationary reference frame. Capacitor *C* is connected at the stator terminals for the self-excitation. For convenience, all values are

assumed to be referred to the stator side and here after "′" is neglected while expressing rotor parameters referred to the stator [3.14].

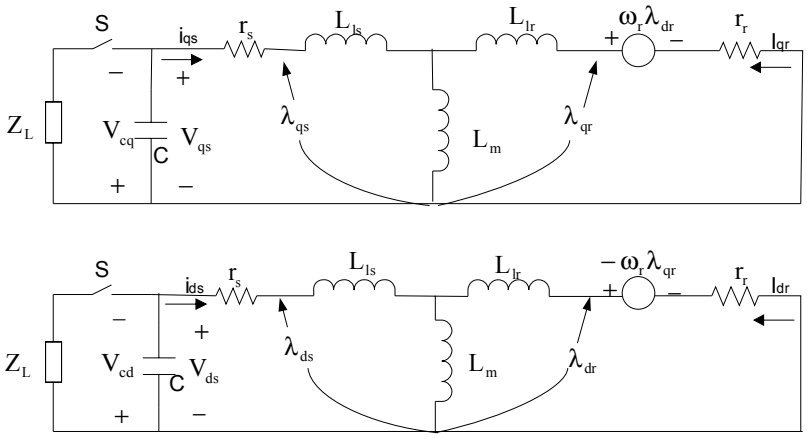

Figure 3.8 *dq* model of SEIG in stationary reference frame (All values referred to stator).

For no-load condition, rearranging the terms after writing loop equations for Figure 3.8, we obtain the following voltage equations expressed in the form of a matrix [3.1, 3.14]:

$$\begin{bmatrix} 0 \\ 0 \\ 0 \\ 0 \end{bmatrix} = \begin{bmatrix} r_s + pL_s + 1/pC & 0 & pL_m & 0 \\ 0 & r_s + pL_s + 1/pC & 0 & pL_m \\ pL_m & -\omega_r L_m & r_r + pL_r & -\omega_r L_r \\ \omega_r L_m & pL_m & \omega_r L_r & r_r + pL_r \end{bmatrix} \begin{bmatrix} i_{qs} \\ i_{ds} \\ i_{qr} \\ i_{dr} \end{bmatrix} + \begin{bmatrix} V_{cqo} \\ V_{cdo} \\ K_q \\ K_d \end{bmatrix} \quad (3.20)$$

Where:

K_d and K_q are constants representing initial induced voltages along the *d*-axis and *q*-axis respectively, due to the remaining magnetic flux in the core.

V_{cqo} and V_{cdo} are initial voltages in the capacitors.

$L_s = L_{ls} + L_m$ and $L_r = L_{lr} + L_m$.

The above equations can further be simplified in the following manner using (3.8)-(3.15):

In the stationary reference frame (3.8) can be written as,

$$V_{qs} = -V_{cq} = r_s i_{qs} + 0 \times \lambda_{ds} + p\lambda_{qs} \tag{3.21}$$

Substituting (3.12) in (3.21), will result

$$0 = V_{cq} + r_s i_{qs} + L_s p i_{qs} + L_m p i_{qr} \tag{3.22}$$

Solving for pi_{qr} by substituting (3.14) and (3.15) in (3.10) yields:

$$pi_{qr} = \frac{1}{L_{lr}}(V_{qr} - r_r i_{qr} + \omega_r L_r i_{dr} + \omega_r L_m i_{ds} - L_m p i_{qs}) \tag{3.23}$$

Substituting (3.23) in (3.22) results in the final expression for i_{qs} as:

$$pi_{qs} = \frac{1}{L}(-r_r L_r i_{qs} - L_m^2 \omega_r i_{ds} + L_m r_r i_{qr} - L_m \omega_r L_r i_{dr} + L_m K_q - L_r V_{cq}) \tag{3.24}$$

Where:

$L = L_s L_r - L_m^2$

Similarly, the expressions for other current components are obtained and the SEIG can be represented in a matrix form as:

$$pI = AI + B \tag{3.25}$$

Where:

$$A = \frac{1}{L}\begin{bmatrix} -L_r r_s & -L_m^2 \omega_r & L_m r_r & -L_m \omega_r L_r \\ L_m^2 \omega_r & -L_s r_s & L_m \omega_r L_r & L_m r_r \\ L_m r_s & L_s \omega_r L_m & -L_s r_r & L_s \omega_r L_r \\ -L_s \omega_r L_m & L_m r_s & -L_s \omega_r L_r & -L_s r_r \end{bmatrix};\ B = \frac{1}{L}\begin{bmatrix} L_m K_q - L_r V_{cq} \\ L_m K_d - L_r V_{cd} \\ L_m V_{cq} - L_s K_q \\ L_m V_{cd} - L_s K_d \end{bmatrix}$$

$$I = \begin{bmatrix} i_{qs} \\ i_{ds} \\ i_{qr} \\ i_{dr} \end{bmatrix};\ V_{cq} = \frac{1}{C}\int i_{qs}\,dt + V_{cq}\Big|_{t=0};\ V_{cd} = \frac{1}{C}\int i_{ds}\,dt + V_{cd}\Big|_{t=0}$$

Any combination of *R*, *L* and *C* can be added in parallel with the self-excitation capacitance to act as load. For example, if resistance *R* is added in parallel with the self-excitation capacitance, then the term *1/pC* in (3.20) becomes *R/(1+RpC)*. The load can be connected across the capacitors, once the voltage reaches a steady-state value [3.7, 3.14].

The type of load connected to the SEIG is a real concern for voltage regulation. In general, large resistive and inductive loads can vary the terminal voltage over a wide range. For example, the effect of an inductive load in parallel with the excitation capacitor will reduce the resulting effective load impedance (Z_{eff}) [3.15].

$$Z_{eff} = R + j\left(\omega L - \frac{1}{\omega C}\right) \tag{3.26}$$

This change in the effective self-excitation increases the slope of the straight line of the capacitive reactance (Figure 3.3), reducing the terminal voltage. This phenomenon is more pronounced when the load becomes highly inductive.

Simulation Results

A model based on the first order differential equation (3.25) has been built in the MATLAB/Simulink to observe the behavior of the self-excited induction generator. The parameters used, obtained from [3.1], are as follows.

Table 3. 1: Induction Machine Parameters

Machine Rating			I_B (abc)	r_r	r_s	X_{ls}	X_{lr}	X_m	J
hp	Volts	rpm	Amps	Ohms	Ohms	Ohms	Ohms	Ohms	Kg.m^2
500	2300	1773	93.6	0.187	0.262	1.206	1.206	54.02	11.06

All the above mentioned values are referred to the stator side of the induction machine and the value of self-exciting capacitance used is 90 micro farads.

From the previous subsection, it can be said that with inductive loads the value of excitation capacitance value should be increased to satisfy the reactive power requirements of the SEIG as well as the load. This can be achieved by connecting a bank of capacitors, across the load meeting its reactive power requirements thereby, presenting unity power factor characteristics to the SEIG. It is assumed in this thesis that, such a

reactive compensation is provided to the inductive load, and the SEIG always operates with unity power factor.

Saturation Curve. As explained in the previous section, the magnetizing inductance is the main factor for voltage build up and stabilization of generated voltage for the unloaded and loaded conditions of the induction generator (Figure 3.3). Reference [3.15] presents a method to determine the magnetizing inductance curve from lab tests performed on a machine. The saturation curve used for the simulation purposes is, obtained from [3.16] by making use of the B-H saturation curve of the magnetic material (silicon iron 1%), shown in Figure 3.9.

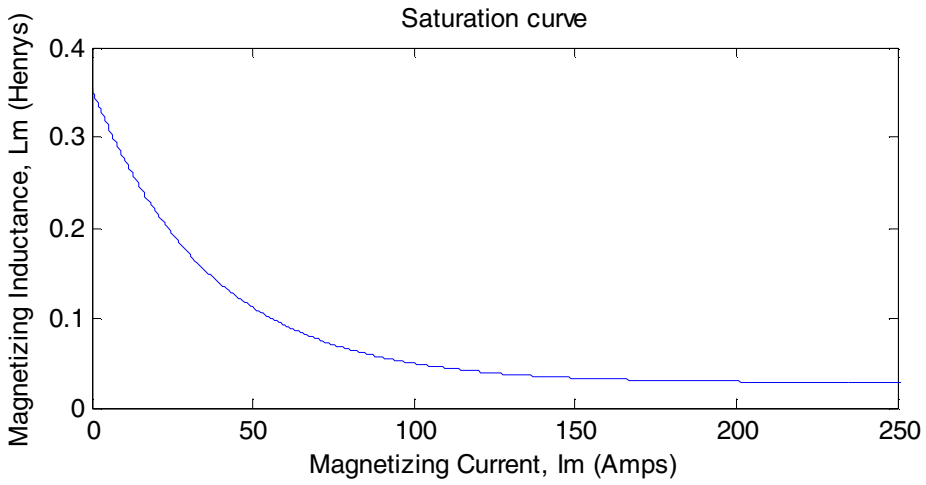

Figure 3.9 Variation of magnetizing inductance with magnetizing current.

Using least square curve fit, the magnetizing inductance L_m can be expressed as a function of the magnetizing current I_m as follows:

$$Lm = 1.1*(0.025+0.2974*\exp(-0.0271*Im)) \tag{3.27}$$

where $I_m = \sqrt{[(i_{ds} + i_{dr})^2 + (i_{qs} + i_{qr})^2]}$.

It must be emphasized that the machine needs residual magnetism so that the self-excitation process can be started. Reference [3.15] gives different methods to recover the residual magnetism in case it is lost completely. For numerical integration, the residual magnetism cannot be zero at the beginning; its role fades away as soon as the first iterative step for solving (3.25) has started.

Process of Self-excitation. The process of self-excitation can be compared with the resonance phenomenon in an *RLC* circuit whose transient solution is of the exponential form $Ke^{p_1 t}$ [3.6], [3.7]. In the solution, K is a constant, and root p_1 is a complex quantity, whose real part represents the rate at which the transient decays, and the imaginary part is proportional to the frequency of oscillation. In real circuits, the real part of p_1 is negative, meaning that the transient vanishes with time. With the real part of p_1 positive, the transient (voltage) build-up continues until it reaches a stable value with saturation of iron circuit. In other terms, the effect of this saturation is to modify the magnetization reactance X_m, such that the real part of the root p_1 becomes zero in which case the response is sinusoidal steady-state corresponding to continuous self-excitation of SEIG.

Any current (resulting from the voltage) flowing in a circuit dissipates power in the circuit resistance, and an increasing current dissipates increasing power, which implies some energy source is available to supply the power. The energy source, referred to above is provided by the kinetic energy of the rotor [3.7].

With time varying loads, new steady-state value of the voltage is determined by the self-excitation capacitance value, rotor speed and load. These values should be such that they guarantee an intersection of magnetization curve and the capacitor reactance line (Figure 3.3), which becomes the new operating point.

The following figures show the process of self-excitation in an induction machine under no-load condition.

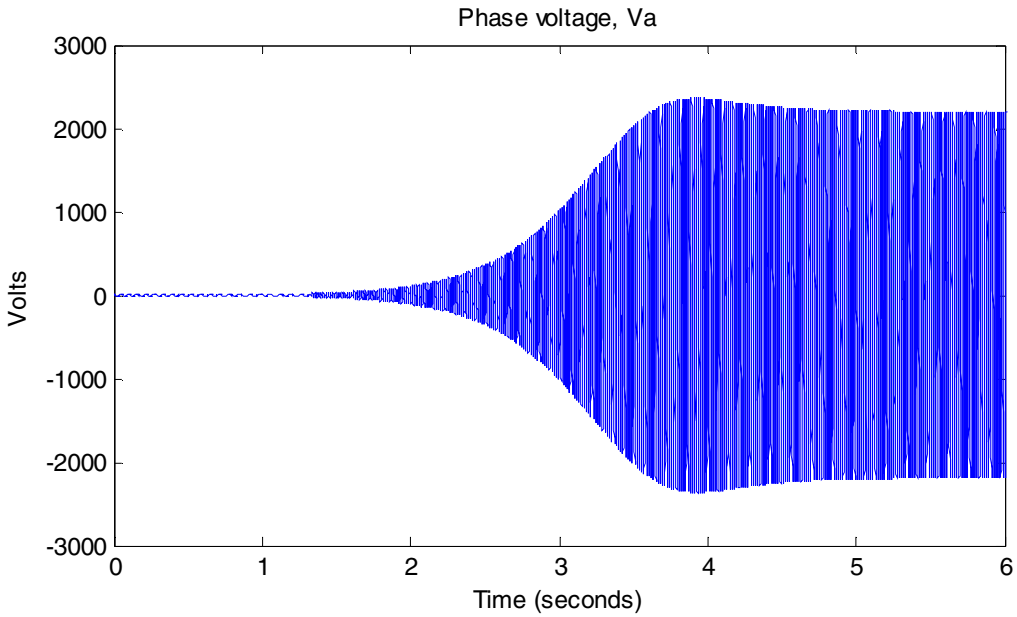

Figure 3.10 Voltage build up in a self-excited induction generator.

From Figures 3.10 and 3.11, it can be observed that the phase voltage slowly starts building up and reaches a steady-state value as the magnetization current I_m starts from zero and reaches a steady-state value. The value of magnetization current is calculated from the instantaneous values of stator and rotor components of currents (see (3.27)). The magnetization current influences the value of magnetization inductance L_m as per (3.27),

and also the capacitance reactance line (Figure 3.3). From Figures 3.10-3.12, we can say that the self-excitation follows the process of magnetic saturation of the core, and a stable output is reached only when the machine core is saturated.

In physical terms the self-excitation process could also be explained in the following way. The residual magnetism in the core induces a voltage across the self-exciting capacitor that produces a capacitive current (a delayed current). This current produces an increased voltage that in turn produces an increased value of capacitor current. This procedure goes on until the saturation of the magnetic filed occurs as observed in the simulation results shown in Figures 3.10 and 3.11.

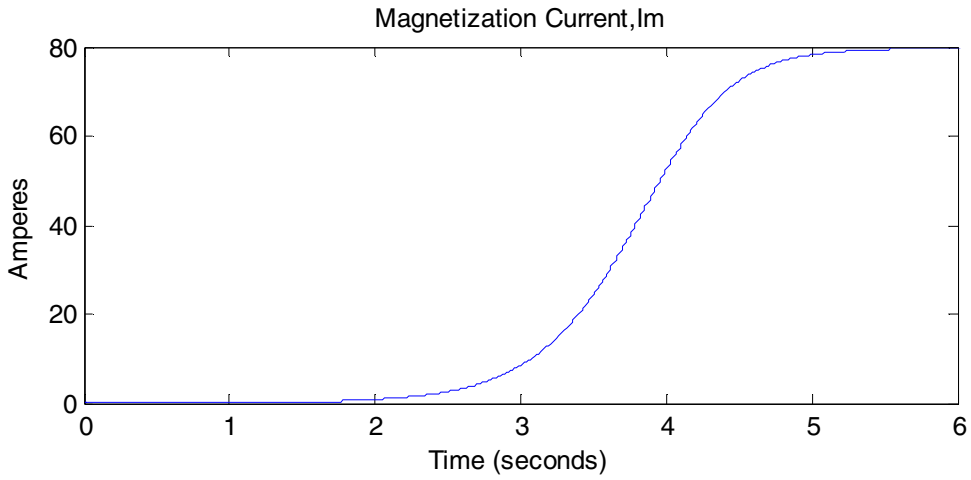

Figure 3.11 Variation of magnetizing current with voltage buildup.

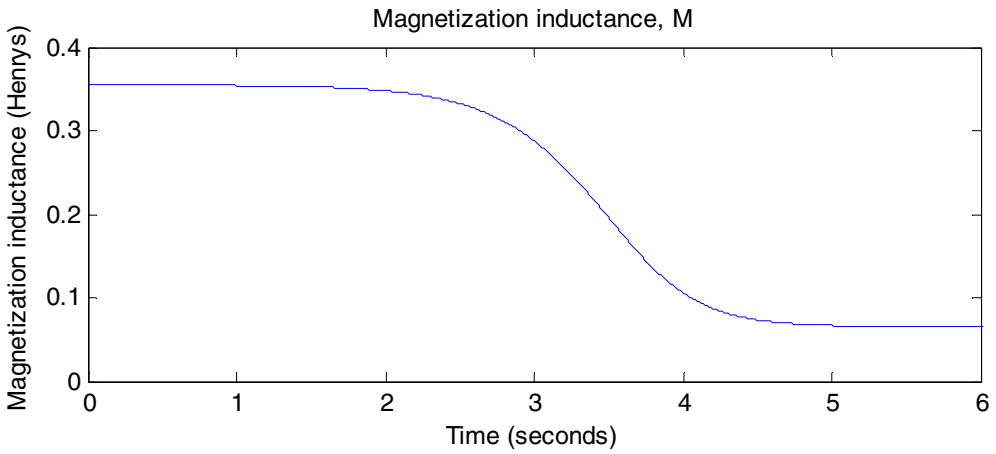

Figure 3.12 Variation of magnetizing inductance with voltage buildup.

For the following simulation results the WECS consisting of the SEIG and the wind turbine (see chapter 1) is driven by wind with velocity of 6 m/s, at no-load. At this wind velocity it can only supply a load of approximately 15 kW. At t=10 seconds a 200 kW load is applied on the WECS. This excess loading of the self-excited induction generator causes the loss of excitation as shown in the Figure 3.13.

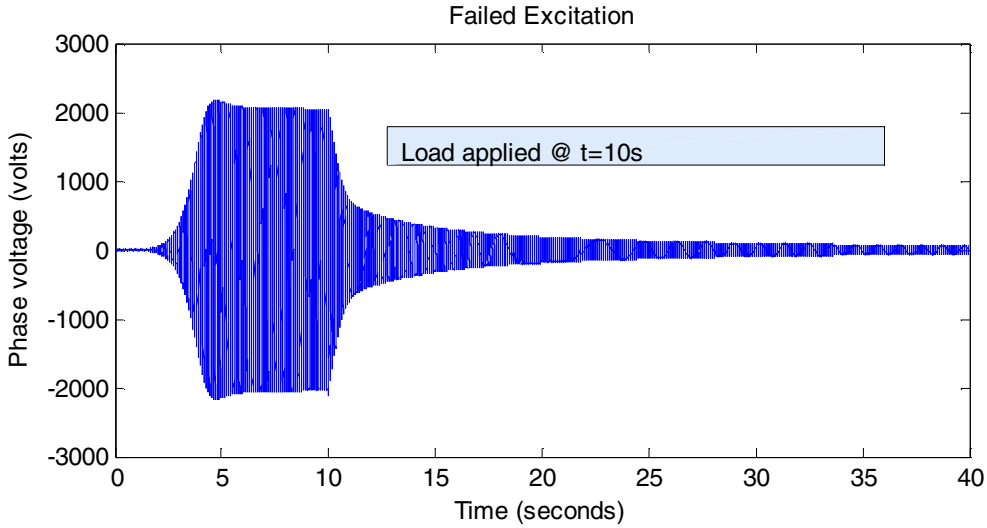

Figure 3.13 Failed excitation due to heavy load.

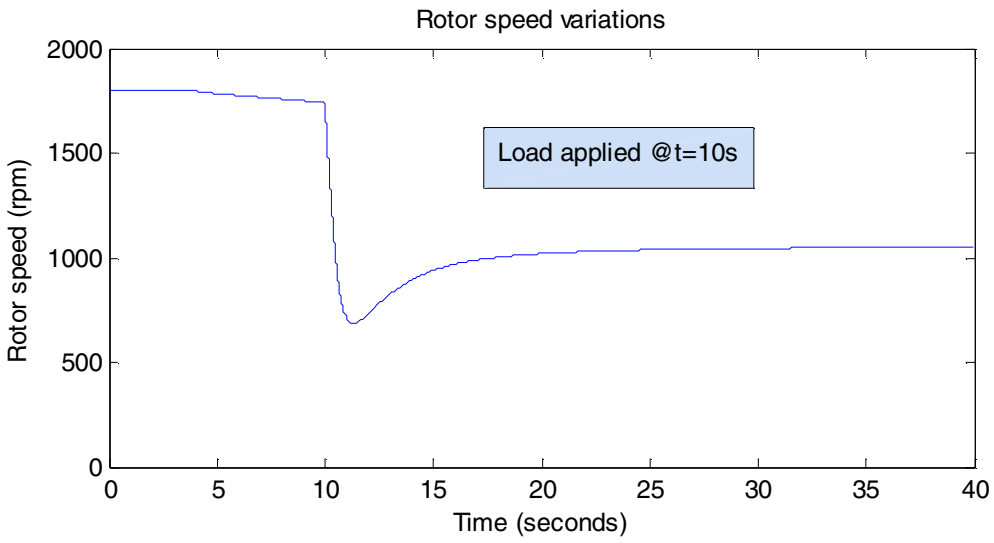

Figure 3. 14 Generator speed (For failed excitation case).

Figure 3.14 shows the rotor speed variations with load during the loss of excitation. The increase in load current should be compensated either by increasing the energy input (drive torque) thereby increasing the rotor speed or by an increase in the reactive power to the generator. None of these conditions were met here which resulted in the loss of excitation. It should also be noted from the previous section that there exists a minimum limit for speed (about 1300 rpm for the simulated machine with the self-excitation capacitance equal to 90 micro-farads), below which the SEIG fails to excite.

In a SEIG when load resistance is too small (drawing high load currents), the self-excitation capacitor discharges more quickly, taking the generator to the de-excitation process. This is a natural protection against high currents and short circuits.

For the simulation results shown below, the SEIG-wind turbine combination is driven with an initial wind velocity of 11m/s at no-load, and load was applied on the machine at

t=10 seconds. At t = 15 seconds there was a step input change in the wind velocity reaching a final value of 14 m/s. In both cases the load reference (full load) remained at 370 kW. The simulation results obtained for these operating conditions are as follows:

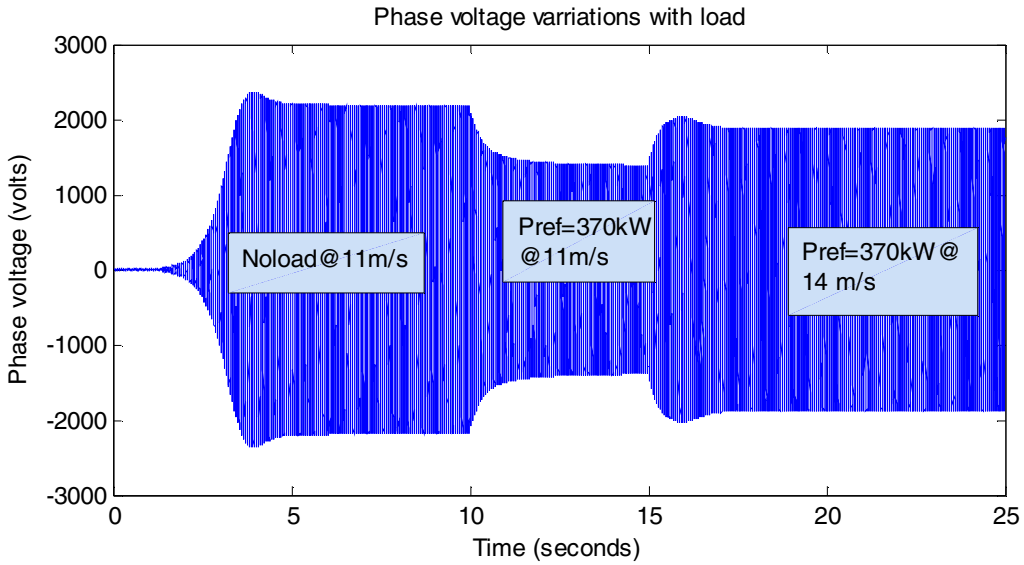

Figure 3.15 SEIG phase voltage variations with load.

For the voltage waveform shown in Figure 3.15, the machine reaches a steady-state voltage of about 2200 volts around 5 seconds at no-load. When load is applied at t=10 seconds, there is a drop in the stator phase voltage and rotational speed of the rotor (shown in Figure 3.18) for the following reasons.

We know that the voltage and frequency are dependent on load [3.14]. Loading decreases the magnetizing current I_m, as seen in Figure 3.16, which results in the reduced flux. Reduced flux implies reduced voltage (Figure 3.15). The new steady-state values of voltage is determined (Figure 3.3) by intersection of magnetization curve and the

capacitor reactance line. While the magnitude of the capacitor reactance line (in Figure 3.3) is influenced by the magnitude of I_m, slope of the line is determined by angular frequency which varies proportional to rotor speed. If the rotor speed decreases then the slope increases, and the new intersection point will be lower to the earlier one, resulting in the reduced stator voltage. Therefore, it can be said that the voltage variation is proportional to the rotor speed variation (Figure 3.18). The variation of magnetizing current and magnetizing inductance are shown in the Figures 3.16 and 3.17 respectively.

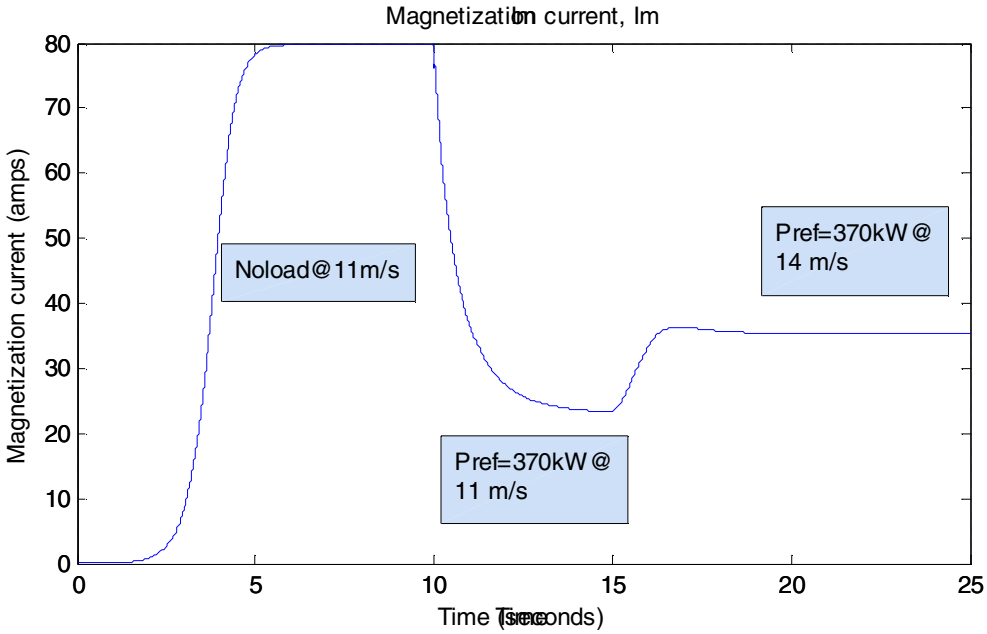

Figure 3.16 Magnetizing current variations with load.

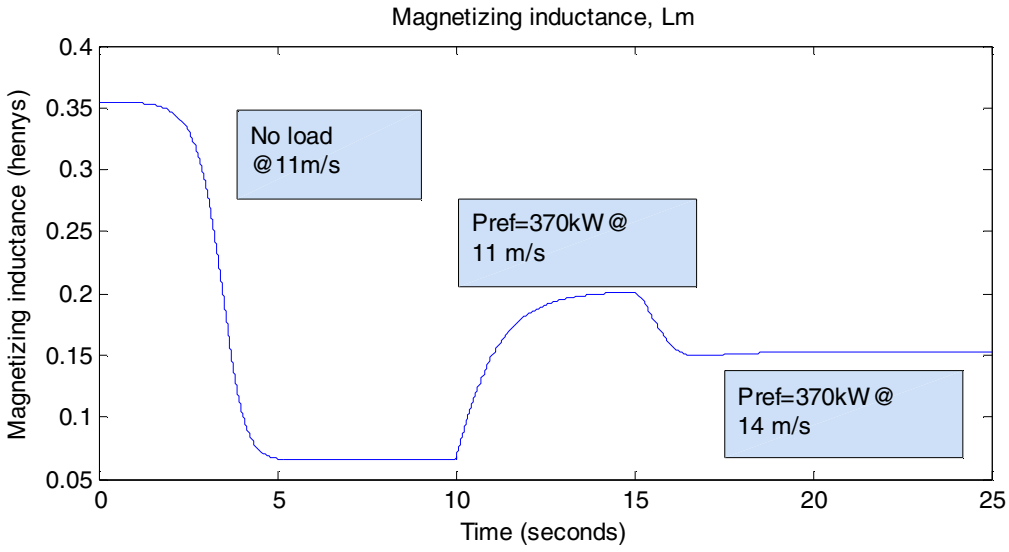

Figure 3.17 Magnetizing inductance variations with load.

Figures 3.16 and 3.17 verify that the voltage is a function of the magnetizing current, and as a result the magnetizing inductance (see (3.27)), which determines the steady-state value of the stator voltage.

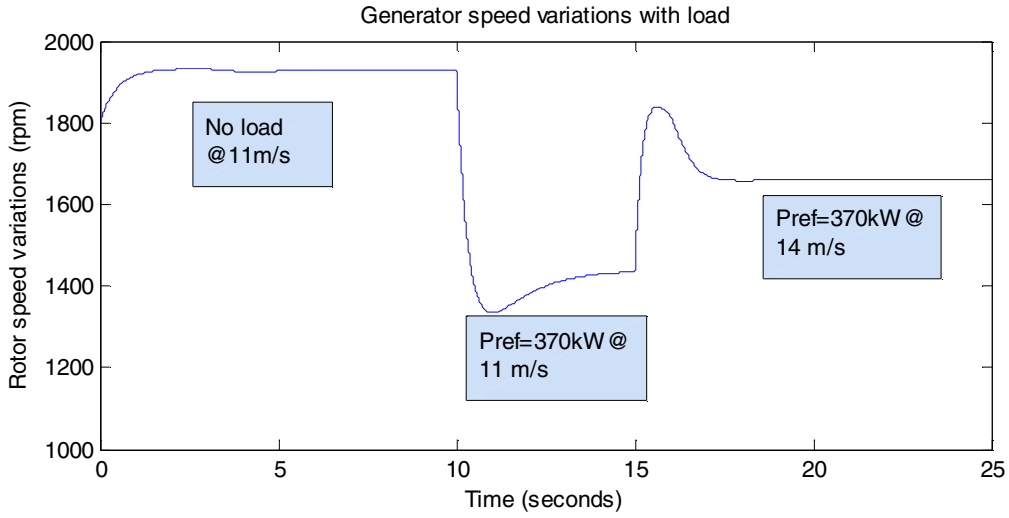

Figure 3.18 Rotor speed variations with load.

Figure 3.18 shows the variations of the rotor speed for different wind and load conditions. For the same wind speed, as load increases, the frequency and correspondingly synchronous speed of the machine decrease. As a result the rotor speed of the generator, which is slightly above the synchronous speed, also decreases to produce the required amount of slip at each operating point.

As the wind velocity increases from 11m/s to 14m/s, the mechanical input from the wind turbine increases (see chapter 1). This results in the increased rotor speed causing an increase in the stator phase voltage, as faster turning rotor produces higher values of stator voltage. The following figures show the corresponding changes in the SEIG currents, WECS torque and power outputs.

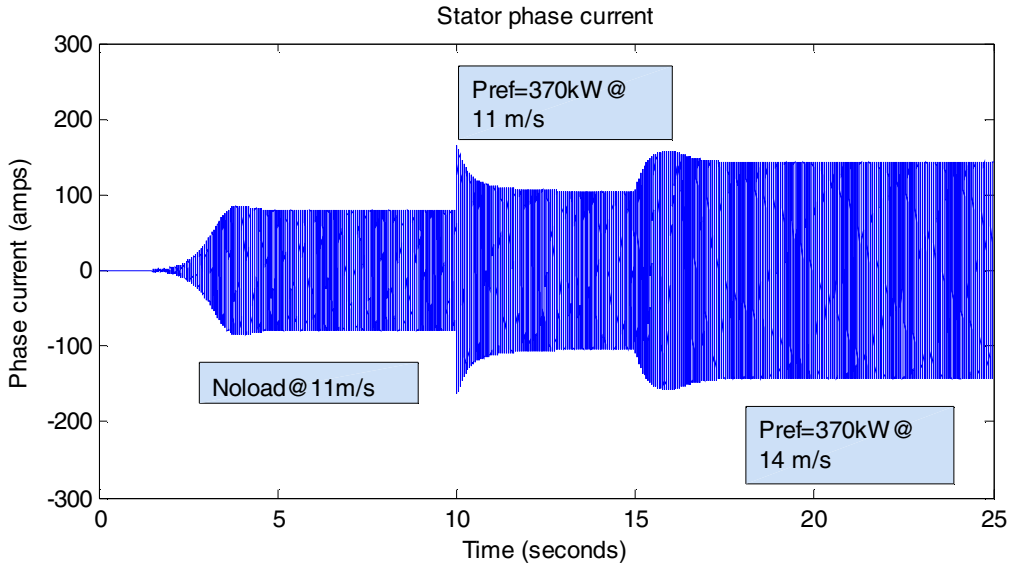

Figure 3.19 Stator current variations with load.

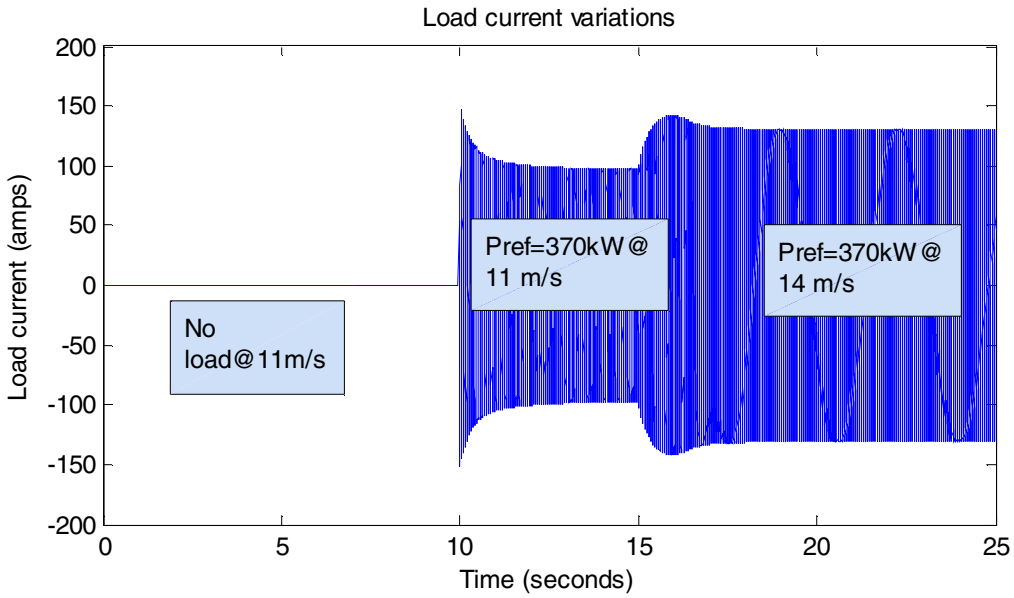

Figure 3.20 Load current variations with load.

From Figures 3.19 and 3.20, we see that as load increases, the load current increases. When the machine is operating at no-load, the load current is zero. When the load is applied on the machine, the load current reaches a steady-state value of 100 amperes (peak amplitude). With an increase in the prime mover power input, the load current further increases and reaches the maximum peak amplitude of 130 amperes. Also, the stator and load currents will increase with an increase in the value of excitation capacitance. Care should be taken to keep these currents with in the rated limits. Notice that, in the case of motor operation stator windings carry the phasor sum of the rotor current and the magnetizing current. In the case of generator operation the machine stator windings carry current equal to the phasor difference of the rotor current and the magnetizing current. So, the maximum power that can be extracted as a generator is more than 100% of the motor rating [3.17].

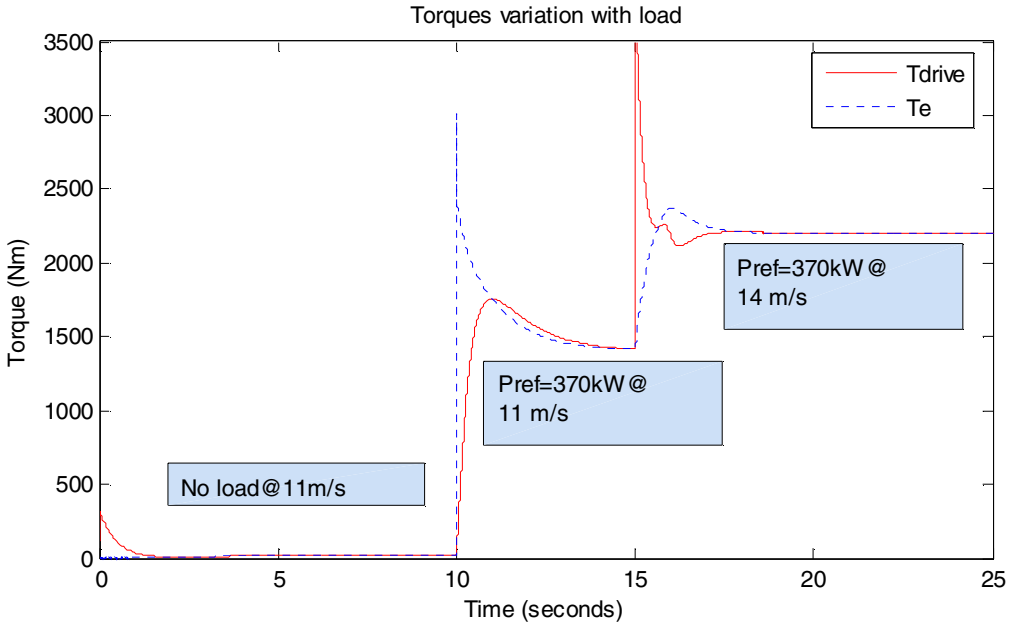

Figure 3.21 Variation of torques with load.

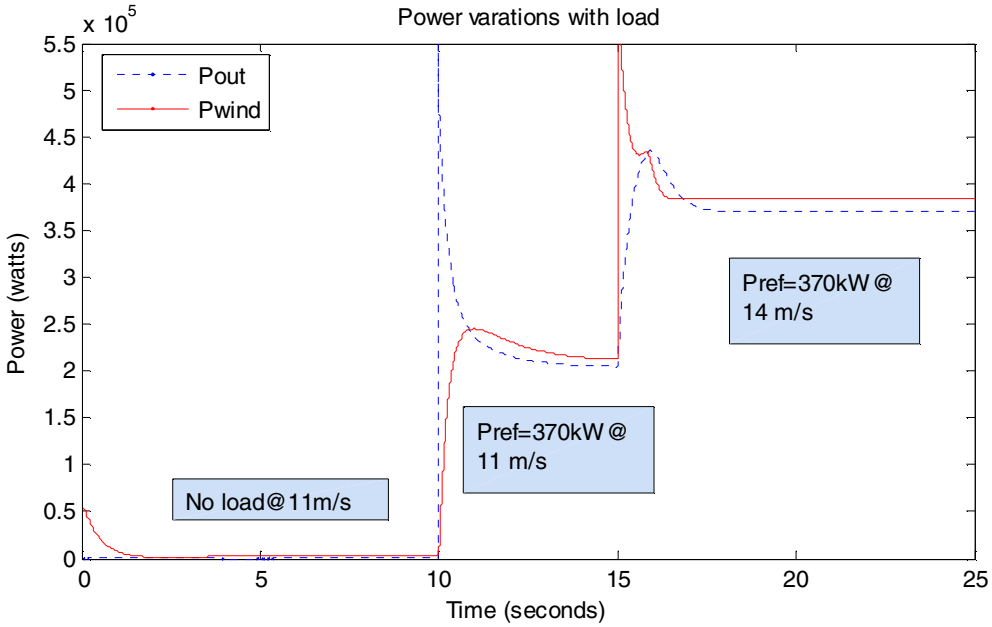

Figure 3.22 Output power produced by wind turbine and SEIG.

Equation (3.17) has been simulated to calculate the electromagnetic torque generated in the induction generator. Figure 3.21 also shows the electromagnetic torque T_e and the drive torque T_{drive} produced by the wind turbine at different wind speeds. At t=0, a small drive torque has been applied on the induction generator to avoid simulation errors in Simulink.

Figure 3.22 shows the electric power output of the SEIG and mechanical power output of the wind turbine. The electric power output of the SEIG (driven by the wind turbine), after t=10 seconds after a short transient because of sudden increase in the load current (Figure 3.20), is about 210 kW at 11 m/s and reaches the rated maximum power (370 kW) at 14 m/s. Pitch controller limits (see chapter 1) the wind turbine output power, for wind speeds above 13.5 m/s, to the maximum rated power. This places a limit on the power output of the SEIG also, preventing damage to the WECS. Since, the pitch controller has an inertia associated with the wind turbine rotor blades, at the instant t=15 seconds the wind turbine output power sees a sudden rise in its value before pitch controller starts rotating the wind turbine blades out of the wind thereby reducing the value of rotor power coefficient. Note that the power loss in the SEIG is given by the difference between P_{out} and P_{wind}, shown in Figure 3.22.

Conclusion. In this chapter the electrical generation part of the wind energy conversion system has been presented. Modeling and analysis of the induction generator, the electrical generator used in this thesis, was explained in detail using dq-axis theory. The effects of excitation capacitor and magnetization inductance on the induction

generator, when operating as a stand-alone generator, were explained. From the simulation results presented, it can be said that the self-excited induction generator (SEIG) is inherently capable of operating at variable speeds. The induction generator can be made to handle almost any type of load, provided that the loads are compensated to present unity power factor characteristics. SEIG as the electrical generator is an ideal choice for isolated variable-wind power generation schemes, as it has several advantages over conventional synchronous machine.

REFERENCES

3.1 Paul.C.Krause, Oleg Wasynczuk and Scott D. Sudhoff, *Analysis of Electric Machinery*, IEEE Press, 1994, ch. 3-4.

3.2 Bimal K. Bose, *Modern Power Electronics and Ac Drives*, Pearson Education, 2003, ch. 2.

3.3 Mukund. R. Patel, *Wind Power Systems*, CRC Press, 1999, ch. 6.

3.4 E. D. Basset and F. M. Potter, "Capacitive excitation of induction generators," *Trans. Amer. Inst. Elect. Eng*, vol. 54, no.5, pp. 540-545, May 1935.

3.5 C. F. Wagner, "Self-excitation of induction motors," *Trans. Amer. Inst. Elect. Eng*, vol. 58, pp. 47-51, Feb. 1939.

3.6 J. M. Elder, J. T. Boys and J. L. Woodward, "Self-excited induction machine as a small low-cost generator," *Proceedings, IEE*, pt. C, vol. 131, no. 2, pp. 33-41, Mar. 1984.

3.7 C. Grantham, D. Sutanto and B. Mismail, "Steady-state and transient analysis of self-excited induction generators," *Proceedings, IEE*, pt. B, vol. 136, no. 2, pp. 61-68, Mar. 1989.

3.8 M. H. Salama and P. G. Holmes, "Transient and steady-state load performance of stand alone self-excited induction generator," *Proceedings, IEE-Elect. Power Applicat.*, vol. 143, no. 1, pp. 50-58, Jan. 1996.

3.9 S. S. Murthy, O. P. Malik and A. K. Tandon, "Analysis of self excited induction generators," *Proceedings, IEE*, pt. C, vol. 129, no. 6, pp. 260-265, Nov.1982.

3.10 N. H. Malik and A. H. Al-Bahrani, "Influence of the terminal capacitor on the performance characterstics of a self-excited induction generator," *Proceedings, IEE*, pt. C, vol. 137, no. 2, pp. 168-173, Mar. 1990.

3.11 L. Ouazene and G. Mcpherson Jr, "Analysis of the isolated induction generator," *IEEE Trans. Power Apparatus and Systems*, vol. PAS-102, no. 8, pp.2793-2798, Aug. 1983.

3.12 T. F. Chan, "Capacitance requirements of self-excited induction generators," *IEEE Trans. Energy Conversion*, vol. 8, no. 2, pp. 304-311, June 1993.

3.13 A. K. Al Jabri and A.I. Alolah, "Capacitance requirements for isolated self-excited induction generator," *Proceedings, IEE*, pt. B, vol. 137, no. 3, pp. 154-159, May 1990.

3.14 Dawit Seyoum, Colin Grantham and M. F. Rahman, "The dynamic characteristics of an isolated self-excited induction generator driven by a wind turbine," *IEEE Trans. Industry Applications*, vol.39, no. 4, pp.936-944, July/August 2003.

3.15 M. Godoy Simoes and Felix A. Farret, *Renewable Energy Systems-Design and Analysis with Induction Generators*, CRC Press, 2004, ch. 3-6.

3.16 Theodore Wildi, *Electrical Machines, Drives, and Power Systems*, Prentice Hall, Third Edition, 1997, pp. 28.

3.17 Rajesh Chathurvedi and S. S. Murthy, "Use of conventional induction motor as a wind driven self-excited induction generator for autonomous applications," in *IEEE-24th Intersociety Energy Conversion Eng. Conf.*, IECEC-89, pp.2051-2055.

CHAPTER 4

MICROTURBINE GENERATION SYSTEM

Introduction

In a hybrid energy system consisting of renewable sources of energy, there should be some storage facility or backup generation to maintain continuity of supply to the load when renewable source alone is not sufficient. The objective this chapter is to present one such generating system that is capable of acting as a backup generator.

This chapter presents the modeling and simulation of a microturbine generation (MTG) system, the nonrenewable source of energy considered in this thesis, suitable for isolated as well as grid-connected operation. The system comprises of a permanent magnet synchronous generator driven by a microturbine. A brief description of the overall system is given and mathematical models for the microturbine and permanent magnet synchronous generator are presented.

MTG systems are gaining popularity in distributed power generation because of their smaller size, high efficiency (with recuperator), and faster response compared to the conventional gas turbines. Microturbines are capable of burning a number of fuels at high and low pressure levels, including natural gas, waste (sour) gas, landfill gas, or propane. Today's microturbine technology is the result of the development work, in small stationary and automotive gas turbines, pursued by the automotive industry beginning in

the 1950's. As a result of which, modern microturbines are able to combine the reliability of on board commercial aircraft generators with the low cost of automotive turbochargers.

In the last section of this chapter, the developed models are simulated in MATLAB/Simulink. The simulated microturbine model is of single shaft type with control systems capable of regulating its output power. Simulation results are presented for the developed model of the MTG system under different load conditions.

Microturbine Generation (MTG) System

Microturbines are small gas turbines which burn gaseous or liquid fuels to create high energy gas stream that turns an electrical generator. There is a growing interest in the application of MTGs as they can start quickly and are especially useful for on-peak power supply for grid support. Other applications include remote power and combined heat and power (CHP) systems by utilizing the heat contained in the exhaust gases to supply thermal energy needs in a building or industrial process [4.1]-[4.4].

Generally MTG systems range from 30 to 400 kilowatts [4.11]-[4.13], while conventional gas turbines range from 500 kW to more than 300 MW [4.9], [4.10].

Microturbines are capable of burring a number of fuels at high and low pressure levels. They generally have marginally lower electrical efficiencies than similarly sized reciprocating engine generators. Without a recuperator the overall efficiency of a

microturbine is 15 to 17%, where as with an 85% effective recuperator the efficiency can be as high as 33 to 37% [4.13]. However, because of their design simplicity and relatively fewer moving parts, microturbines have the potential for simpler installation, higher reliability, reduced noise and vibration, lower maintenance requirements, lower emissions, continuous combustion and possibly lower capital costs compared to reciprocating engines [4.1], [4.4], [4.12]. Microturbines emissions can be up to eight times lower than diesel generators, and currently available ones produce less than 50% of the NOx emissions of a state of the art natural gas lean-burn engine [4.1].

Types of Microturbine Systems. There are mainly two types of microturbine systems available, single-shaft models and two shaft models. In single-shaft designs, a single expansion turbine turns both the compressor and the generator. As a result they operate at high-speeds, some in excess of 100,000 rpm, and generate electrical power at high frequency (in the order of kHz). Two-shaft models on the other hand, uses a turbine to drive the compressor on one shaft and a power turbine on a separate shaft connected to a conventional generator via a gear box which generates AC power at 60 Hz or 50 Hz [4.17]. In a single-shaft design, since the generator provides a high frequency AC voltage source, a power electronic interface between the MTG system and the AC load is required. For a two-shaft design, on the other hand, there is no need for such interfacing. This thesis considers the modeling single-shaft type only.

Basic Process and Components of a MTG System.

The basic components of a microturbine generation system are: compressor, turbine, recuperator, high-speed generator and power electronics interfacing. In the following paragraphs a brief description of each component is given, followed by a detailed modeling of microturbine and high-speed generator. Figure 4.1 shows the schematic diagram of a single-shaft microturbine based generation system [4.1], [4.5].

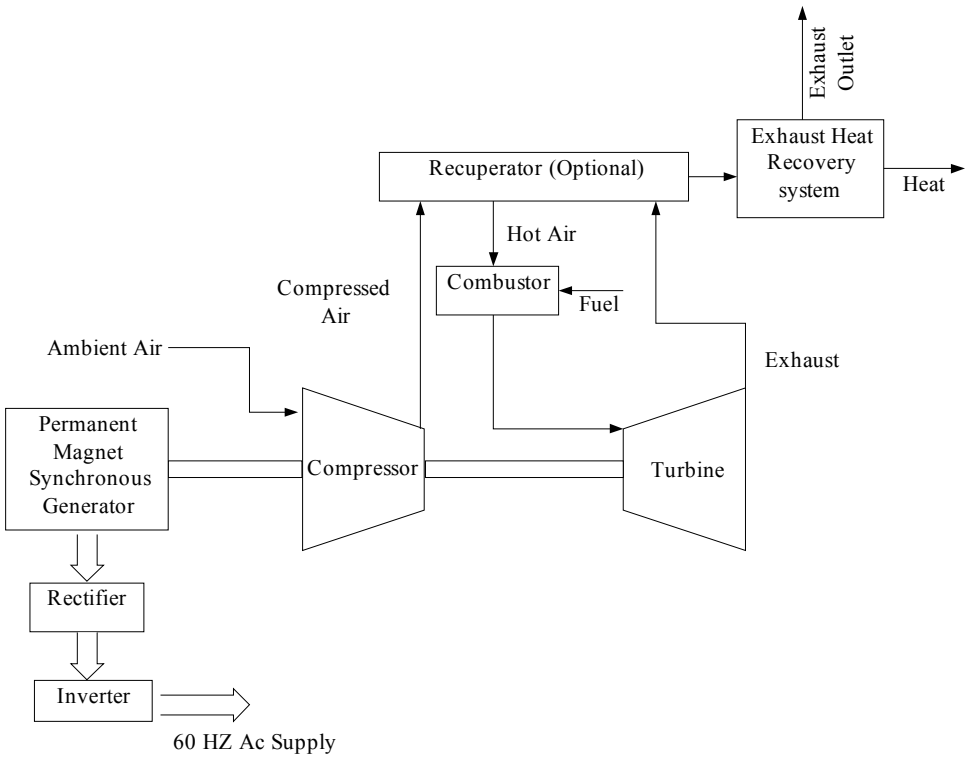

Figure 4.1 Microturbine based CHP system (Single-Shaft Design).

Microturbines, like large gas turbines, operate based on the thermodynamic cycle known as the Brayton cycle [4.1]. In this cycle, the inlet air is compressed in a radial (or centrifugal) compressor. The compressed air is mixed with fuel in the combustor and

burned. The hot combustion gas is then expanded in the turbine section, producing rotating mechanical power to drive the compressor and the electric generator, mounted on the same shaft (single-shaft design). In a typical microturbine air to gas heat exchanger called recuperator is added to increase the overall efficiency. The recuperator uses the heat energy available in the turbine's hot exhaust gas to preheat the compressed air before the compressed air goes into the combustion chamber thereby reducing the fuel needed during the combustion process.

The high-speed generator of the single shaft design usually employs a permanent magnet synchronous generator (PMSG), and requires that the high frequency AC output in the order of kHz be converted to 60 Hz (or 50 Hz) for general use. This power conditioning involves rectifying the high frequency AC to DC and then inverting the DC to 60 Hz (or 50 Hz) AC. Power electronic interfacing is a critical component in the single-shaft design and is generally designed to handle transient and voltage spikes [4.1].

The model presented in this thesis concentrates on the slow dynamics of the MTG system, suitable for power management of MTG combined with other types of distributed generation (DG) systems. It is reasonable, while modeling the microturbine for the above purpose, to assume that the system is operating under normal operating conditions by neglecting fast dynamics of the microturbine (e.g., start-up, shutdown, internal faults and loss of power). Also, since the electromechanical behavior of the MTG system is of main interest the recuperator is not included in the model as it only serves to increase the turbine efficiency [4.17].

Mathematical Representation of a Microturbine

There exists a large literature on the modeling of gas turbines, with varying level of complexity depending on the intended application. The concept of gas turbine system presented in this section is based on the paper presented by Rowen [4.6]. He proposed a single-shaft design, generator driven gas turbine model which includes speed control, temperature control and fuel system. This model was successfully adopted by the several authors for gas turbine simulations [4.7]-[4.10] as well as for microturbine simulations with smaller time constants [4.11], [4.12].

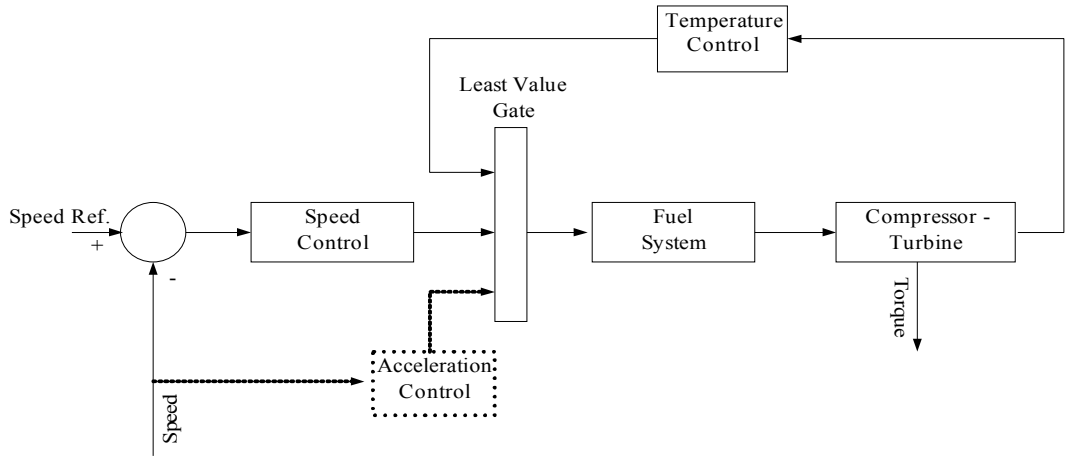

Figure 4.2 Block diagram of a microturbine.

The three control functions of the microturbine are: speed control acting under part load conditions, temperature control acting as an upper output power limit, and acceleration control to prevent over speeding. The output of these control function blocks are all inputs to a least value gate (LVG), whose output is the lowest of the three inputs

and results in the least amount of fuel to the compressor-turbine as shown in Figure 4.2. This figure shows the per-unit representation of a microturbine, along with its control systems [4.6]. Each subsystem of the microturbine is discussed in the following subsections.

Speed and Acceleration Control. The speed control operates on the speed error formed between a reference (one per-unit) speed and the MTG system rotor speed. It is the primary means of control for the microturbine under part load conditions. Speed control is usually modeled by using a lead-lag transfer function [4.6], or by a PID controller [4.8]. In this work a lead lag transfer function has been used to represent the speed controller, as shown in Figure 4.3. In this figure K is the controller gain, T_1 (T_2) is the governor lead (lag) time constant, and Z is a constant representing the governor mode (droop or isochronous). A droop governor is a straight proportional speed controller in which the output is proportional to the speed error. An isochronous speed controller is a proportional-plus-reset speed controller in which the rate of change of the output is proportional to the speed error.

Acceleration control is used primarily during turbine startup to limit the rate of the rotor acceleration prior to reaching operating speed. If the operating speed of the system is close to its rated speed, the acceleration control could be eliminated in the modeling [4.6], which is the case in this study.

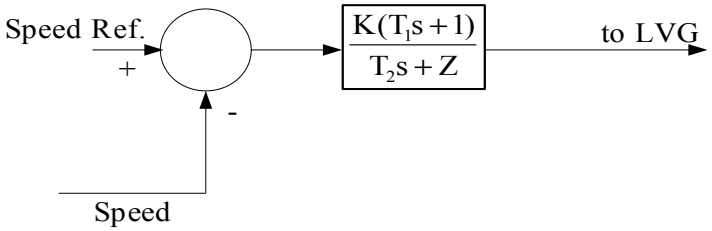

Figure 4.3 Speed controller for the microturbine.

Fuel System. The fuel system consists of the fuel valve and actuator. The fuel flow out from the fuel system results from the inertia of the fuel system actuator and of the valve positioner [4.6], [4.8], whose equations are given below.

The valve positioner transfer function is:

$$E_1 = \frac{K_v}{T_v s + c} F_d \tag{4.1}$$

and the fuel system actuator transfer function is:

$$Wf = \frac{K_f}{T_f s + c} E_1 \tag{4.2}$$

In (1) and (2), K_v (K_f) is the valve positioner (fuel system actuator) gain, T_v ,T_f are the valve positioner and fuel system actuator time constants, c is a constant, F_d and E_1 are the input and outputs of the valve positioner and Wf is the fuel demand signal in p.u.

The output of the LVG, V_{ce}, represents the least amount of fuel needed for that particular operating point and is an input to the fuel system. Another input to the fuel

system is the per-unit turbine speed N (limited by the acceleration control). The per-unit value for V_{ce} corresponds directly to the per-unit value of the mechanical power on turbine at steady-state. The fuel flow control as a function of V_{ce} is shown in Figure 4.4.

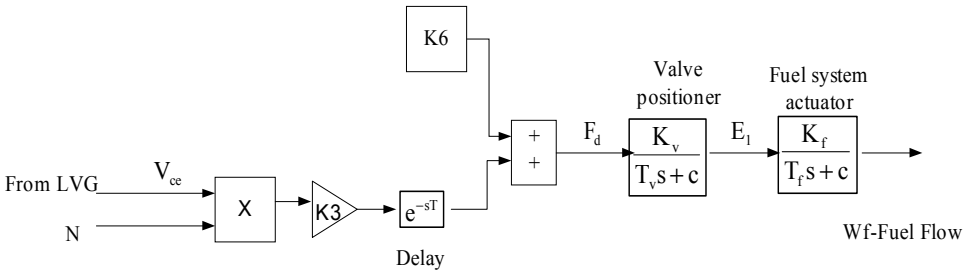

Figure 4.4 Block diagram of the fuel system.

The value of V_{ce} is scaled by the gain *K3* (*K3*= (1-*K6*)), then delayed and offset by the minimum amount of fuel flow *K6* to ensure continuous combustion process in the combustion chamber. *K6* is essentially the minimum amount of fuel flow at no-load, rated speed.

Compressor-Turbine. The compressor-turbine is the heart of the microturbine and is essentially a linear, nondynamic device (with the exception of the rotor time constant) [4.6]. There is a small transport delay T_{CR}, associated with the combustion reaction time, a time lag T_{CD}, associated with the compressor discharge volume and a transport delay T_{TD} , for transport of gas from the combustion system through the turbine. The block diagram of the compressor-turbine package is shown in Figure 4.5. In this figure both the torque and the exhaust temperature characteristics of the single-shaft gas turbine are

essentially linear with respect to fuel flow and turbine speed and are given by the following equations [4.6]:

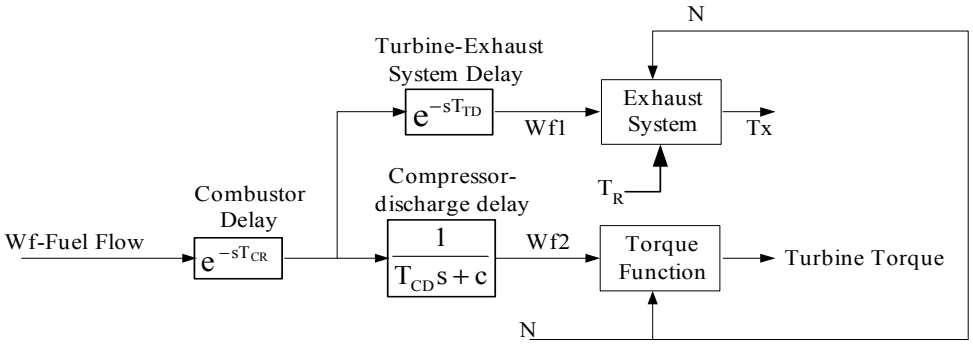

Figure 4.5 Compressor-Turbine package of a microturbine.

$$Torque = K_{HHV}\,(W_{f2}\text{-}0.23)+0.5(1\text{-}N)\ (Nm) \tag{4.3}$$

$$Exhaust\ Temp.,\ Tx = T_R\text{-}700(1\text{-}W_{fl})+550(1\text{-}N)\ (^{\circ}F) \tag{4.4}$$

where K_{HHV} is a coefficient which depends on the enthalpy or higher heating value of the gas stream in the combustion chamber and T_R is the reference temperature [4.6], [4.9]. The K_{HHV} and the constant 0.23 in the torque expression cater for the typical power/fuel rate characteristic, which rises linearly from zero power at 23% fuel rate to the rated output at 100% fuel rate.

The input to this subsystem is the p.u. fuel demand signal *Wf* and outputs are the p.u. turbine torque and exhaust temperature (˚F).

Temperature Control. Temperature control is the normal means of limiting the gas turbine output power at a predetermined firing temperature, independent of variation in

ambient temperature or fuel characteristics. The fuel burned in the combustor results in turbine torque and in exhaust gas temperature. The exhaust temperature is measured using a series of thermocouples incorporating radiation shields as shown in the block diagram of the temperature controller (Figure 4.6). In Figure 4.6, T_t is the temperature controller integration rate and T_3, T_4 are time constants associated with the radiation shield and thermocouple, respectively. K_4 and K_5 are constants associated with radiation shield and T_5 is the time constant associated with temperature controller. The output from the thermocouple is compared with a reference temperature, which is normally higher than the thermocouple output. This forces the output of the temperature control to stay on the maximum limit permitting the dominance of speed control through the LVG (Figure 4.2). When the thermocouple output exceeds the reference temperature, the difference becomes negative, and the temperature control output starts decreasing. When this signal (Figure 4.2) becomes lower than the speed controller output, the former value will pass through the LVG to limit the turbine's output, and the turbine operates on temperature control. The input to the temperature controller is the exhaust temperature (T_x) and the output is the temperature control signal to the LVG [4.6], [4.9].

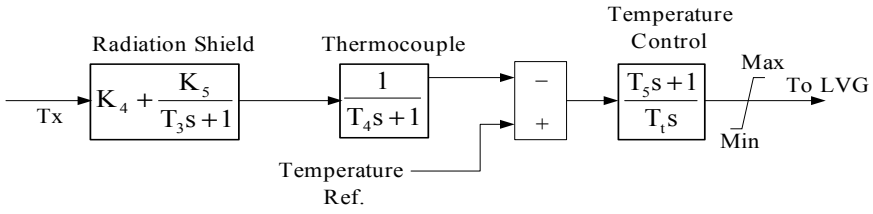

Figure 4.6 Temperature controller.

Permanent Magnet Synchronous Generator (PMSG)

Microturbine produces electrical power via a high-speed generator directly driven by the turbo-compressor shaft. Small gas turbines benefit in particular when the gearbox that reduces the shaft speed to the speed of conventional electrical machines is eliminated, as is the case with the single-shaft designs considered here. The result is a more efficient, compact and reliable machine and the shaft speed is normally above 30,000 rev/min and may exceed 100,000 rev/min. High energy permanent magnets and high yield-strength materials like neodymium-iron-boron (NdBFe) or Samarium-cobalt magnets have proved very suitable for high-speed electrical machines [4.1], [4.5].

In the following sections the equivalent circuit of a permanent magnet synchronous machine (PMSM) is presented along with a brief description of its construction, operation and the permanent magnet materials.

In a permanent magnet synchronous machine, the dc field winding of the rotor is replaced by a permanent magnet. The advantages are elimination of filed copper loss, higher power density, lower rotor inertia, and more robust construction of the rotor. The drawbacks are loss of flexibility of field flux control and possible demagnetization. The machine has higher efficiency than an induction machine, but generally its cost is higher [4.15].

Permanent Magnet Materials. The property of a permanent magnet and the selection of the proper materials are very important in the design of a permanent magnet

synchronous machine (PMSM). A good permanent magnet should produce a high magnetic field with a low mass, and should be stable against the influences which would demagnetize it. The desirable properties of such magnets are typically stated in terms of the *remanence* and *coercivity* of the materials, and are quoted in Tesla, the basic unit for magnetic field B.

Iron, nickel, cobalt and some of the rare earth metals exhibit a unique magnetic behavior which is called ferromagnetism. Ferromagnets tend to stay magnetized to some extent after being subjected to an external magnetic field. The fraction of the saturation magnetization retained (remanence) when the driving filed is removed is an important factor for the selection of the permanent magnets. All ferromagnetic materials have a maximum temperature known as *Curie temperature*, where the ferromagnetic property disappears. Consequently, the range of temperatures plays an important role in the operation of a PMSM [4.14].

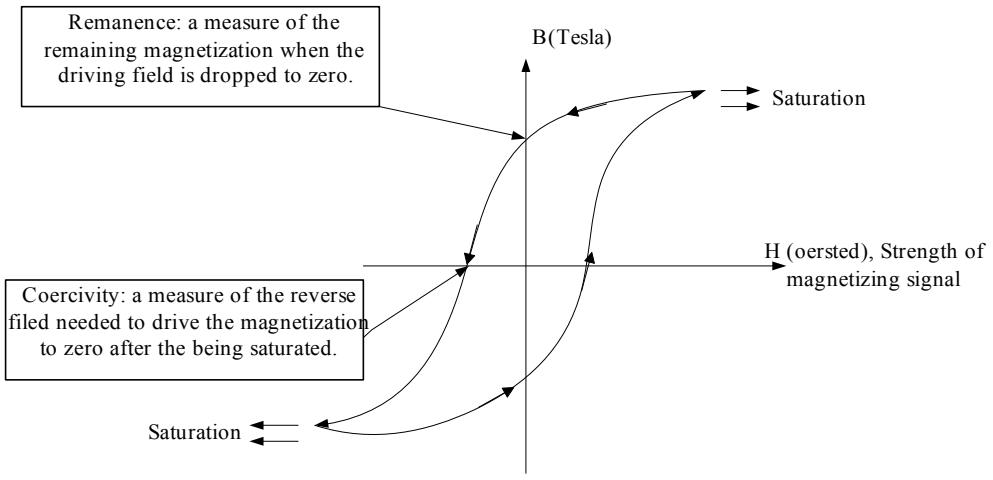

Figure 4.7 Hysteresis loop in the form of magnetization B and magnetic field strength H.

Operating Region of a PMSM. Figure 4.8 shows the demagnetization segment of the B-H curve where the permanent magnet is usually designed to operate [4.15].

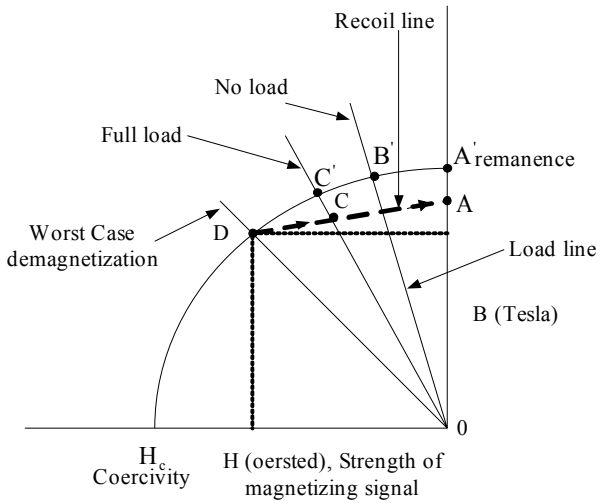

Figure 4.8 Permanent magnet machine operating points on B-H curve.

The maximum flux density B_r corresponding to A' will be available initially (no airgap). When the magnet is installed in the machine, the air gap will have some demagnetization effect and the operating point B' will correspond to the no-load line as shown in Figure 4.8. When current flows in the stator winding, the magnetic axis (direct axis) armature reaction effect can have further demagnetization effect, which will reduce the air gap flux density further. A load line representing worst-case demagnetization (may be due to starting, transient or machine fault condition) is also shown in Figure 4.8. Once the operating point reaches the D and the demagnetization effect is removed, the magnet will recover along the recoil line (DA). Subsequently, the stable operating point will be determined by the intersection of the load line and the recoil line. The magnet is

therefore permanently demagnetized at no-load operation, corresponding to the vertical distance between A' and A. If the permanent magnet material has a straight-line demagnetization curve, the recoil line will coincide with the demagnetization line irrespective of the worst case magnetization point (i.e., permanent demagnetization will be negligible). The characteristics for several possible permanent magnet materials are given in reference [4.15].

dq Axis Representation of a PMSM. In a PMSM, the permanent magnets are glued on the rotor in surface sinusoidal magnet machine (SPM), and are mounted inside the rotor in case of an interior or buried magnet synchronous machine (IPM). The stator has three-phase sinusoidal winding, which creates a synchronously rotating air gap flux. If the machine is rotated by a prime mover, the stator windings generate balanced three-phase sinusoidal voltages. The *dq* axis representation of a permanent magnet synchronous machine (for a balanced system the *0*-axis quantities are equal to zero), where is shown in the Figure 4.9 [4.15], [4.16], [4.18]. In this figure the finite core loss is represented by the dotted damper windings.

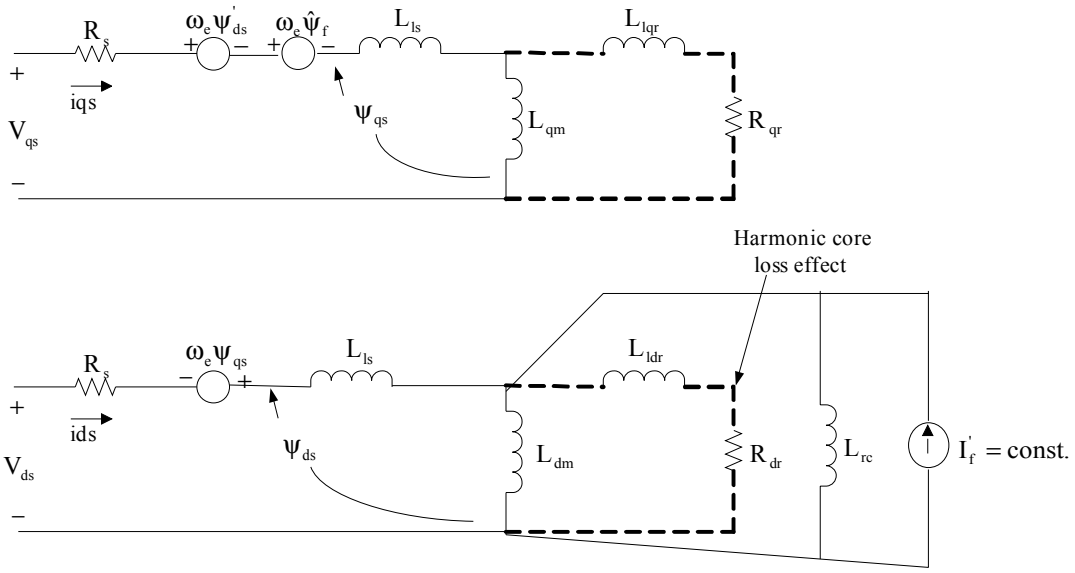

Figure 4.9 Synchronously rotating frame equivalent circuits of a PMSM.

Ignoring core loss, the circuit equations can be written as (equations are valid for both IPM as well as SPM (for SPM L_{dm}=L_{qm}):

$$V_{qs} = R_s i_{qs} + \omega_e \psi'_{ds} + \omega_e \hat{\psi}_f + \frac{d\psi_{qs}}{dt} \tag{4.5}$$

$$V_{ds} = R_s i_{ds} - \omega_e \psi_{qs} + \frac{d\psi_{ds}}{dt} \tag{4.6}$$

where the flux linkages are given by the following equations:

$$\hat{\psi}_f = L_{dm} I'_f \tag{4.7}$$

$$\psi'_{ds} = i_{ds}(L_{ls} + L_{dm}) = i_{ds} L_{ds} \tag{4.8}$$

$$\psi_{ds} = \hat{\psi}_f + \psi'_{ds} \tag{4.9}$$

$$\psi_{qs} = i_{qs}(L_{ls} + L_{qm}) = i_{qs}L_{qs} \tag{4.10}$$

The electromagnetic developed in the machine air gap is given by:

$$T_e = \frac{3}{2} \times \frac{P}{2}(\psi_{ds} i_{qs} - \psi_{qs} i_{ds}) \tag{4.11}$$

Substituting (4.5)-(4.8) in (4.3), (4.4) and (4.9) and simplifying, we have

$$\frac{di_{qs}}{dt} = \frac{1}{L_{qs}}\left[V_{qs} - R_s i_{qs} - L_{ds}\omega_e i_{ds} - \hat{\psi}_f \omega_e\right] \tag{4.12}$$

$$\frac{di_{ds}}{dt} = \frac{1}{L_{ds}}\left[V_{ds} - R_s i_{ds} + \omega_e L_{qs} i_{qs}\right] \tag{4.13}$$

$$T_e = \frac{3P}{4}[\hat{\psi}_f i_{qs} + (L_{ds} - L_{qs}) i_{qs} i_{ds}] \tag{4.14}$$

The rotor speed is obtained from the dynamics of the mechanical system as follows:

$$\frac{d\omega_r}{dt} = \frac{1}{J}(T_e - T_{shaft}) \tag{4.15}$$

where ω_e, ω_r are electrical and mechanical angular velocities of the rotor (rad/sec), V_{qs}, V_{ds} (I_{qs}, I_{ds}) are q and d axis voltage (current) components and L_{qs} and L_{ds} are q and d axis inductances of the stator respectively. L_{dm} is the common d-axis mutual inductance of the stator lumped with the damper windings and the permanent magnet inductance L_{rc} (associated with the recoil slope).

I_f is an equivalent field current of the permanent magnets and $I_f^{'}$ is its equivalent referred to the stator side,

Ψ_f ($\psi_f = L_{dm} I_f^{'} = consant$) denotes flux linkage induced by the permanent magnets of the rotor in stator phases,

J is the inertia of the rotor (Kgm^2),

T_{shaft} is the shaft torque produced by the microturbine (Nm),

T_e is the electric torque generated by the PMSG (Nm), and

P is the number of poles.

Note that the signs for the generated torque T_e and shaft torque T_{shaft} are positive for motor operation and negative for generator operation.

Simulation Results

A mathematical model of the microturbine as explained in the previous section is built in MATLAB/Simulink using SimPowerSystems blockset. An inbuilt model of the permanent magnet synchronous machine in the SimPowerSystems blockset, based on (4.12)-(4.15), is used to simulate the PMSG by applying negative torque to the model. All the parameters values used for the simulation are given below. The block diagram of the simulated MTG system is given in Figure 4.10 followed by the simulation results for different operating conditions.

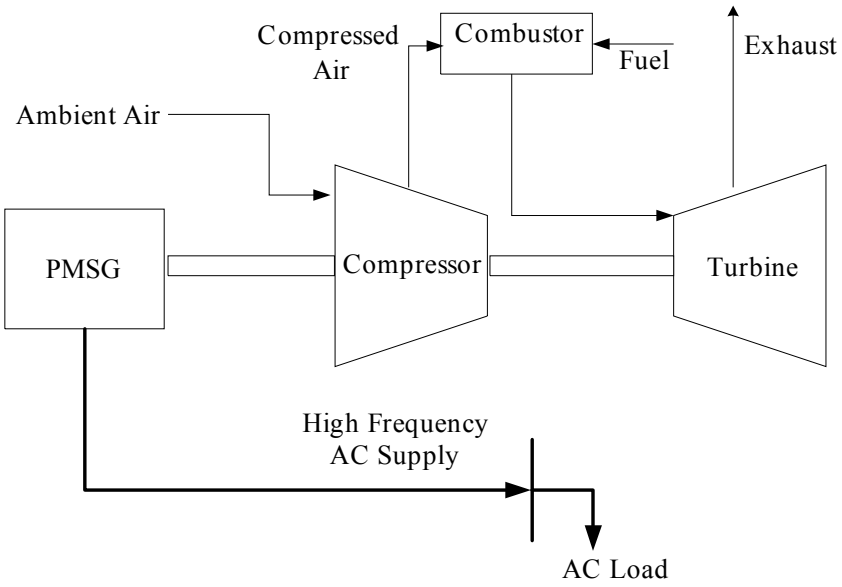

Figure 4.10 Block diagram of the simulated MTG system.

Parameters are obtained form [4.6], [4.9], [4.10], and adopted for this simulation. All time functions are in seconds.

Microturbine ratings: 400 kW, 70000 rpm.

Speed controller parameters (Figure 4.3):

K=25, T_1=0.4, T_2=1.0, Z=3.

Fuel system parameters (Figure 4.4):

K_v=1, T_v=0.05, c=1, $K3$=0.77, $K6$=0.23, K_f=1, T=0, T_f=0.04.

Compressor-turbine combination parameters (Figure 4.5):

T_{CR}=0.01, T_{TD}=0.04, T_{CD}=0.2, K_{HHV}=1.2.

Temperature controller parameters (Figure 4.6):

K_4=0.8, K_5=0.2, T_3=15, T_4=2.5, T_5=3.3, T_t=450 ˚F, T_R=950 ˚F.

Parameters used for the PMSG simulation [4.4], [4.18].

R_s=12.5m Ohms, L_d=L_q=165e-6 Henrys, Ψ_f=0.2388 wb, P=4, J=0.011 kg m^2.

Speed reference was kept constant at 1 p.u. for all simulations. All values are referred to a base power rating of 1 MVA. The response of the developed MTG system is given in the following simulation results:

Initially the system is operating at no-load. At t =10 seconds a load of 200kW is applied on the MTG system, and at t = 15 seconds, the load is increased to 400 kW. Figure 4.11 shows the output power of the MTG system, responding to the above load variations. Figure 4.12 shows the fuel consumed by the microturbine for the applied load conditions. The fuel demand is equal to 23% (0.23 p.u.) until the load is applied on the system at t=10 seconds, increasing the amount of fuel required to keep the combustion process alive. Note that the fuel demand signal is 0.62 p.u. at 200kW load and increasing to 1 p.u. at full load (400kW).

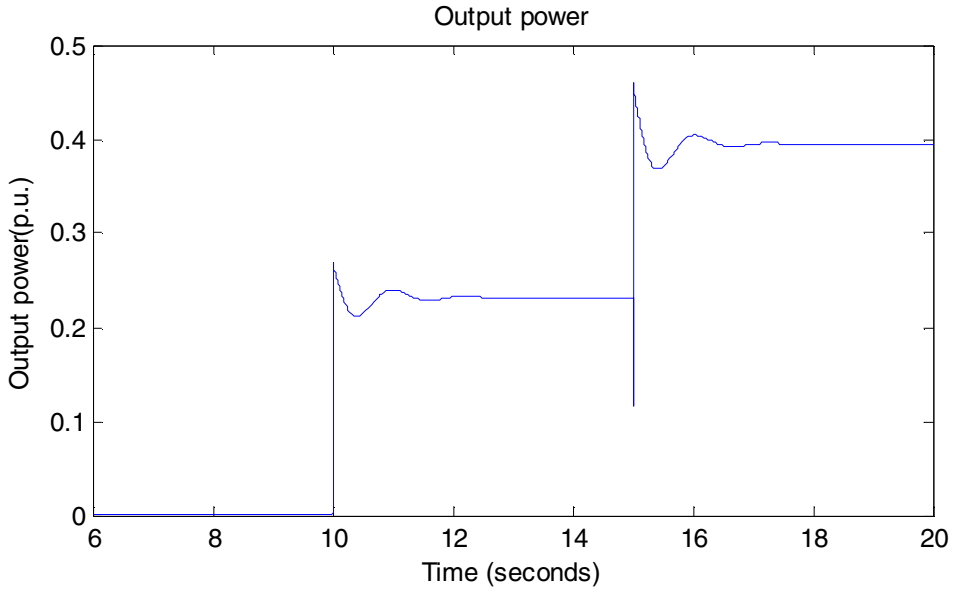

Figure 4.11 Power output from the MTG system.

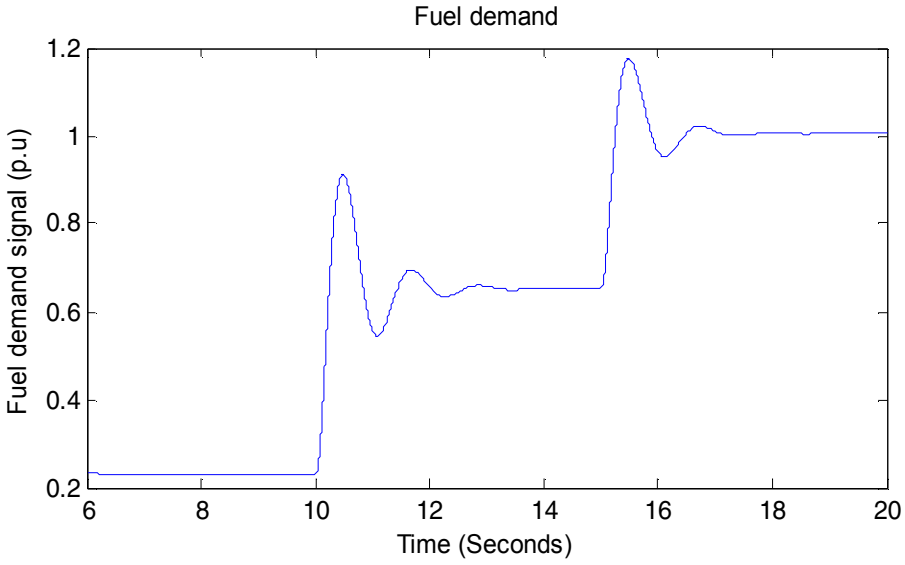

Figure 4.12 Fuel demand signal of the microturbine.

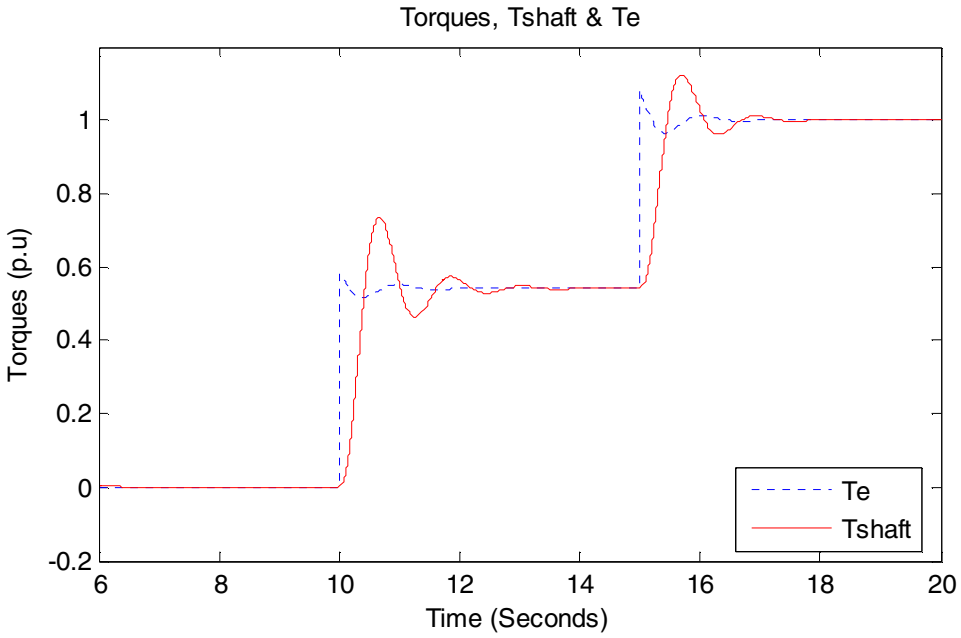

Figure 4.13 Variation of shaft torque and electric torque generated.

Figure 4.13 shows the shaft torque (T_{shaft}) produced by the microturbine, which drives the PMSG, and the electromagnetic torque (T_e) generated by the PMSG. The generator torque is approximately same as the shaft torque produced by microturbine at steady-state. At no-load the electromagnetic torque is equal to zero; it increases to about 50% of its base value at 200kW and to 1 p.u. at full load.

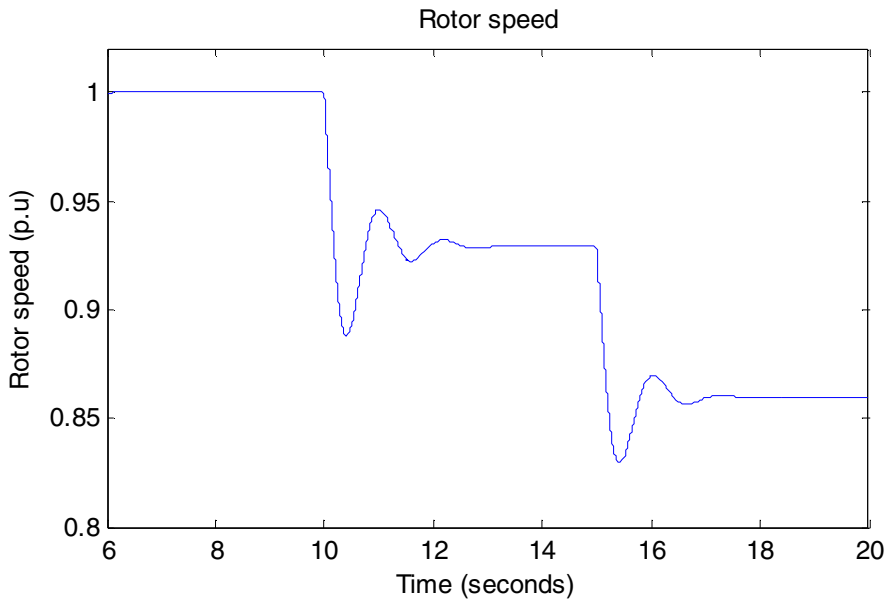

Figure 4.14 Rotor speed variations with load.

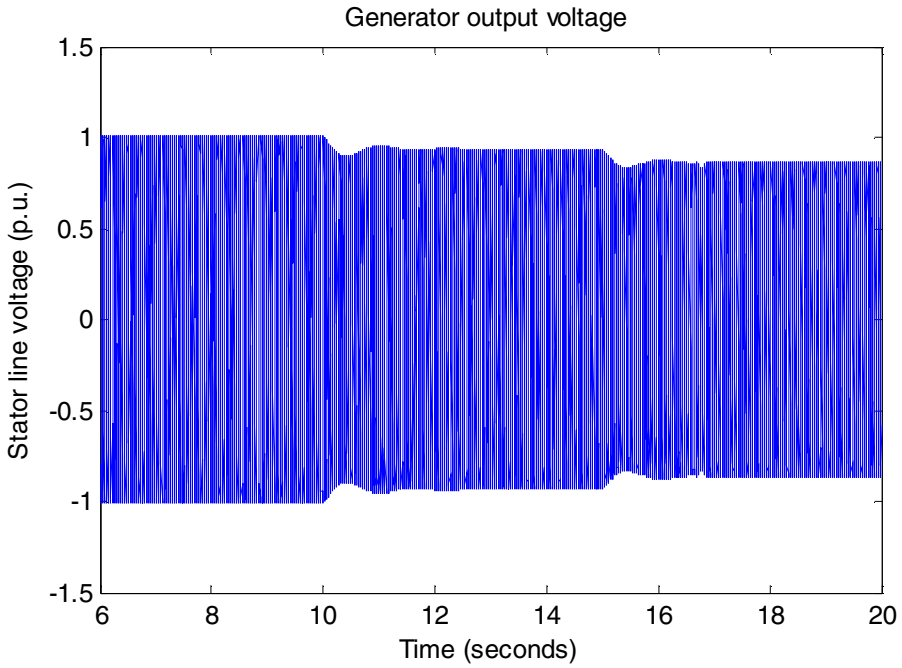

Figure 4.15 Voltage across the stator terminals of PMSG.

Figures 4.14 and 4.15 show the rotor speed and output voltage of the PMSG. When the MTG is operating at no-load, the speed of the rotor is equal to 1 p.u. and the stator line voltage of the PMSG reaches no-load steady-state value of 1.p.u. (1p.u.=6000 volts peak, Figure 4.15). When the PMSG is loaded at t =10 seconds, the voltage decreases from no-load value to 0.94 p.u. and the frequency of the voltage waveform decreases from 2.33 kHz to 2.17 kHz. At t=15 seconds, as the load is increased again, the rotor speed (Figure 4.14) and the stator voltage decrease further to 0.86 p.u. and 0.865 p.u., respectively.

Conclusion. The modeling of a single-shaft microturbine generation system suitable for power management in DG applications is presented in this chapter. The model is good for both, power only and CHP applications. Detailed mathematical modeling of the control systems of the microturbine is given and simulation of the developed MTG system model is carried out. A MATLAB/Simulink model of the proposed MTG system was implemented in the SimPowerSystems blockset. Different load conditions are applied on the MTG system. The simulation results show that the developed model of the MTG system has the ability to meet the power requirements of the load, within MTG's rating.

REFERENCES

4.1 Larry Goldstein, Bruce Hedman, Dave Knowles, Steven I. Freedman, Richard Woods and Tom Schweizer., "Gas-fired distributed energy resource technology characterizations," National Renewable Energy Laboratory, NREL/TP-620-34783, Nov. 2003.

4.2 Robert Lasseter, "Dynamic models for micro-turbines and fuel cells," in *Proceedings, IEEE PES Summer Meeting*, vol. 2, 2001, pp. 761-766, Jul. 2001, Vancouver, BC, Canada.

4.3 Hans B. Puttgen, Paul R. Macgregor and Frank C. Lambert, "Distributed generation: Semantic hype or the dawn of a new era," *IEEE Power and Energy Magazine*, vol. 1, no. 1, pp. 22-29, Jan. /Feb. 2003.

4.4 Anders Malmquist, "Analysis of a gas turbine driven hybrid drive system for heavy vehicles," Ph.D. dissertation, School of Electrical Engineering and Information Technology, KTH, Stockholm, Sweden, 1999.

4.5 Anders Malmquist, Ola Aglen, Edgar Keller, Marco Suter and Jari Wickstrom., "Microturbines: Speeding the shift to distributed heat and power," *ABB Review*, no. 3, pp. 22-30, Mar. 2000.

4.6 W. I. Rowen, "Simplified mathematical representations of heavy duty gas turbines", *Journal of Engineering for Power, Transactions ASME*, vol. 105, no. 4, pp. 865-869, Oct, 1983.

4.7 Working Group on Prime Mover and Energy Supply Models for System Dynamic Performance Studies, "Dynamic models for combined cycle plants in power system studies," *IEEE Transactions on Power Systems*, vol. 9, no. 3, pp. 1698-1708, August 1994.

4.8 Francisco Jurado and Jose Ramon Saenz, "Adaptive control of a fuel cell-microturbine hybrid power plant," *IEEE Transactions on Energy Conversion*, vol. 18 no.2, pp. 342-347, June 2003.

4.9 L. N. Hannet and Afzal Khan, "Combustion turbine dynamic model validation from tests," *IEEE Transactions on Power Systems*, vol. 8, no. 1, pp. 152-158, Feb. 1993.

4.10 L. M. Hajagos and G. R. Berube, "Utility experience with gas turbine testing and modeling," in *Proceedings, IEEE PES Winter Meeting*, vol. 2, 2001, pp. 671-677 Jan. / Feb. 2001, Columbus, OH.

4.11 Amer Al-Hinai, Ali Feliachi, "Dynamic model of a microturbine used as a distributed generator," in *Proceedings, 34th Southeastern Symposium on system Theory*, Huntsville,pp.209-213, Alabama, March 2002.

4.12 F. Jurado and A. Cano, "Use of ARX algorithms for modeling micro-turbines on the distribution feeder," in *IEE Proceedings: Generation Transmission and Distribution*, vol. 151, no. 2, pp. 232-238, Mar. 2004.

4.13 Anne-Marie Borbely and Jan F. Kreider, *Distributed Generation-The Power Paradigm for the new millennium*, CRC Press, 2001.

4.14 Web link: http://hyperphysics.phy-astr.gsu.edu/hbase/solids/magperm.html

4.15 Bimal K.Bose, *Modern Power Electronics and AC Drives*, Pearson Education, 2003.

4.16 Chee-Mun Ong, *Dynamic Simulation of Electric Machinery*, Prentice Hall, 1998.

4.17 Y. Zhu and K. Tomsovic, "Development of models for analyzing the load-following performance of microturbines and fuel cells," *Journal of Electric Power Systems Research*, vol. 62, pp. 1-11, 2002.

4.18 MATLAB/Simulink Documentation. Available: http://www.mathworks.com

CHAPTER 5

HYBRID WIND-MICROTURBINE GENERATION SYSTEM

Introduction

In this chapter power management of a hybrid (wind-microturbine) generation system is presented. A brief description of the power electronic interface is given, through which the output of the each generating unit is passed before they are connected to a common load.

Two major problems have to be addressed when employing non-dispatchable distributed generation sources, such as wind (the renewable source of energy considered in this thesis), for electric power generation. The first issue is the unpredictable nature of wind and the subsequent need for standby energy systems to ensure continuity of supply. The second issue is the usage of induction generator as an electrical generator. While these machines are well suited for variable speed nature of wind turbines, they can not operate without reactive power support from the network to which they are connected. Therefore, the ability to provide a reliable supply to the load depends on successful integration of the renewable resources (wind energy, in this case) with existing non-renewable sources of energy; addressing the above mentioned concerns.

In this thesis, a microturbine generation system (MTG) is considered as the backup generator, to meet the energy requirements when wind energy is not sufficient. Thus, we

have a hybrid system consisting of a wind energy conversion system (WECS) and a microturbine supplementing each other. Such a system could also be referred as a virtual power plant and could be operated either in grid-connected mode (not discussed in this thesis) or in a stand-alone (isolated) mode. Hybrid systems in general are influenced by factors like input (wind) and load conditions, which may affect their voltage and frequency, necessitating the use of power electronics to control and maintain these system variables at desired values. The power electronics interface used in this thesis is taken from [5.1] and has been adapted for the system under consideration.

In the last section of this chapter, a hybrid configuration comprising of a WECS and a MTG system interconnected through a power electronics interface is simulated. The power electronic controls presented have the ability to manage the real and reactive power components at prescribed level. The system response under different load conditions and the load management ability of the power electronics are shown through simulations studies carried out in MATLAB/Simulink.

Hybrid Wind-Microturbine System

A hybrid generation system consisting of a 370kW WECS and a 400kW MTG system along with the power electronics interfacing is presented in this section.

Although a hybrid plant may use other combinations of energy sources, the combination of wind generation and MTG systems are particularly complimentary [5.1], [5.2]. Wind power generation is high on capital cost and low on operational cost; Once

installed there no ongoing fuel costs and the maintenance costs are also very low. On the other hand, gas turbine generation is low on capital cost and high on operational cost compared to wind turbine due to its need for fuel and maintenance. This combination is also environmentally friendly in that the emission of greenhouse gases from the microturbine is very low compared to the conventional fossil fuel steam turbines. Figure 5.1 shows the block diagram of the proposed system.

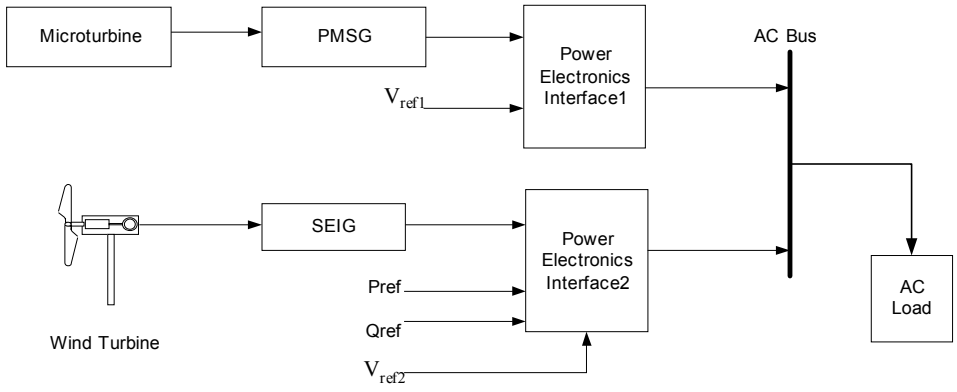

Figure 5.1 Block diagram of the hybrid generation system.

Description of the System

The hybrid system, shown in Figure 5.1, consists of models for WECS, MTG, and power electronics interfacing connected to an AC bus which supplies an AC load. The WECS and MTG system were presented in chapters 2, 3 and 4, respectively. In the following paragraph, a brief description the power electronics interfacing [5.3] is given.

Power Electronics Interface

In order to realize a hybrid system, the output voltage and frequency of each component should be maintained at a predetermined level so that the interconnection between the different components of the hybrid system can be achieved. This is made possible by employing power electronics interface which has the ability to control the system output variables such as voltage, frequency, active and reactive power to keep or bring them to match their reference values after a disturbance. In the hybrid configuration considered, the WECS and the MTG system each have their own *dq* transformed [5.4] power electronics interface and the control logic is the same in both cases. The power electronics interface comprises of a rectifier and voltage source inverter. A pulse width modulation (PWM) controller was used to control the inverter in order to satisfy the voltage regulation as well as to achieve real and reactive power control [5.3]. A brief description of each sub system of this block is given in the following sections.

The power electronics interface used has the ability to control the real and reactive power by controlling the inverter output voltage, angle and frequency [5.3]. This is realized by converting AC power output from the generator in to DC and then in to AC. A 3-phase uncontrolled rectifier made up of six bridge connected diodes has been used to rectify the generator output from AC to DC. A voltage source inverter (VSI) is then employed to convert the DC output from the rectifier to AC. Control of voltage source inverter is achieved by means of two control loops namely, the inner current control loop

and the outer voltage regulator loop. The overall system along with its control strategies is shown in Figure 5.2.

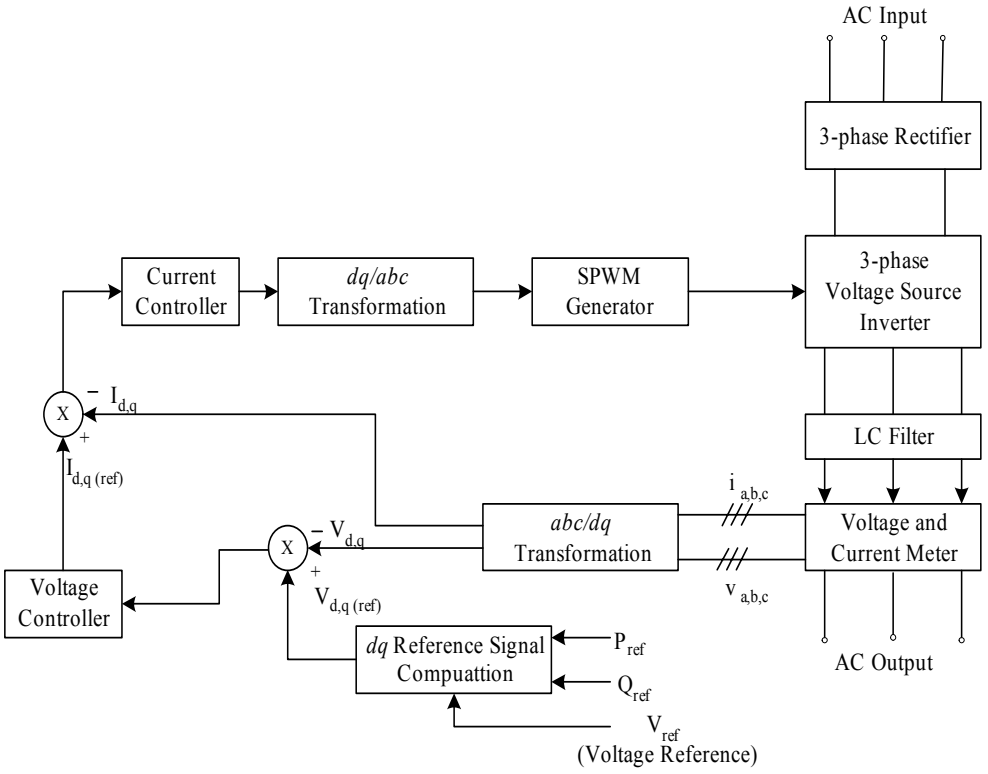

Figure 5.2 Block diagram of the power electronics interfacing.

The "*abc/dq* Transformation" block takes the time varying currents and voltages (in *abc* coordinates) from the voltage and current measurement devices and converts them into *dq* (time-invariant) values. The voltage controller takes the error signals between the actual output in *dq* frame ($V_{d,q}$) and the reference voltage ($V_{d,q(ref)}$) and generates the current reference signals ($I_{d,q(ref)}$) for the current controller loop. The current controller produces the *dq* control signals, which are converted back to the control signals in *abc* coordinates through the "*dq/abc* Transformation" block. These control signals are used

generate the gating pulses for the inverter to control its output voltage, using sinusoidal pulse-width modulation (SPWM) generator. In the following paragraphs the control principle of the power electronics interfacing along with the control loops are presented.

Control Principle. Consider a circuit having a sending end voltage of $V_s \angle \delta$ and receiving end voltage equal to $V \angle 0^0$, connected through a coupling impedance of (R+jX), as shown in Figure 5.3.

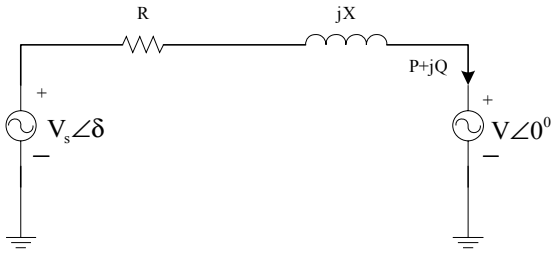

Figure 5. 3 Power flow between two points.

The real and reactive power transferred between the source and load end are [5.3]:

$$P = \frac{VV_s}{Z} cos(\theta_z - \delta) - \frac{V^2}{Z} cos(\theta_z) \tag{5.1}$$

$$Q = \frac{VV_s}{Z} sin(\theta_z - \delta) - \frac{V^2}{Z} sin(\theta_z) \tag{5.2}$$

Where $Z = \sqrt{R^2 + X^2}$ and $\theta_z = tan^{-1}(X/R)$.

From (5.1) and (5.2) it is clear that the real and reactive powers delivered are completely determined by the amplitude and angle of the sending voltage source, i.e. the

output voltage of the inverter. On the other hand, if the desired values of real and reactive power are given, the values of V_s and δ can be determined from (5.3) and (5.4):

$$V_s = \left[\frac{Z^2}{V^2}\left(P^2 + Q^2\right) + V^2 + 2PZcos(\theta_z) + 2QZsin(\theta_z) \right]^{\frac{1}{2}} \tag{5.3}$$

$$\delta = \theta_z - cos^{-1}\left(\frac{ZP}{VV_s} + \frac{V}{V_s} cos(\theta_z) \right) \tag{5.4}$$

The corresponding *dq0* component values of V_s in (5.3) can be obtained through *abc/dq* transformation, as discussed in chapter 3. In Figure 5.2, the "*dq* Reference Signal Computation" block uses (5.3) and (5.4) to calculate the magnitude and angle of the filtered output voltages of the inverter and then convert them into *dq* voltage reference signals using *abc/dq* transformation.

3-Phase Voltage Source Inverter. The DC power output from the uncontrolled rectifier is converted to AC by a 3-phase voltage source inverter, and delivered to a load as shown in Figure 5.4. It also shows the connection to the AC load bus through *LC* filters and coupling inductors [5.3].

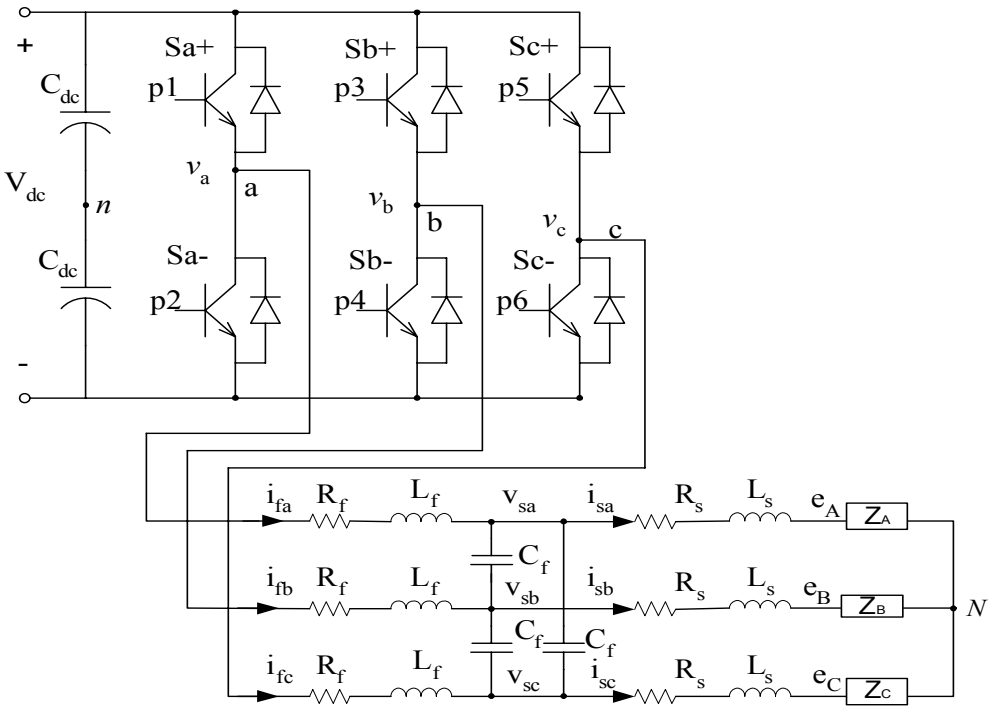

Figure 5.4 Three-phase DC/AC voltage source inverter.

In the Figure 5.4, *R*, *L* and *C* denote resistance, inductance and capacitance values. Z_A denotes the load impedance of phase *A*. The subscripts *f* and *s* denote filter and coupling inductor parameters respectively. *N* is the common reference point and *n* is a virtual neutral point. V_{dc} is the DC bus voltage. The output phase potentials of the inverter, v_a, v_b and v_c, can be obtained as $v_a = v_{an} + v_n, v_b = v_{bn} + v_n, v_c = v_{cn} + v_n$, where v_{an}, v_{bn} and v_{cn}, the inverter output voltages between each phase and its virtual neutral point *n*. The voltage of phase *A* at the receiving end (load end) is given by e_A.

Current Controller. Current control forms the inner control loop of the overall control system and is designed to respond faster than the voltage control loop so that the two control loops can be designed independently. As a result, when dealing with the inner

loop, we take the voltage control loop as a constant input (i.e., $I_{d,q(ref)}$ is constant in Figure 5.2). The current controller employed is a PI controller and the parameters used are obtained from [5.3]. The block diagram of the current controller is shown in Figure 5.5.

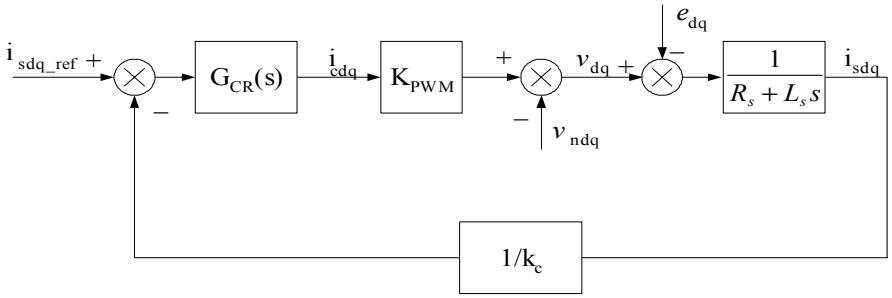

Figure 5.5 Block diagram of the current control loop for the inverter.

In Figure 5.5, $G_{CR}(s) = k_{cp} + \frac{k_{ci}}{s}$ is the current regulator, I_{cdq} is dq component of the current regulator output, K_{PWM} is the overall gain of the PWM generator for the inverter, $\frac{1}{R_s + L_s}$ is the equivalent admittance of the combination of LC filter, power transformer, coupling inductor and transmission line, and $1/k_c$ is the current transducer ratio. v_{ndq} is the dq component of the virtual neutral point voltage[1].

---

[1] $\begin{bmatrix} v_a \\ v_b \\ v_c \end{bmatrix} K_{abc/dq} = \begin{bmatrix} v_{an} + v_n \\ v_{bn} + v_n \\ v_{cn} + v_n \end{bmatrix} K_{abc/dq} = v_{dq} + v_{ndq}$, where $K_{abc/dq}$ is the abc to dq transformation matrix.

Voltage Controller. A PI controller is employed to implement voltage controller. As discussed above, this controller forms the outer loop in Figure 5.2 and is slower compared to the inner current control loop [5.3]. This facilitates the approximation of the current control loop (in Figure 5.2) as a simple lag block when analyzing the voltage controller. The block diagram of the voltage controller is shown in the Figure 5.6:

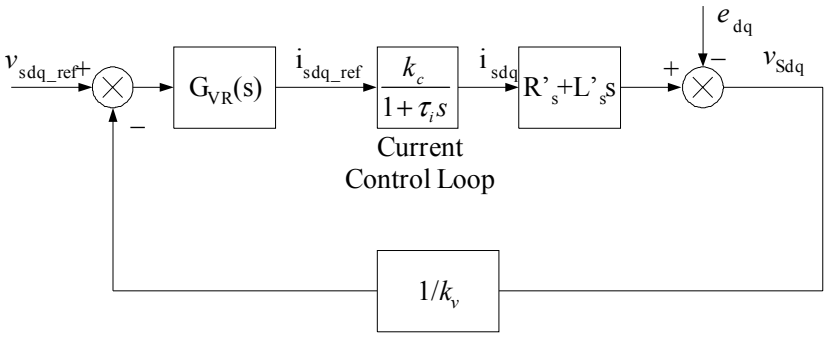

Figure 5.6 Block diagram of the voltage control loop for the inverter.

In Figure 5.6, $G_{VR}(s) = k_{vp} + \frac{k_{vi}}{s}$ is the voltage regulator, $\frac{k_c}{1+\tau_i s}$ is the lag approximation for the inner current loop, $(R_s' + L_s' s)$ is the equivalent impedance of the combination of the power transformer, coupling inductor and transmission line, and $1/k_v$ is the voltage transducer ratio.

The parameters of the current and voltage controllers are as follows [5.3].

Table 5.1 Parameters of the controllers for 3-phase VSI.

K_{ci}	K_{cp}	K_{vi}	K_{vp}
250	2.5	25	0.25

Simulation Results

A model for the hybrid wind-microturbine generation system, shown in Figure 5.1, is built in the MATLAB/Simulink. This is achieved by integrating the dynamic models of the WECS and the MTG system through the power electronics interfacing. The maximum power output from the WECS is 370kW and that of the MTG system is 400kW. So, the hybrid system is capable of supplying 400kW at any time of the day irrespective of prevailing wind conditions. Simulation parameters used for the WECS can be found in chapter 2 and 3, and the MTG system parameters are given in chapter 4. The following paragraph explains the control principle behind the power management of the hybrid generation system. Simulation results for the hybrid generation system under different wind and load conditions follows next. The simulink diagrams of the hybrid system are given in the appendix, at the end of this thesis.

The power reference P_{ref}, (Figure 5.1), for the WECS power electronics interfacing is obtained by using the wind turbine simulations results (see chapter 2). Figure 2.8 gives the power output of the wind turbine for different wind velocities. This can be represented in the form of a look-up table whose input is wind velocity, and output is the power reference (P_{ref}). The reactive power reference Q_{ref} for the WECS is kept constant at zero as the SEIG of the WECS is assumed to be operating on unity power factor. The voltage references V_{ref1} and V_{ref2} for the MTG system and WECS (Figure 5.1) are kept constant at 1p.u. in order to maintain AC bus voltage (at 1.p.u.). As a result, whenever there is not enough power output from the wind turbine, to meet the load requirement, the

voltage at the load terminals tends to drop from 1 per-unit. The power electronics interface connected to the MTG system counters this drop by increasing the power output from the microturbine and thereby maintaining the load voltage at a constant value of 1 per-unit. Since the output voltage levels of the PMSG and SEIG are different (Figures 3.15 and 4.15), a transformer with 1:2 turns ratio is used in between the inverter output and the AC load (in side the *power electronics interface2*), to increase the output voltage of the SEIG to an acceptable level.

For the following simulation results, all values are referred to a base power rating of 1MVA and a base voltage rating of 2400 volts. The speed reference for the microturbine is kept constant at 1 per-unit. Initially the wind turbine is not connected to the hybrid system and the MTG system is supplying the total load demand. At t=10 seconds, the WECS is connected to the MTG system. Although with the help of power electronic interfacing it is possible to get some reactive power output from the WECS, in this study, it is assumed that the reactive power contribution from the WECS is zero. Accordingly, Q_{ref} (in Figure 5.1) is kept constant at zero for all simulations. Different wind and load conditions are applied, and results are presented in the following paragraphs. Simulation results of the hybrid generation system including responses of the subsystems, for the first case, are given with a brief discussion of each result. Power and voltage outputs of the hybrid generation system are presented for remaining case studies.

Case 1. (Rise in wind input –Constant load)

The wind velocity remained constant at 9m/s, until t=15 seconds and then starts ramping up reaching a final value of 12m/s at *t*=16 seconds. This change in the wind velocity is shown in Figure 5.7. As said above, MTG system is supplying the total load demand of (0.4+j0.2) per-unit until the WECS is connected to the MTG system at *t*=10 seconds.

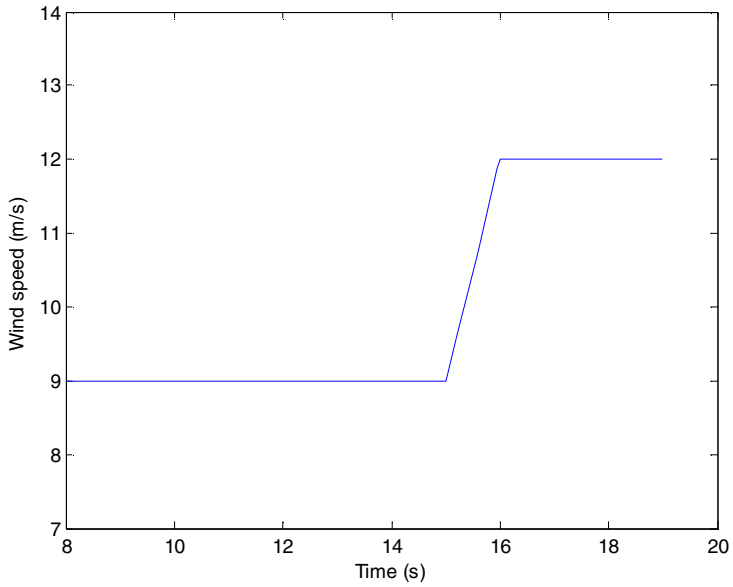

Figure 5.7 Wind input to the hybrid generation system.

The real power outputs of the MTG system and the WECS for the above mentioned wind and load conditions are shown in Figures 5.8 and 5.9, respectively.

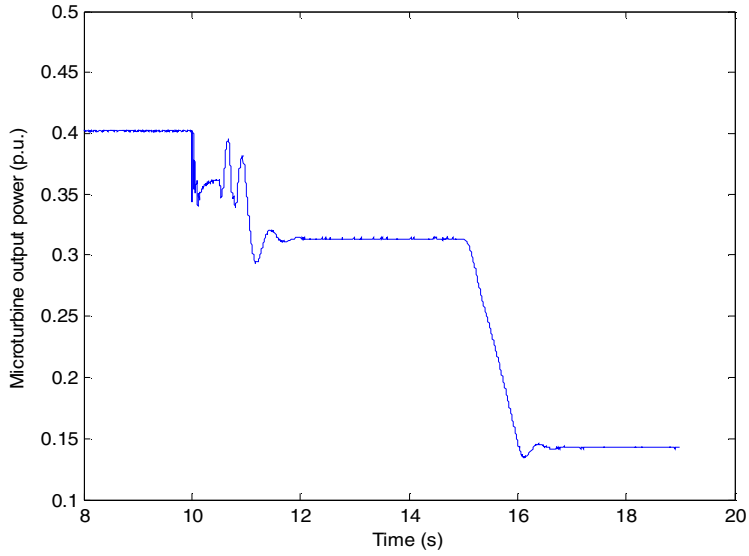

Figure 5.8 MTG system real power output variations with wind.

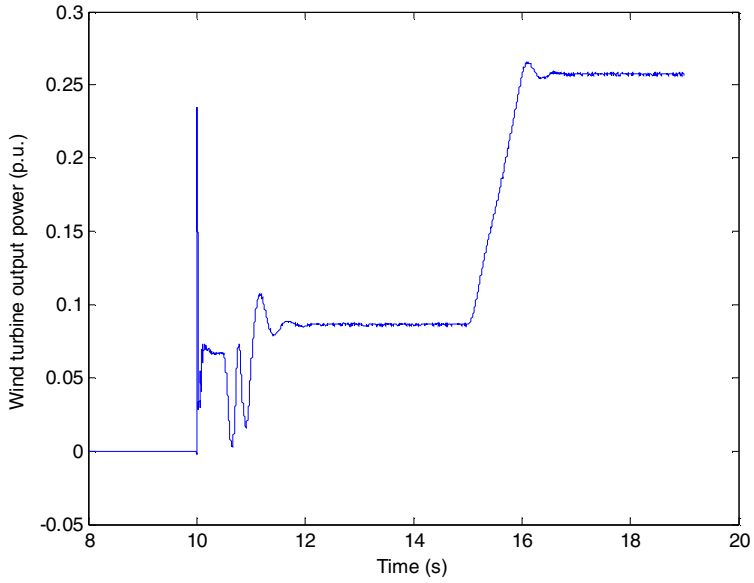

Figure 5.9 WECS real power output variations with wind.

Figure 5.8, shows that the MTG system alone is capable of supplying the total real power requirement of the load (400 kW) before the WECS is connected to the hybrid generation system. At t=10 seconds, the WECS is connected to the hybrid system and the

real power output from the MTG drops which corresponds to an increase in the WECS output power. From the chapter 2 (Figure 2.8) simulations, it is known that the wind turbine output for a wind velocity of 9 m/s is about 85 kW. This will be the output of the look-up table which is fed to the *power electronics interface2* as P_{ref} in p.u. (85 kW=0.085 p.u.). Figure 5.9 shows the output power produced by the WECS which is about 0.085 p.u. (85 kW). Since the load power requirement is 0.4 p.u. (400 kW) the remaining 0.315 p.u. is produced by the MTG system to maintain the AC bus (load) voltage at 1 per-unit. As the wind velocity changes from 9 m/s to 12 m/s, between t=15 and 16 seconds, the wind turbine is capable of producing more power. Correspondingly, P_{ref} (Figure 5.1) to the *power electronics interface2* is also increased to 0.275 p.u. (Figure 2.8). Observe that the output from the MTG system decreases from 315 kW (0.315 p.u.) at t=15 seconds to 0.14 p.u. around t=16.5 seconds. During the same time the WECS output increases from 0.085 p.u. to 0.26 p.u. (Figure 5.9). From Figures 5.8 and 5.9, it can be observed that at any point of time the real power requirement of the AC load connected to the hybrid generation system is satisfied. Note that, the difference between the reference power and the output power of the WECS is more pronounced at higher power output. This is expected; as the output power increases correspondingly power losses in the interfacing components between the hybrid generation system and the load (e.g. the transmission line and the power electronic interfacing) are also increased.

Figures 5.10 and 5.11 show the output reactive power variations of the MTG and WECS, respectively, for the given wind conditions shown in Figure 5.7. It was noted in

chapter 3, that the SEIG (of the WECS) fails to self-excite if the reactive power provided by the excitation capacitor is not sufficient to satisfy the combined reactive power requirement of the induction generator and inductive component of the AC load (if there is any). Consequently, in the hybrid generation system, the reactive power requirements are met by the MTG system and the SEIG supplies the active power whenever there is sufficient wind (with the presence of power electronics interfacing, it is possible to extract reactive power from the WECS also).

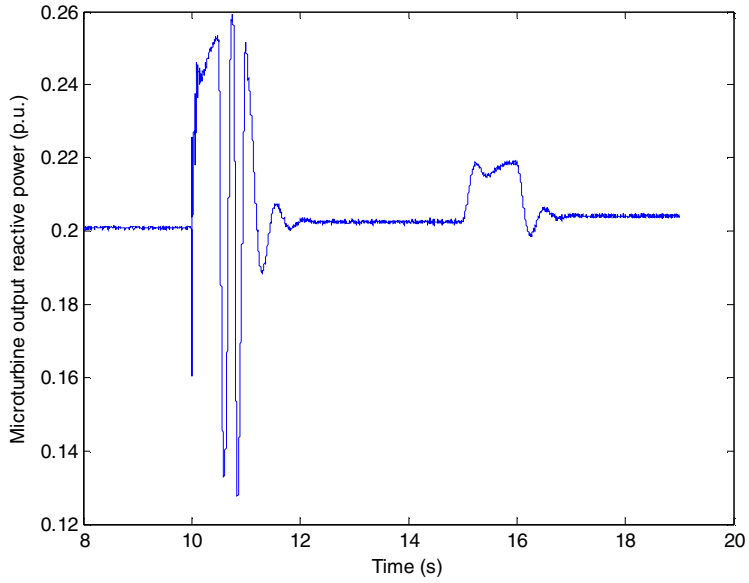

Figure 5.10 MTG system output reactive power variations with wind.

Figure 5.10 shows that the MTG system meets the reactive power needed by the AC load (0.2 p.u.). The reactive power output from the WECS (Figure 5.11), as explained in the above paragraph, remained at zero (followed Q_{ref}=0) following a disturbance in the wind after short transient periods.

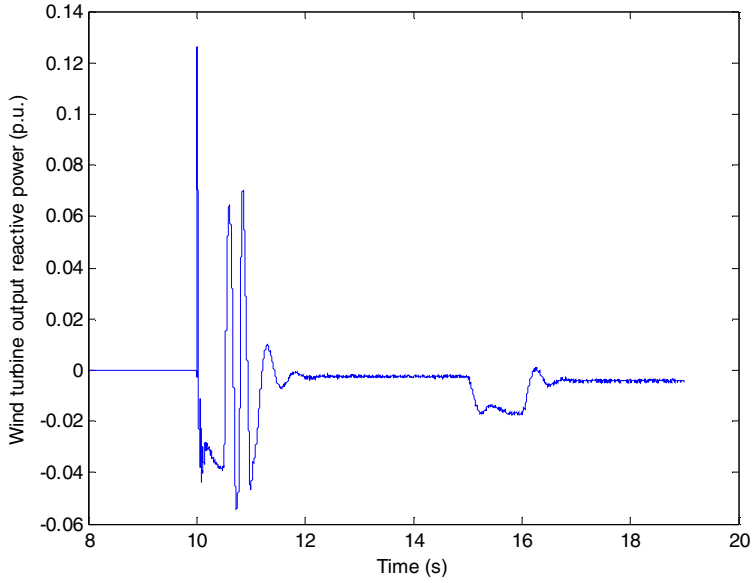

Figure 5.11 WECS output reactive power variations with wind.

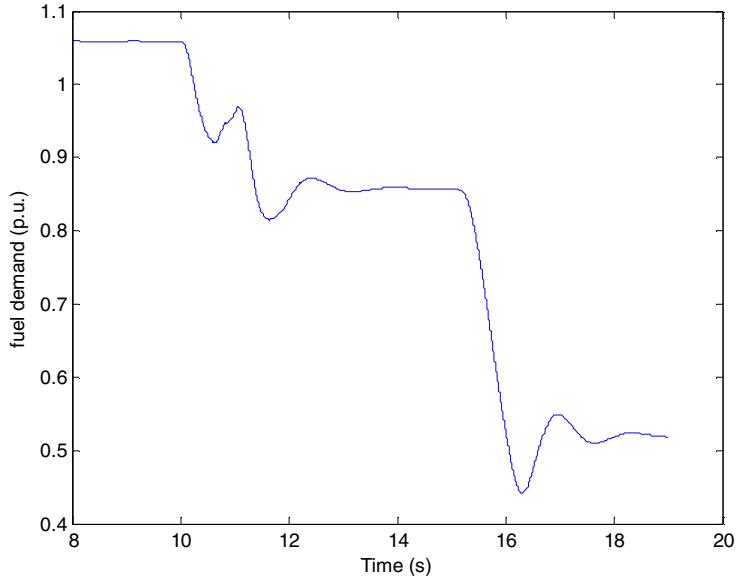

Figure 5.12 Fuel demand signal of the microturbine.

Figure 5.12 shows fuel consumed by the microturbine for the applied load conditions. It can be observed that the fuel demand signal is slightly higher than 1.p.u. when

operating at full load. This is possible as the microturbine tries to meet the losses associated with power electronics interface. The fuel demand signal is about 0.85 p.u. at 0.315 p.u. load and drops to 0.52 p.u. after t=15 seconds, as the power produced by the WECS increases with increased wind velocity.

Figures 5.13 and 5.14 show the rotor speed variations of the microturbine and the SEIG, respectively.

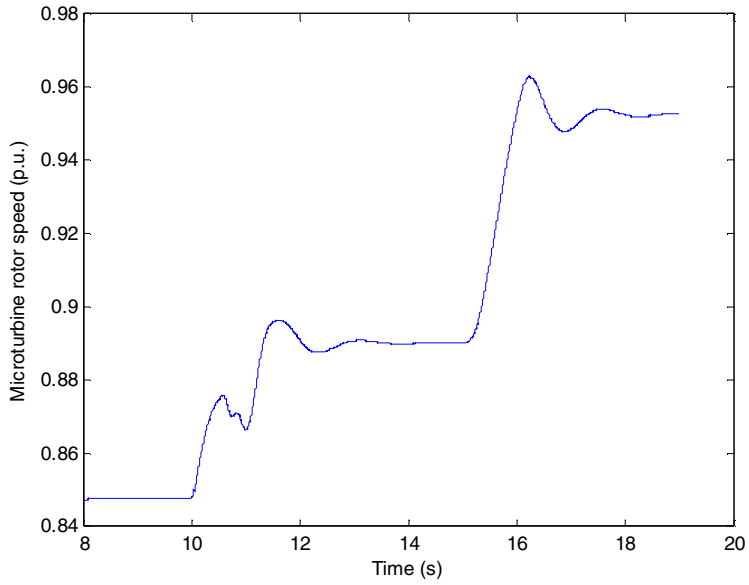

Figure 5.13 Microturbine rotor speed variations.

The microturbine rotor speed (Figure 5.13) has a value of 0.85 p.u. (1 p.u.= 70000 rpm) at full load and increases as the load demand on the MTG system decreases. Correspondingly, the speed of the SEIG (Figure 5.14) during same time period is 1 p.u. (base speed =1500 rpm) as it is rotating freely under no-load conditions. At t=10 seconds, the WECS is connected to the hybrid generation system. As a result, the WECS starts

supplying the AC load and the rotor speed drops from 1.p.u. to 0.775 per-unit. As the wind input increases from 9 m/s to 12 m/s (Figure 5.7), turning the wind turbine blades at a faster rate and as a result, the rotor speed increases to 0.92 per-unit. This rise in rotor speed results in increased power output (Figure 5.9), which causes a further decrease in the power requirement from the MTG system. As a result the microturbine rotor speed increases to 0.95 p.u. (Figure 5.13).

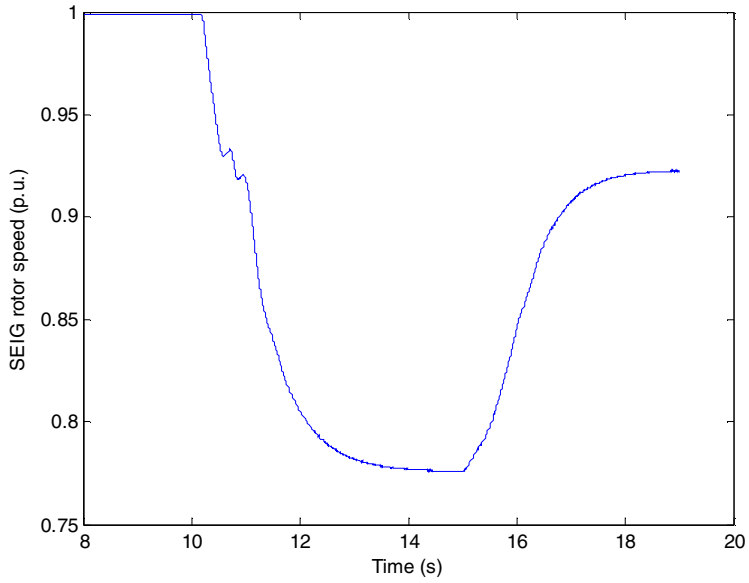

Figure 5.14 SEIG rotor speed variations.

Figure 5.15 shows the variation of the DC bus voltage at the output of the 3-phase rectifier on the MTG side (Figure 5.2). The DC bus voltage increases form 4720 volts to 5000 volts as the load demand reduces from full load (0.4 p.u.) to 0.315 per-unit. Also, it can be seen that as the microturbine rotor speed (Figure 5.13) increases form 0.92 p.u. to

0.95 p.u., the DC bus voltage increases from 5000 volts at 0.315 p.u. load to 5450 volts at a decreased load demand of 0.14 p.u.

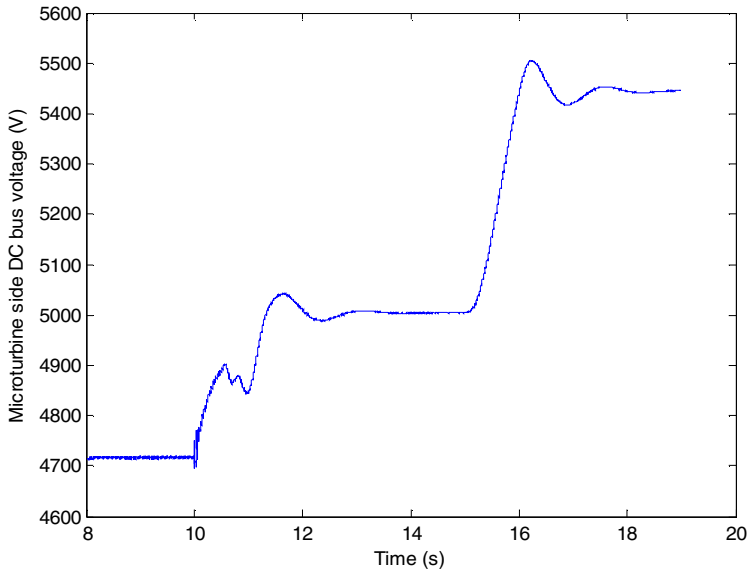

Figure 5.15 Variation of DC bus voltage on the MTG side.

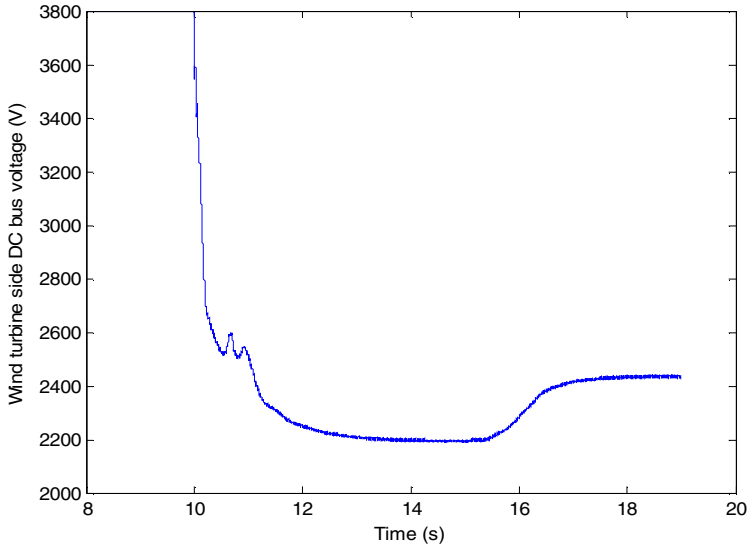

Figure 5.16 Variation of the DC bus voltage on the WECS side.

Figure 5.16 shows the variation of the DC bus voltage on the WECS side of the hybrid generation system (Figure 5.1). The DC bus voltage decreases form 3800 volts to 2200 volts when the load demand increases from no-load to 0.085 p.u. with a rotor speed equal to 0.775 p.u. (Figure 5.14). At t=15 seconds, with an increase in the wind speed the rotor speed increases and correspondingly (the output voltage and thereby) the DC bus voltage of the WECS increases to 2450 volts. Unlike microturbine, here we can see that the voltage is greatly dependent on rotor speed, which is in turn based on the wind speed, and the load.

Figures 5.17 and 5.18 show the voltage levels of the hybrid generation system at the output terminals of *power electronics interface1* and *power electronics interface2*, respectively (Figure 5.1).

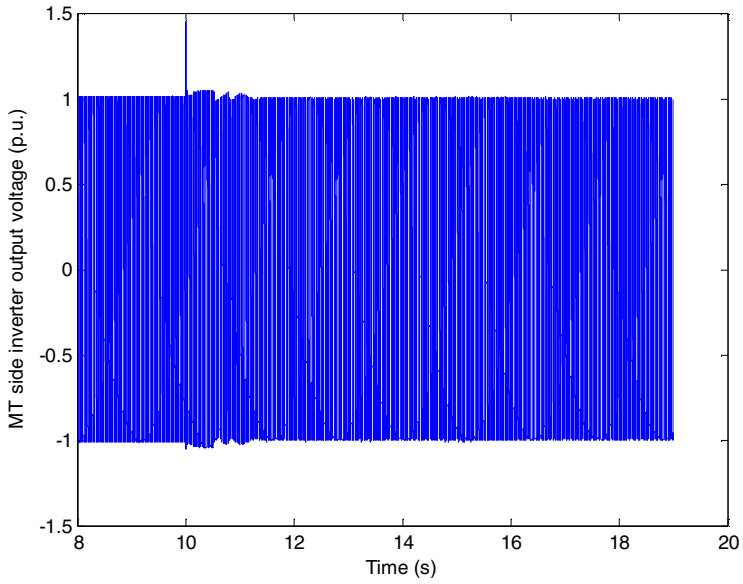

Figure 5.17 MTG side inverter output voltage.

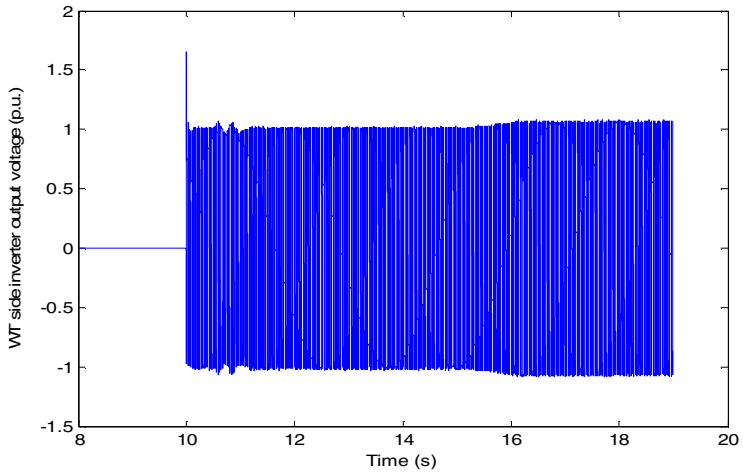

Figure 5.18 WECS side inverter output voltage.

The above figures show that the output voltages at the terminals of the 3-phase inverters of the MTG system and the WECS are maintained at the same level of 1.p.u. at all times, with the exception of small disturbances during load switching. This demonstrates the ability of the power electronics interfacing (Figure 5.2) to maintain the inverter output voltage at the prescribed levels of voltage and frequency (60Hz). Figure 5.17 shows the voltage level on the MTG side, along with the transients when it is connected to the WECS. Figure 5.18 voltage level, on the WECS side, when it is connected to the system at t=10 seconds. After t=10 seconds, the voltage and frequency levels remained the same irrespective of the variations in the DC bus voltages (Figures 5.15 and 5.16), rotor speeds (Figures 5.13 and 5.14), except that the WECS side inverter is slightly higher than 1 p.u. at higher power output (at wind velocity of 12m/s).

Case 2. (Drop in wind input-Constant load)

The wind velocity remained constant at 14m/s, until t=14 seconds and decreased to a final value of 12m/s at t=15 seconds. This change in wind velocity is shown in Figure 5.19. To begin with the MTG system is supplying the total load demand of (0.4+j0.2) per-unit. At t=10 seconds the WECS is connected to the MTG system.

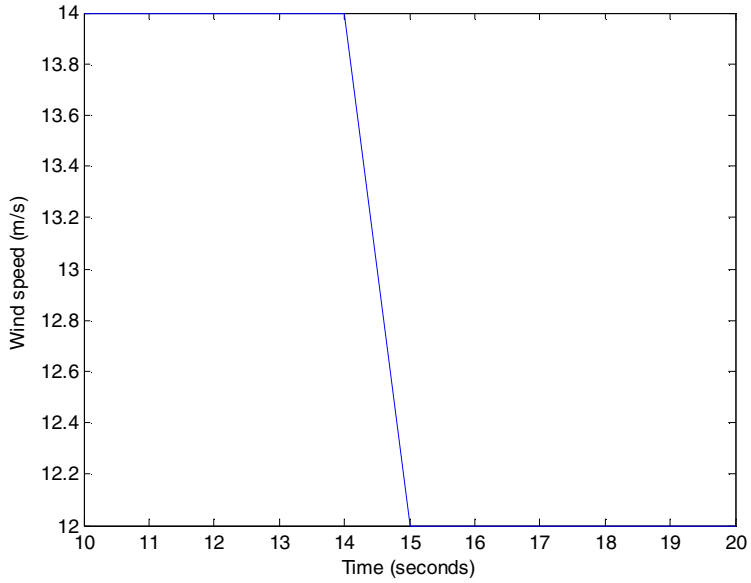

Figure 5. 19 Wind input to the hybrid generation system.

The real power outputs of the MTG system and the WECS for the above mentioned wind and load conditions are shown in Figures 5.20 and 5.21, respectively. These figures demonstrate the ability of the MTG system acting as a backup generator for the WECS, as explained in the following paragraph.

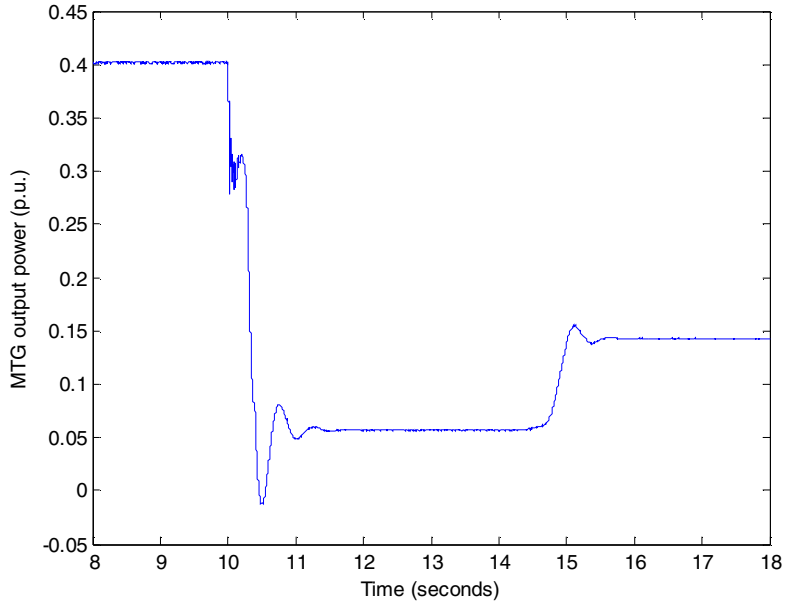

Figure 5. 20 MTG system real power output variations with wind.

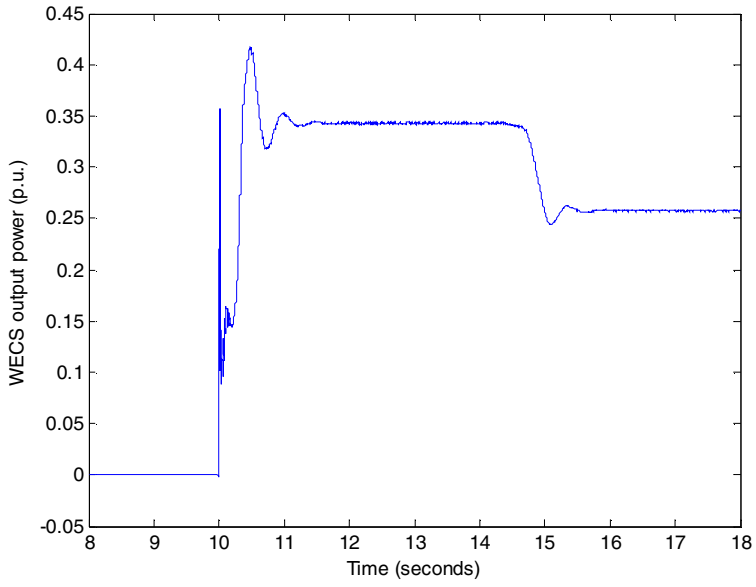

Figure 5. 21 WECS real power output variations with wind.

Figure 5.20, shows the decrease in real power output of the MTG system from 400 kW to about 50 kW when WECS starts supplying the load at t=10 seconds. At a wind

velocity of 14m/s the wind turbine has the capability to produce its rated output, 370 kW. Considering the losses, associated with the wind turbine, SEIG and the power electronic interfacing, the net output at the SEIG output terminals is about 350 kW. So, together the MTG and the WECS supply 400 kW power to the load with most of the load demand met by the WECS. At t=15 seconds, with reduced wind input, the output of the WECS falls to about 260 kW and the MTG picks up the remaining load of 140 kW.

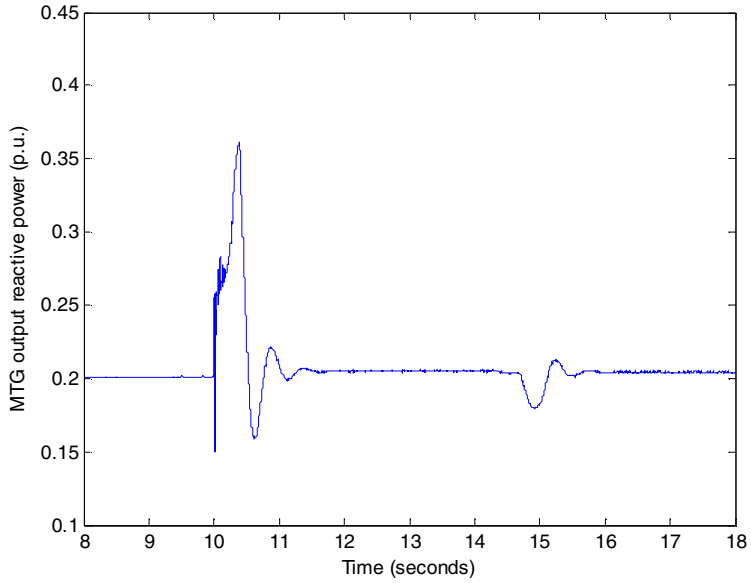

Figure 5. 22 MTG system reactive power variations with wind.

Figure 5.22 shows the reactive power supplied by the MTG system to the load. It can be observed from the figure that the entire reactive power is supplied by the MTG system as the reactive power output from the WECS follows its reference value which is zero (Figure 5.23). The MTG system output shows a transient when the WECS is connected, but otherwise remains fairly constant.

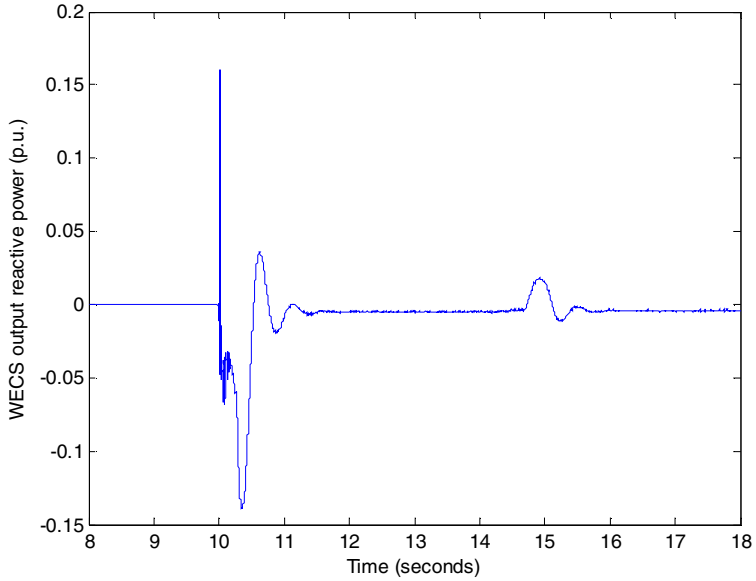

Figure 5. 23 WECS reactive power variations with wind.

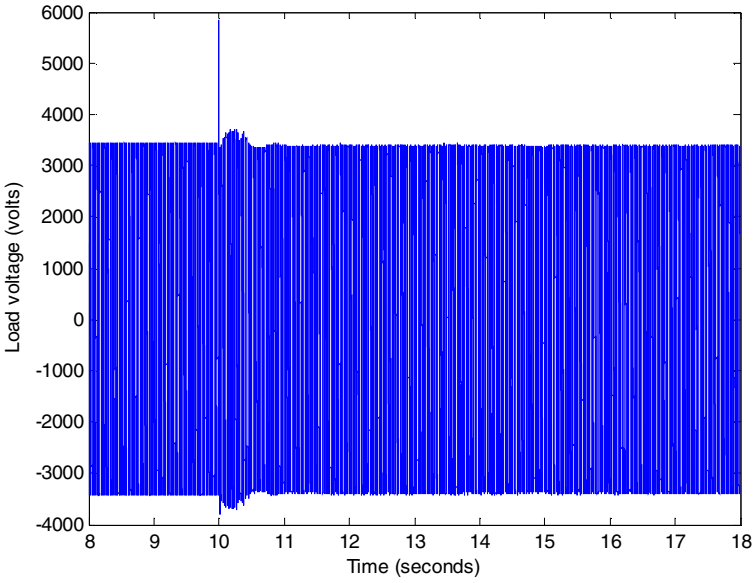

Figure 5. 24 Voltage at the load terminals.

Figure 5.24, shows the voltage at the AC load terminals. It can be observed that the voltage matches well with the voltage reference (2400 volts RMS), and remained constant, except for a switching transient at *t*=10 seconds.

Case 3. (Rise in load demand-Constant wind)

In this case, the input wind velocity remained constant at 9.3 m/s and the load demand changed from (0.25+j0.1) per-unit to (0.4+j0.2) per-unit at t=11 seconds, as shown in Figure 5.25. Initially, the MTG system is supplying the total load demand; the WECS is connected in parallel to the MTG system at *t*=10 seconds. The step change in load is applied at *t*=11 seconds, without giving much time for the wind turbine output to reach a steady state value.

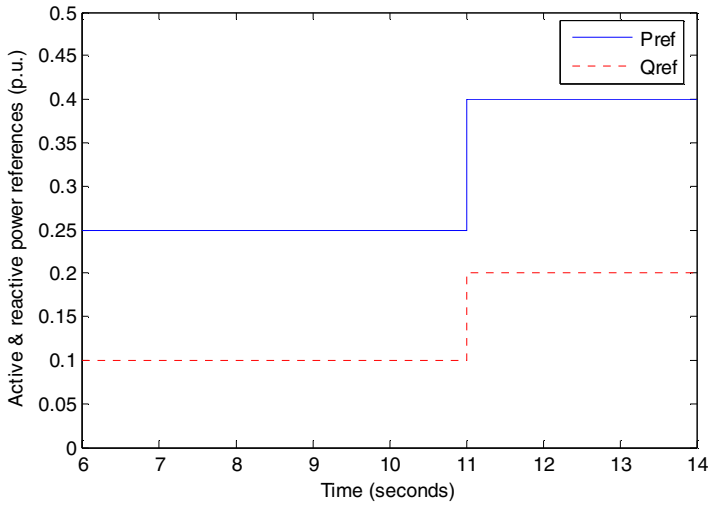

Figure 5. 25 Load demand of the hybrid generation system.

The real power outputs of the MTG system and the WECS for the above mentioned wind and load conditions are shown in Figures 5.26 and 5.27, respectively. These figures

demonstrate the ability of the hybrid system in power management, as explained in the following paragraph.

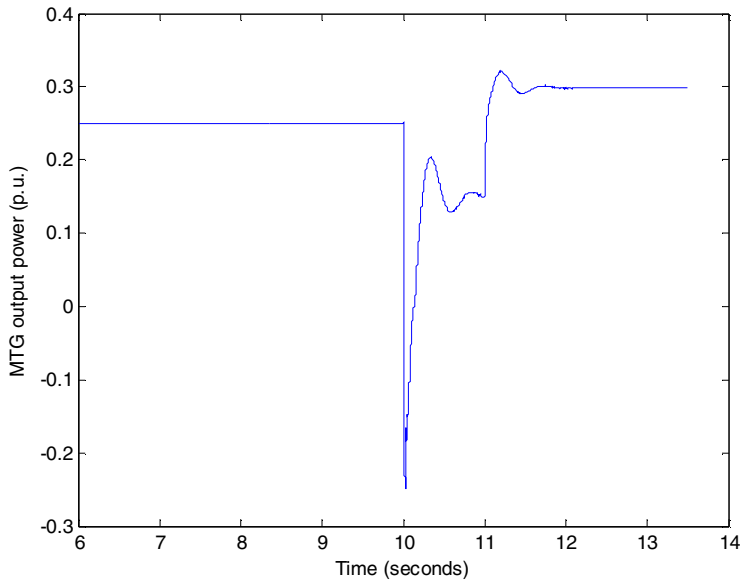

Figure 5. 26 MTG system real power output variations with load.

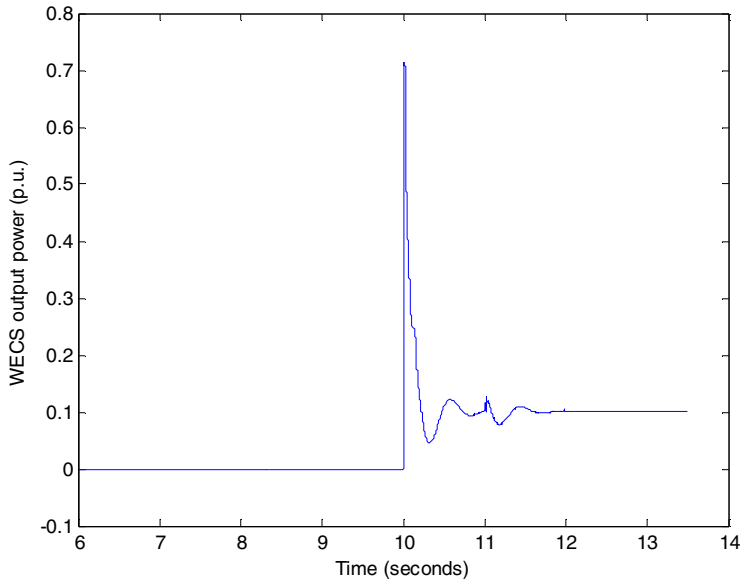

Figure 5. 27 WECS real power output variations with load.

Figure 5.26, shows the decrease in real power output of the MTG system from 250 kW to about 150 kW when WECS starts supplying the load at *t*=10 seconds. At the wind velocity of 9.3m/s, the wind turbine has the capability to produce an output power of 100 kW. As load demand increases from 250 kW to 400 kW at *t*=11 seconds, the microturbine picks up the additional load and its output reaches a final value of 300 kW. During the same period, as the wind velocity remained constant, the WECS output remained constant (Figure 5.27) at 100 kW.

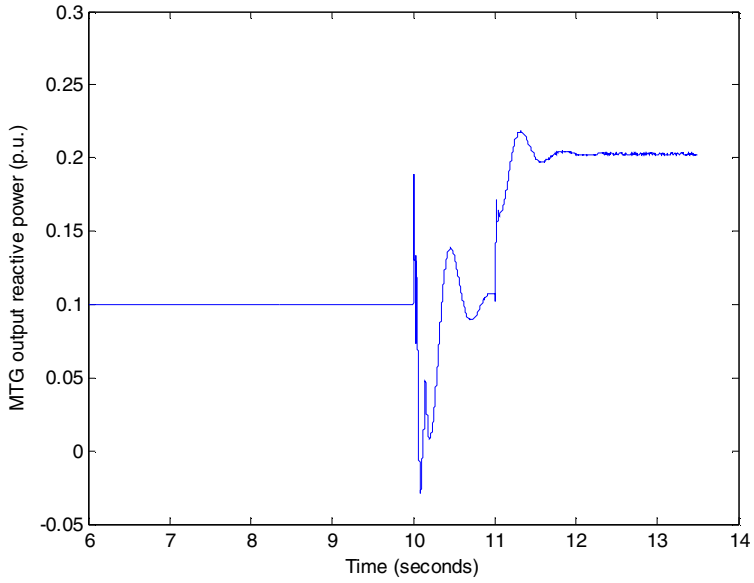

Figure 5. 28 MTG system reactive power variations with load.

Figure 5.28 shows the reactive power supplied by the MTG system to the load. The MTG system reactive power output remains constant at 0.1 p.u. until t=11 seconds, except for the transients at the instants of switching of WECS and load, and then rises to 0.2 p.u. to pick up the reactive power demand of the load. The WECS output reactive

power output (Figure 5.29) reaches its reference value equal to zero after the load switching transients.

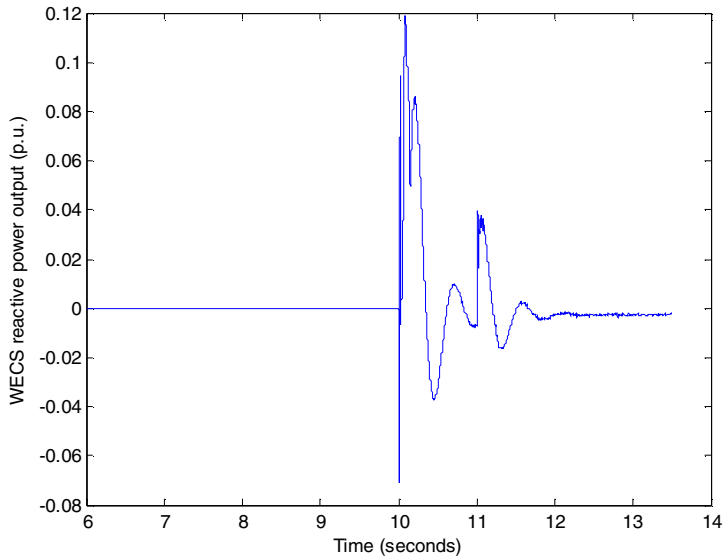

Figure 5. 29 WECS reactive power variations with load.

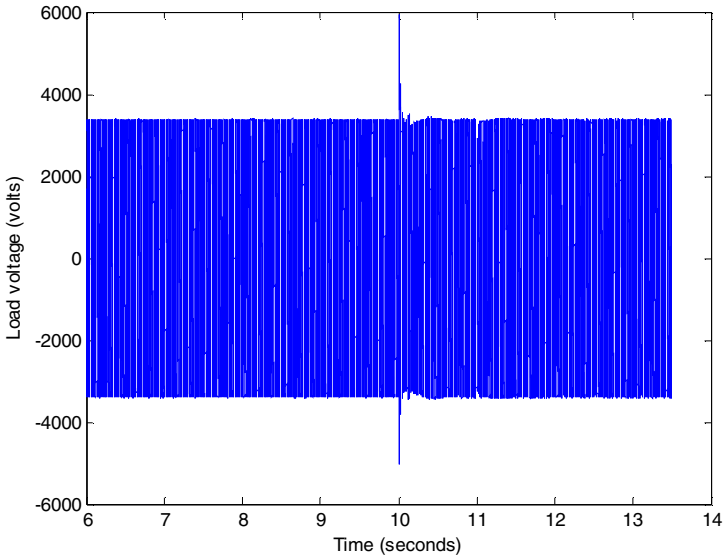

Figure 5. 30 Voltage at the load terminals.

Figure 5.30, shows the voltage at the AC load terminals, which is at its reference value of 2400 volts (RMS), irrespective of the changing load conditions except for a switching transient at t=10 seconds.

Case 4. (Rise in load demand-Constant wind)

This case is similar to the case 3 except that the wind turbine output is allowed to reach a steady state value, before applying additional load on the hybrid generation system. The input wind velocity remained constant at 9.3 m/s and there is a step increase in the load demand at t=12 seconds as shown in Figure 5.31.

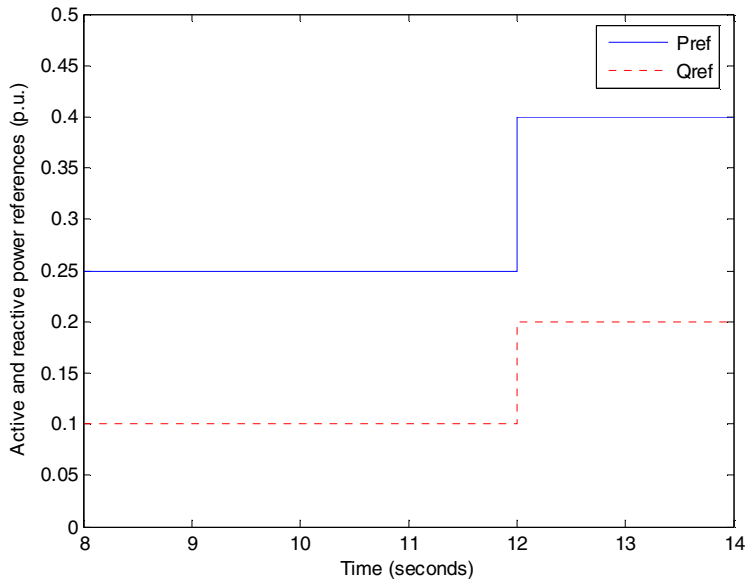

Figure 5. 31 Load demand of the hybrid generation system.

The real power outputs of the MTG system and the WECS for the above mentioned wind and load conditions are shown in Figures 5.32 and 5.33, respectively.

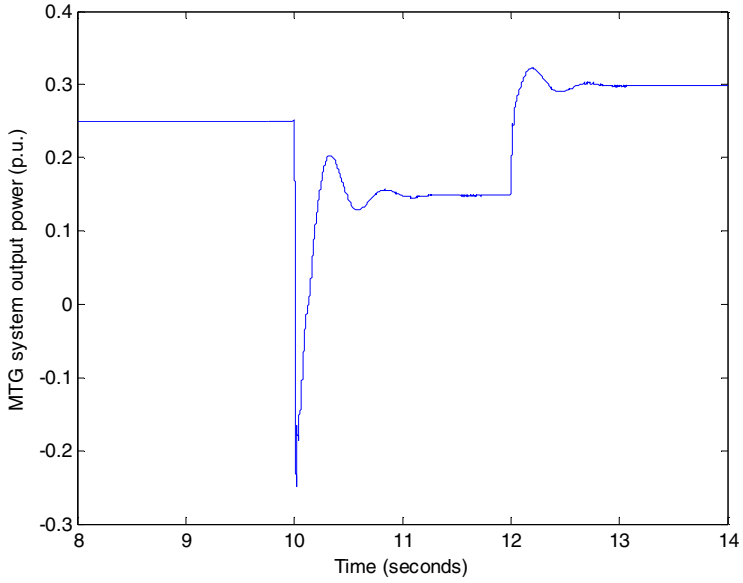

Figure 5. 32 MTG system real power output variations with load.

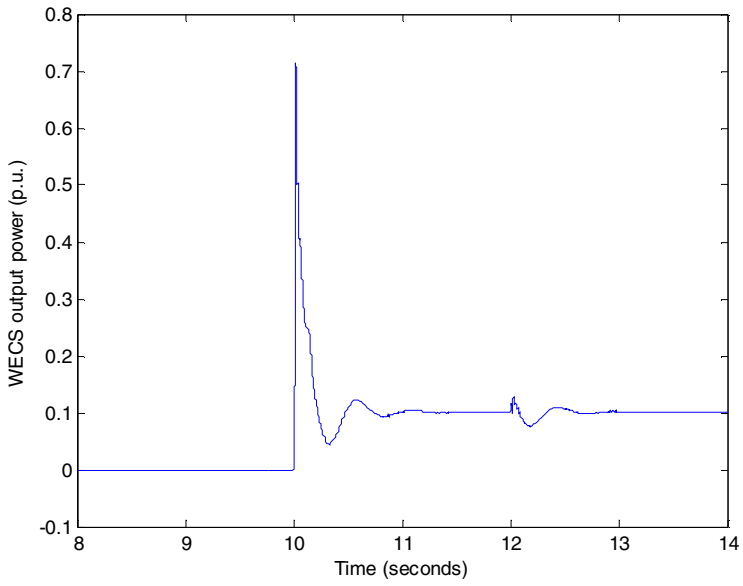

Figure 5. 33 WECS real power output variations with load.

Figure 5.32, shows the decrease in real power output of the MTG system from 250 kW to about 150 kW when WECS starts supplying the load at t=10 seconds as the wind

turbine output at the wind velocity of 9.3m/s is 100 kW. As load demand increases from 250 kW to 400 kW at *t*=12 seconds, the microturbine picks up the additional load and its output reaches a final value of 300 kW. During the same period, as the wind velocity remained constant, the WECS output remained constant (Figure 5.33) at 100 kW.

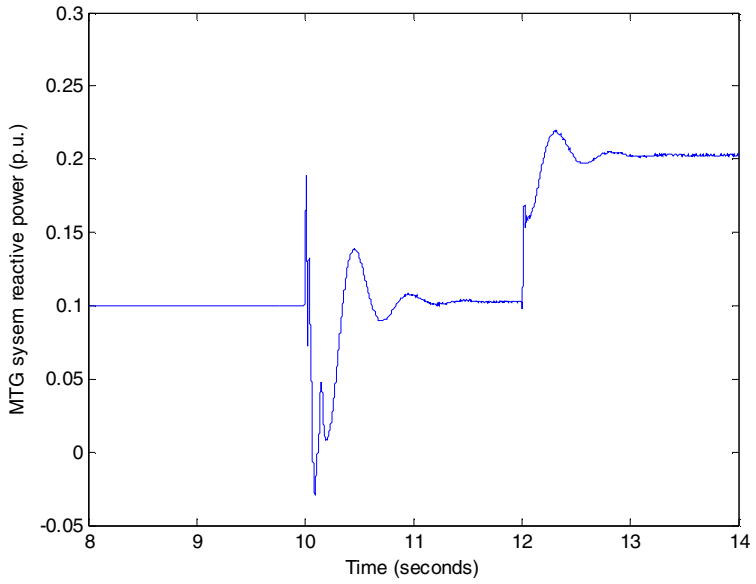

Figure 5. 34 MTG system reactive power variations with load.

Figures 5.34 and 5.35 show the reactive power supplied by the MTG system and the WECS, respectively. These figures show that the MTG system contributes the total reactive power requirements of the load, and the WECS (Figure 5.35) follows its reactive power reference which is set at zero. The MTG system reactive output remains constant at 0.1 p.u. until *t*=12 seconds, except for the transients at the instants of switching of WECS and load, and then rises to 0.2 p.u. following the load demand.

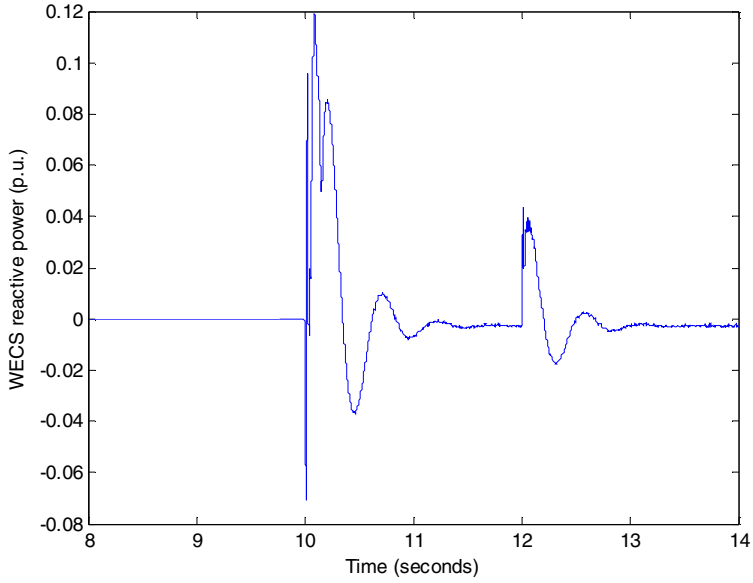

Figure 5. 35 WECS reactive power variations with load.

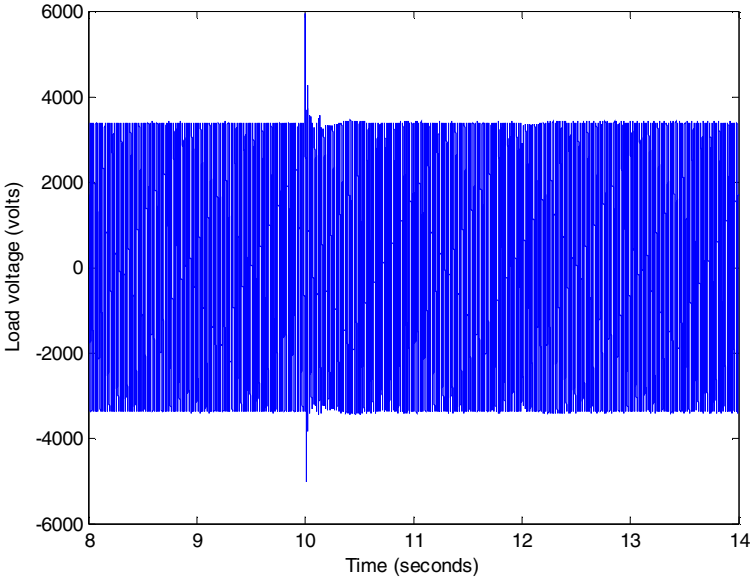

Figure 5. 36 Voltage at the load terminals.

Figure 5.36, shows the AC load terminal voltage in volts. The voltage at the load terminals matches well with its reference value of 2400 volts (RMS), irrespective of the applied load conditions, except for the switching transient at t=10 seconds.

Conclusion. A Simulink based computer simulation model of a hybrid generation system comprised of a wind energy conversion system and a microturbine generation system is presented. This model is used to evaluate the performance of the proposed stand-alone hybrid generation system with varying wind speeds and different load conditions. A *dq*-transformed power electronic controller is employed to regulate the output voltage and frequency throughout the period of operation. Simulation results indicate that the proposed model has the ability to meet both real and reactive power requirements of the load, maintaining prescribed values of voltage and frequency, with the help of the power electronic controls.

REFERENCES

5.1 M.F.Gillie and W.E.Leithead "Operation and regulation of a wind and gas virtual power plant," in *17th intl. conf. Electricity Dist*., Barcelona, May 20003.

5.2 MATLAB/Simulink SimPowerSystems Documentation. Available: http://www.mathworks.com

5.3 C. Wang, M. H. Nehrir and H. Gao, "Control of Grid-Connected PEM Fuel Cell Power Systems," under review for publication in the *IEEE Transactions on Energy Conversion*.

5.4 Paul.C.Krause, Oleg Wasynczuk and Scott D. Sudhoff, *Analysis of Electric Machinery*, IEEE Press, 1994, ch. 3-4.

5.5 J. D. Glover, M.S. Sarma, *Power System Analysis and Design*, 3rd Edition, Wadsworth Group. Brooks/Cole, 2002.

CHAPTER 6

CONCLUSION OF THE THESIS AND FUTURE WORK

Conclusion of the Thesis

Modeling of a hybrid wind-microturbine generation system suitable for power management in DG applications is presented in this thesis. A complete model of the hybrid generation system is achieved by developing dynamic models for each of the system components namely, WECS and MTG system. The developed model of the WECS consists of a SEIG driven by a wind turbine. The dynamic model of the SEIG is complete with its saturation characteristic and is suitable for isolated operation as well as grid connected operation. A mathematical model of a microturbine driving a permanent magnet synchronous generator is used to represent dynamics of the MTG system. These two systems (WECS and MTG system) were integrated through a power electronic interface, feeding an AC load, and simulated in MATLAB/Simulink.

The simulation results presented in the previous chapters suggest the role of the hybrid generation system as a reliable power source and the suitability of developed model for power management studies of hybrid distributed generation systems. In particular the ability of the WECS in picking up the load whenever wind is available, and the ability of the MTG system (working as a backup generator) in meeting the load demand whenever there is not sufficient wind, are demonstrated. Also, simulations results

show that the power electronics interfacing maintained the output voltage and frequency of the 3-phase inverter at the prescribed values during the entire period of operation.

Future Work

Some of the areas worth future investigation, but not limited to, are summarized in the following paragraphs.

A detailed model for wind input can be used which includes noise, gust effects etc, instead of the average wind input used in this study. Also, in the regions below rated wind speeds, the generator speed could be controlled to follow the ideal speed curve; resulting in the optimum value of *TSR* and correspondingly maximum power output. This can be achieved by employing methods like flux control, vector control etc., to control the generator torque thereby controlling the rotor speed.

In this thesis it is assumed that the SEIG always sees a unity power factor load connected to its stator terminals. This topic could be further extended to SEIG under inductive loads, provided techniques are developed to determine the capacitance value that needs to be connected across the load terminals meeting its reactive power requirement. This capacitance should be added or removed with the connection or disconnection of the inductive load. Modern static reactive compensators are a good practical solution. Also, intelligent controls could be very helpful in designing methods to estimate and vary the capacitance value for the above said purpose.

The MTG system starts as a motor until it attains a predetermined rotor speed, with the help of an external storage or device (such as a battery), and then starts to function as a generating system. These start-up dynamics associated with the MTG system are not considered in this thesis. Inclusion of these dynamics represents a significant improvement to the model presented. Also in the microturbine model, for combined heat and power (CHP) applications, recuperator model could be added to increase the overall efficiency. Speed of the PMSG can be controlled, to operate the MTG system in the most efficient regions, to get the optimum output with least fuel consumption.

Addition of storage devices helps to bring down the maximum ratings of the subsystems (MTG and WECS, in this case) and increases the hybrid system's overall efficiency. Other issues related to the hybrid generation systems that are of concern are, its impacts on the overall transmission and distribution system; when connected to an existing network. In such cases, the hybrid energy systems could alter power flow direction or can cause voltage, frequency fluctuations as well as "islanding" where a hybrid plant might energize a dead power line.

APPENDIX A

SIMULATION DIAGRAMS

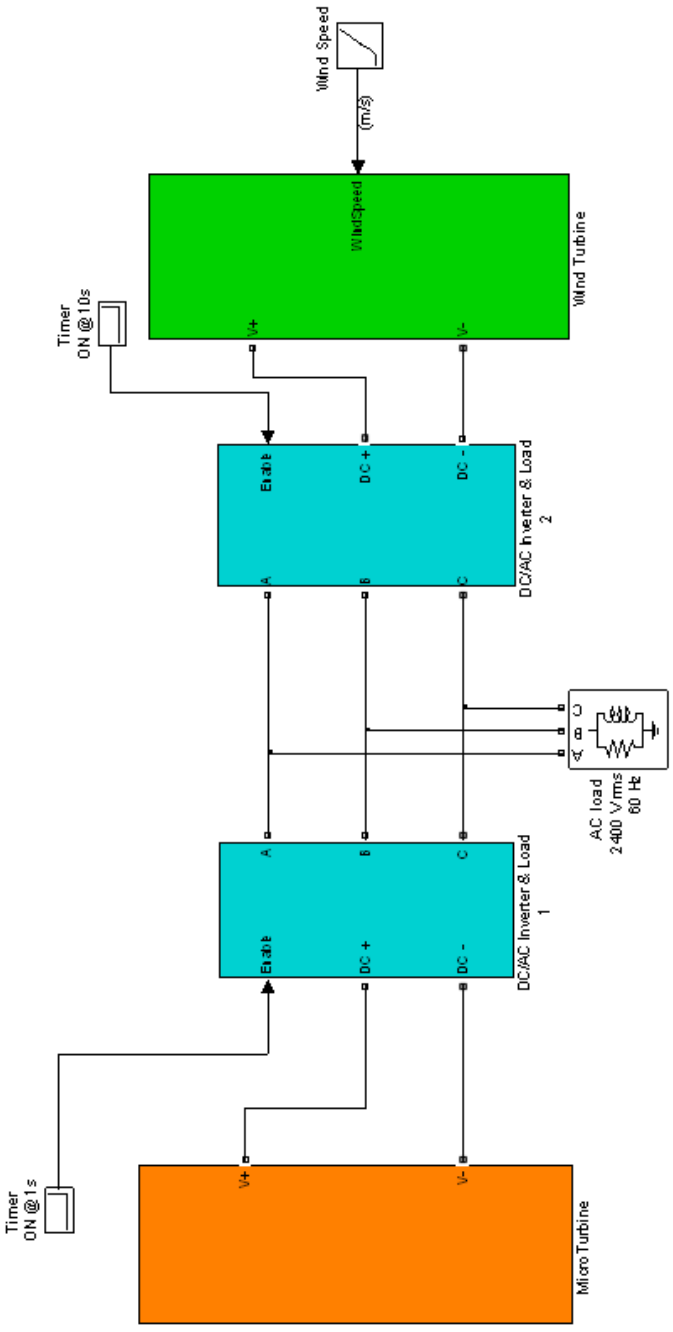

Figure A1. Simulink model of the hybrid generation system

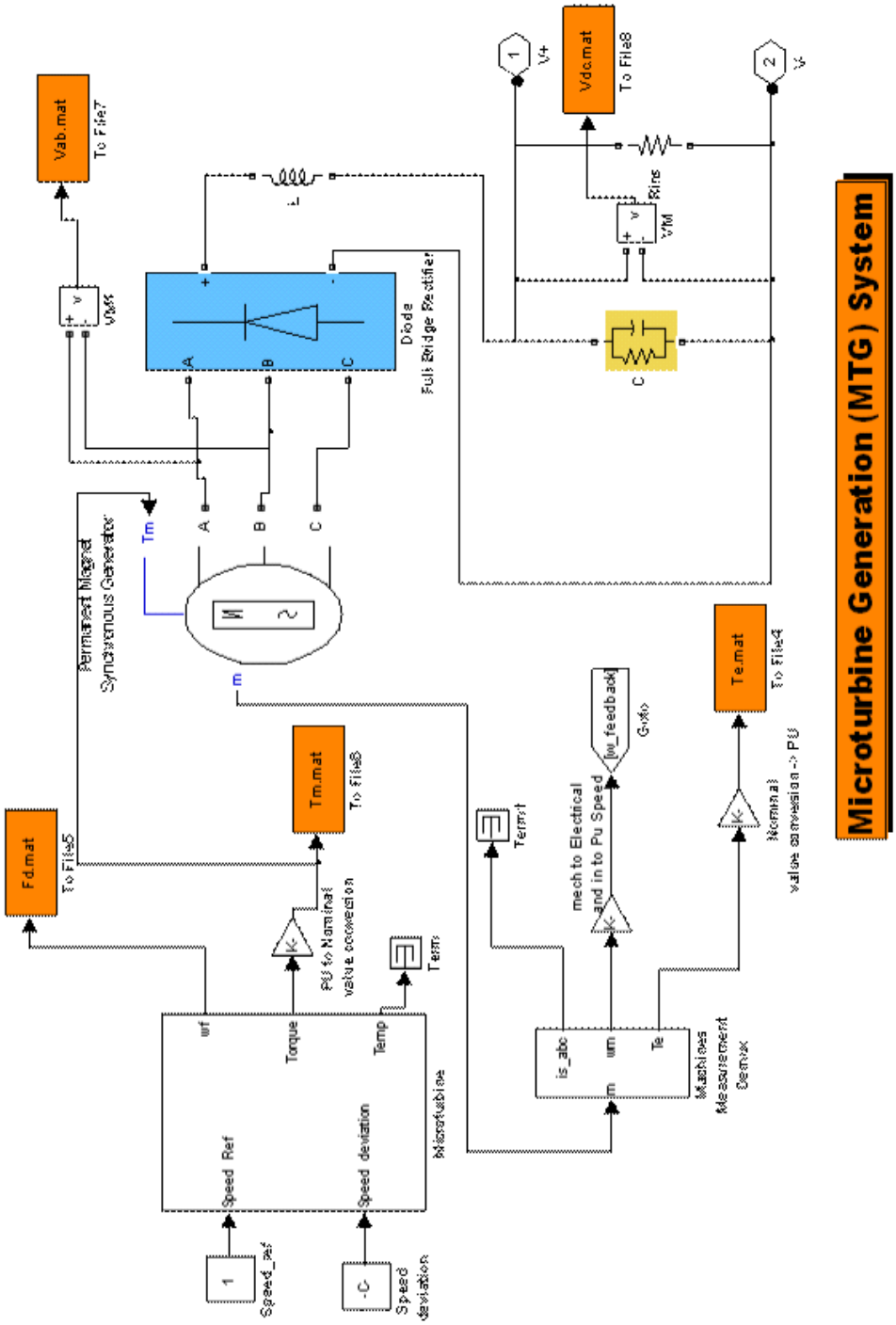
Microturbine Generation (MTG) System
Vab.mat
To File7
Vdc.mat
To File8
Rins
Vdc
Vab
Diode
Full Bridge Rectifier
C
Permanent Magnet
Synchronous Generator
Tm
Fd.mat
To File5
Tm.mat
To File6
Te.mat
To File4
Terms
mech to Electrical
and in to Pu Speed
w_feedback
Gain
Nominal
values conversion -> PU
Pu to Nominal
value conversion
Speed_ref
Speed
deviation
Speed Ref
Speed deviation
wrf
Torque
Temp
Microturbine
is_abc
wm
Te
Machines
Measurement
Demux

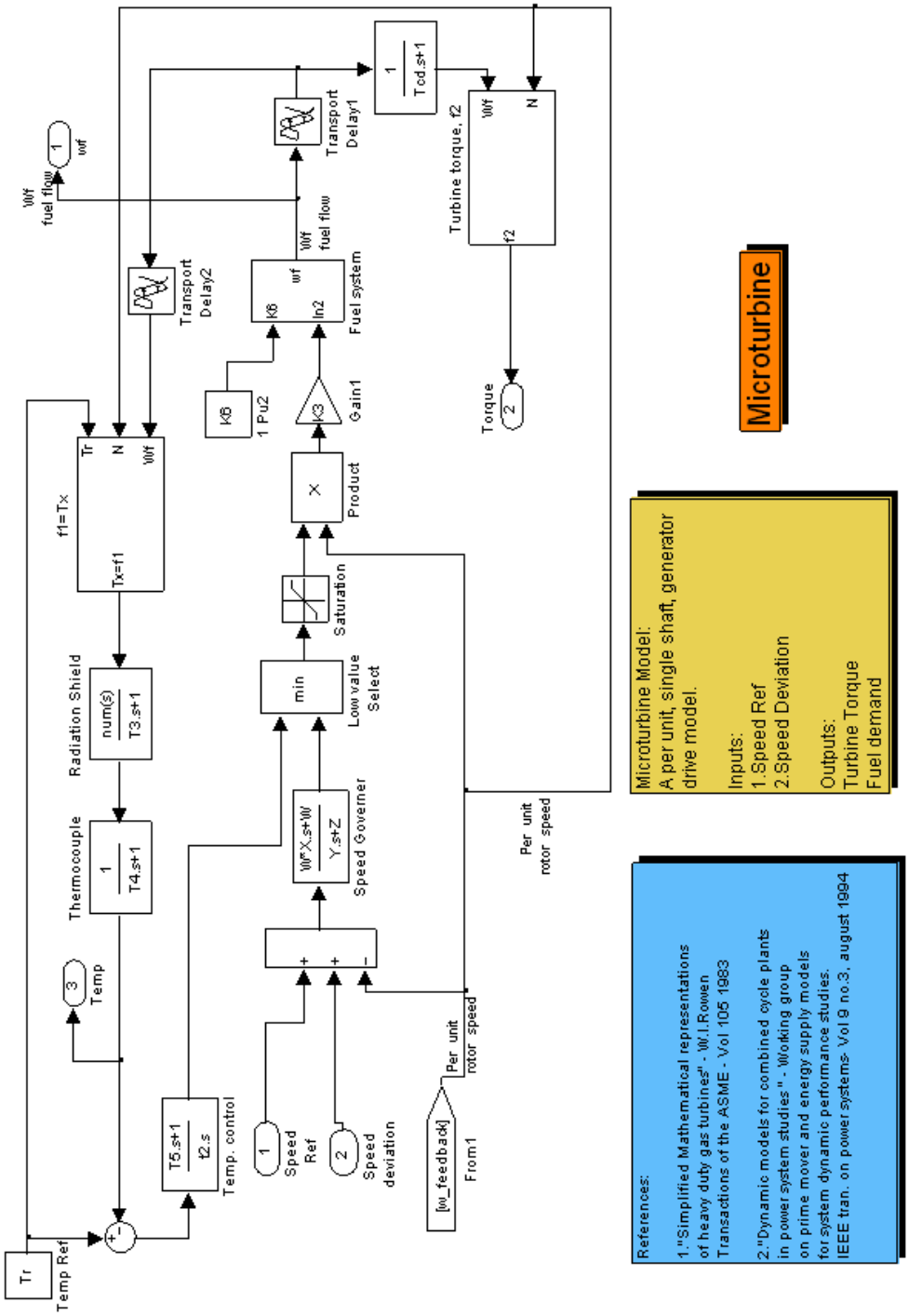

Figure A3. Simulink model of the microturbine

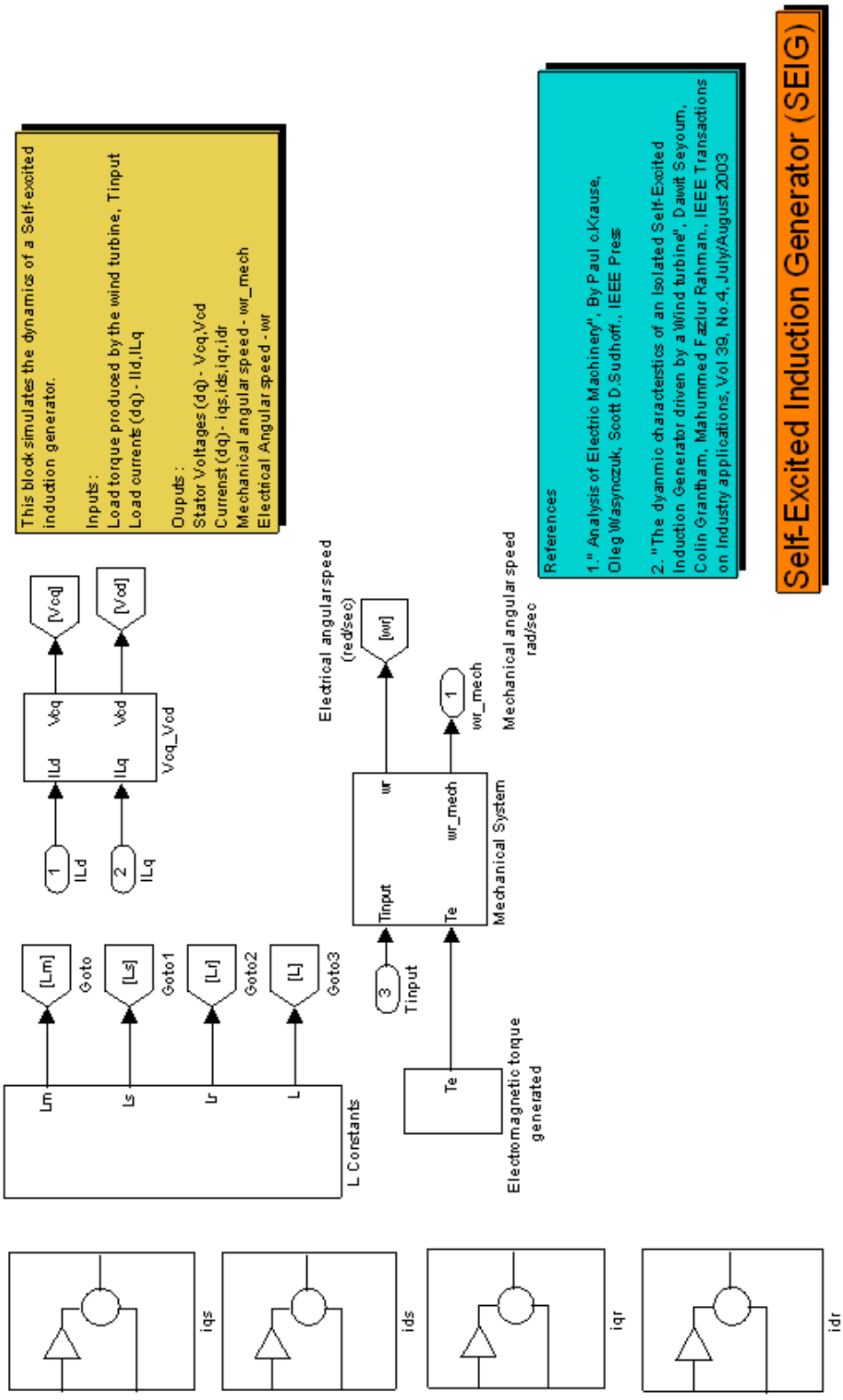

Figure A 4. Simulink model of the self-excited induction generator

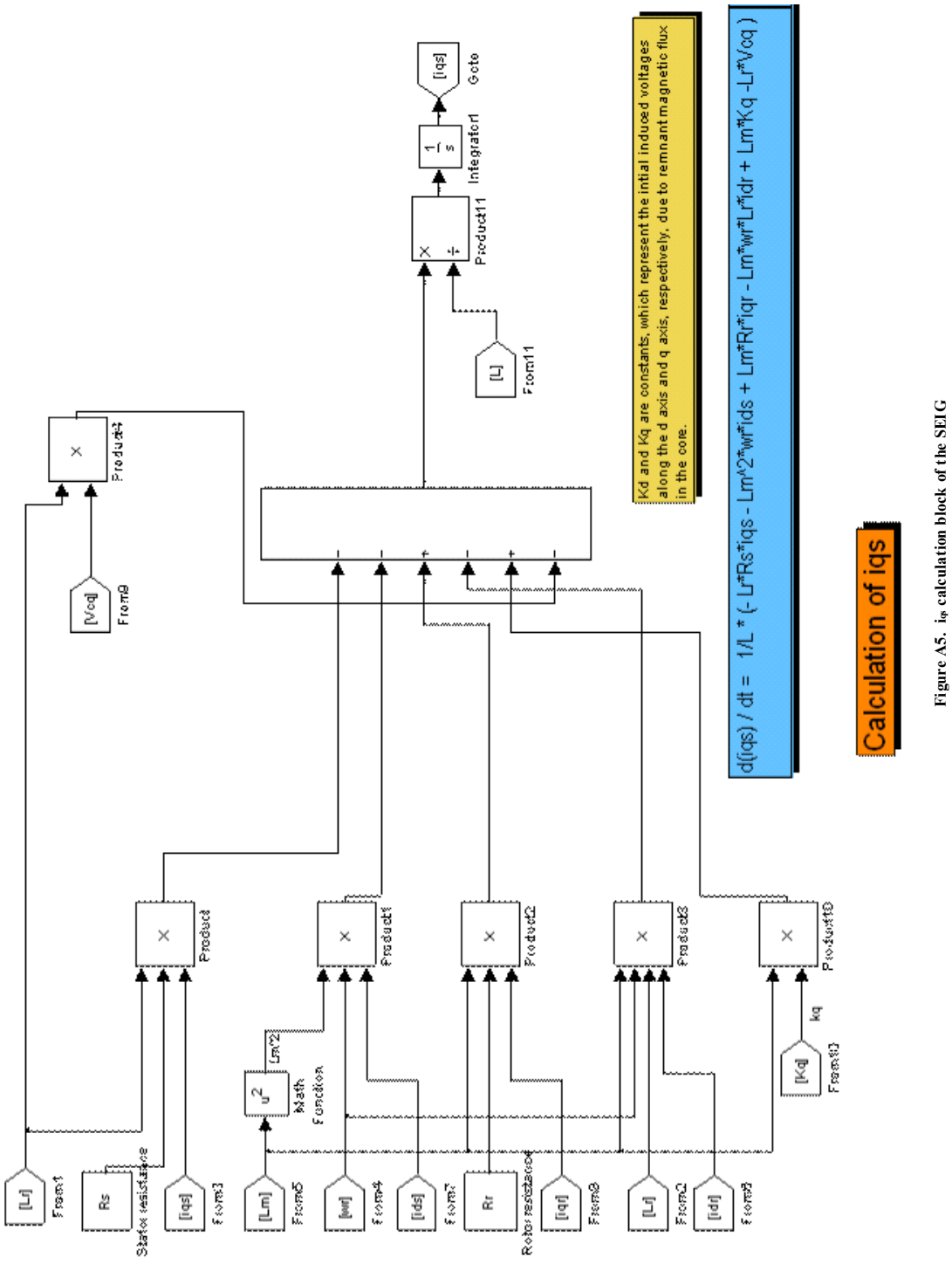

Figure A5. i_{qs} calculation block of the SEIG

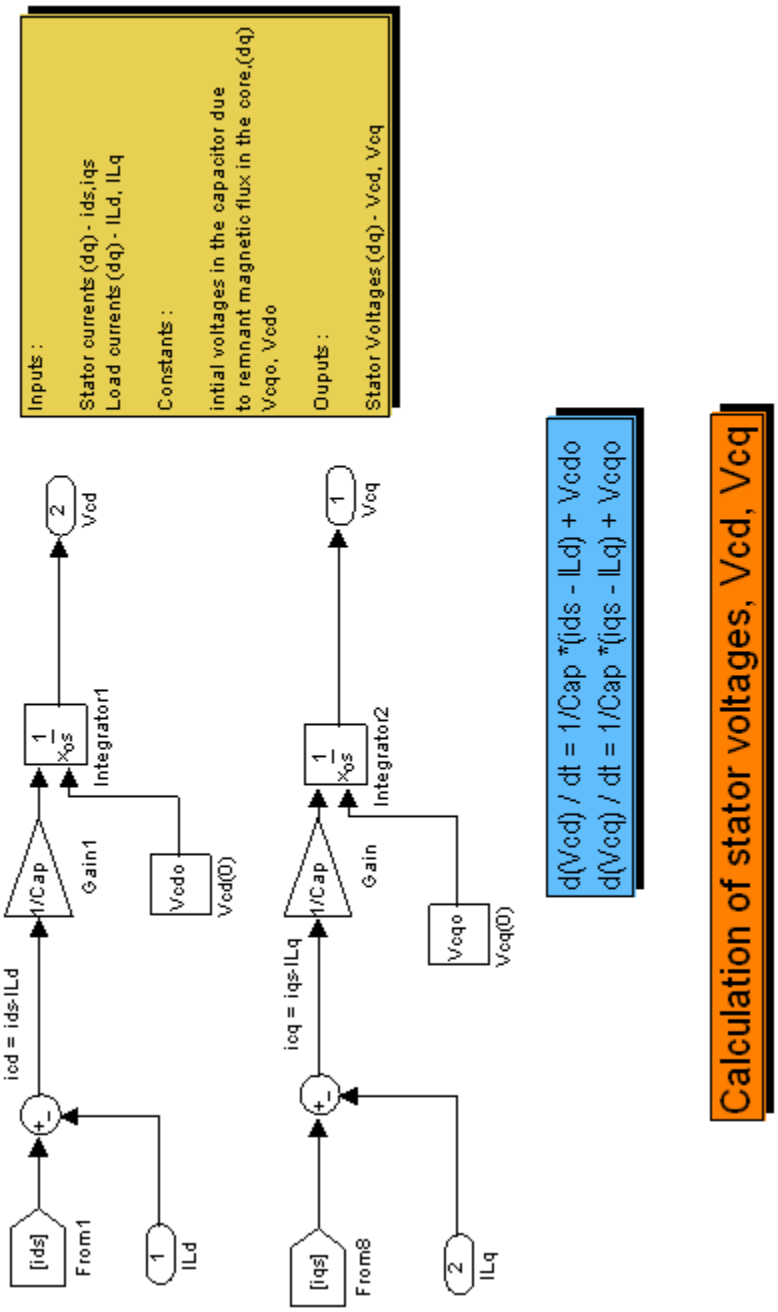

Figure A6. Calculation of V_{cq}, V_{cd} of the SEIG

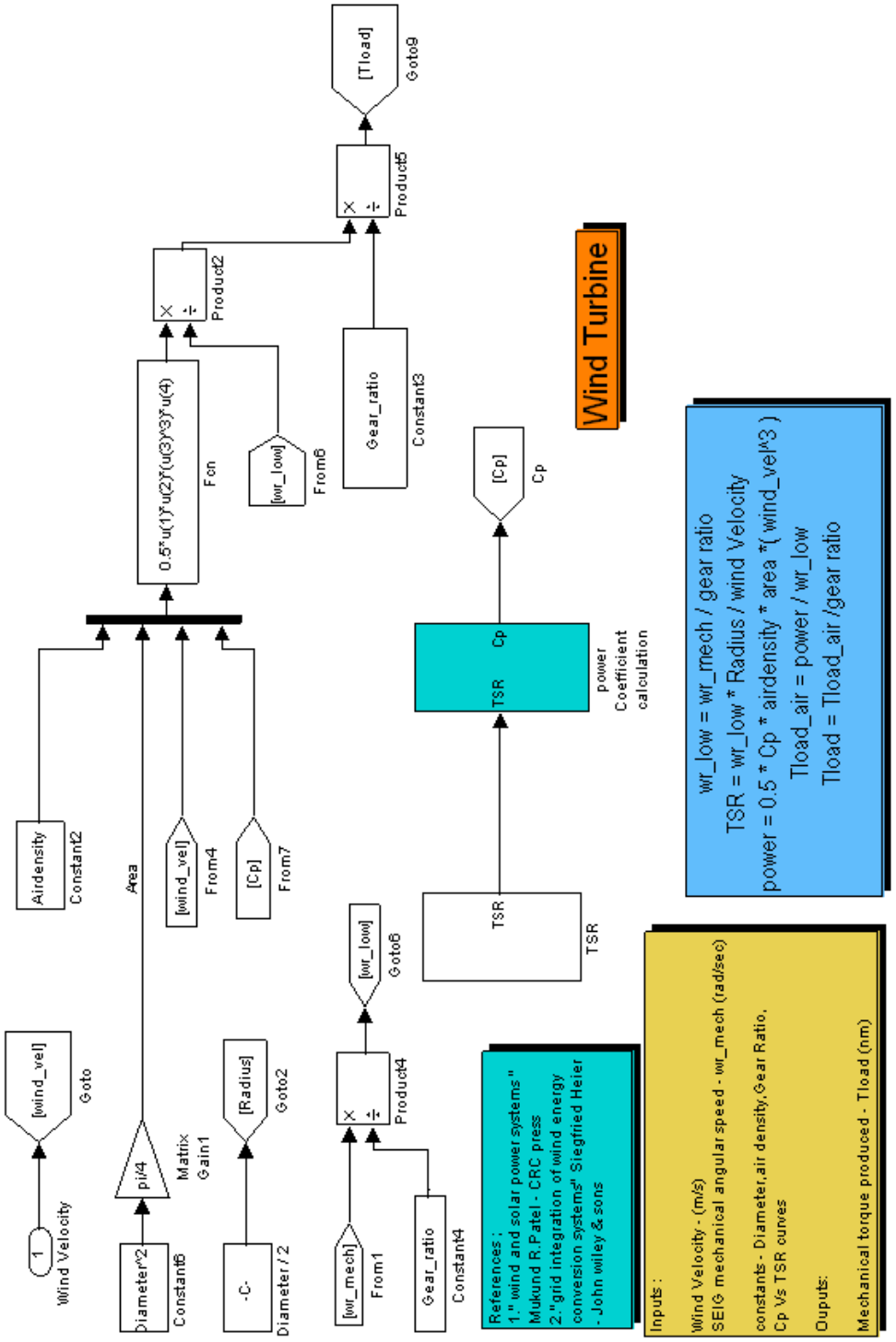

Figure A7. Simulink model of the wind turbine